NTNU
Norwegian University of
Science and Technology

One-pot conversion of biomass to chemicals

Björn Frederik Baumgarten

Chemical Engineering and Biotechnology
Submission date: June 2017
Supervisor: De Chen, IKP

Norwegian University of Science and Technology
Department of Chemical Engineering

Master Thesis

One-pot conversion of Biomass to Diols

By Björn Baumgarten

Supervisor: De Chen

Norwegian University of Science and Technology

Department of Chemical Engineering

Catalysis Group

June 25, 2017

Abstract

One-pot conversion of biomass to diols can be a simple and fast alternative to other methods of biomass conversion. The catalyst for this conversion is required to be bifunctional, catalysing both hydrogenation and retro-aldol condensations. Hydrogenation is realized by usage of transition metals like Ru, Ni and alternativly copper. Retro-aldol condensations are catalyzed by various tungsten compounds, amphoteric and basic metal oxides or basic sites.

New amphoteric and basic catalysts were tested, La_2O_3, MgO, Al_2O_3 and nitrogen doped carbon spheres. The metal oxides were dispersed on carbon nano tubes and copper as hydrogenation catalyst added, while the carbon spheres were used as support and copper dispersed on them.

La_2O_3 proved to be the most promising catalyst with yields of 20,3% ethylene glycol and 19,1% PG.

In order to demonstrate the importance of optimizing the ratio between hydrogenation and retro-aldol condensation catalyst, additives which are solely active for one function were added. Thereby, it was possible to show that La_2O_3 is very active for retro-aldol condensations and more hydrogenation catalyst is required. With hydrogenation additive (Ru/CNT), a yield of 28,2% EG and 19,2 % PG could be reached.

By usage of the additives and a novel liquid sampling mechanism enabling sampling mid-reaction, more insight into the reaction mechanism could be gained. Indicators for too strong activities of both reactions could be identified.

Too high hydrogenation activity is indicated by formation of persistent erythritol and sorbitol amounts. In contrast, forming of small sorbitol amounts and subsequent consumption during the reaction is desired and limits the amount of degradation products.

Too high retro-aldol condensation activity leads to the formation of 5-HMF degradation and polymerisation, manifesting in a large void volume peak.

Additionally, the reaction network could be completed and adjusted for copper-based hydrogenation catalysts.
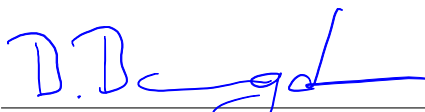
Preface

I would like to thank all members of the catalysis group for their help and guidance during the project. Especially Professor De Chen for his scientific advice.

I would also like to thank Cornelis van der Wijst for his help with the laboratory equipment and his advice as well as Haakon Rui for his help with the analysis of products and his training regarding the HPLC. Many thanks go to Greg Rutkowski for his help with SEM analysis, Petter Kaalstad for the shared struggle with analysis and his moral support.
My parents and especially my son Arne deserve special thanks for their support and the constant reminder that life is great and is ought to be enjoyed.

I declare that this is an independent work according to the exam regulations of the Norwegian University of Science and Technology (NTNU).

Trondheim, June 25, 2017

Björn Baumgarten

Contents

1 Introduction

Today's economy is based upon fossil fuels and chemicals which are mostly based on crude oil.

This causes a range of issues, partly manifesting already, partly in the foreseeable future. Usage of fossil resources liberates CO_2 which was stored in the earth crust. This leads to an increasing concentration of CO_2 in the atmosphere and thereby causes Global Warming. Another problem is the limited supply of fossil resources. Even though the resources are expected to last for another 150 years, extraction will become more and more difficult and expensive [1]. Additionally, the limitation to one source leads to a huge dependency on its cost. In the past, the crude oil cost proved to be quite volatile, causing the Oil Crisis in the 1970s. Afterwards the price became very low, just to reach a new high in 2011. After the development of fracking technologies mainly in the US, it again plummeted to a new low.

Given the economic and environmental risk of relying on crude oil, it is important to use other sources for both Energy and Chemicals.

For Energy, a wide range of different sources is possible and many routes to replace fuels are getting explored. The technologies used are quite diverse, ranging from Solar Energy, Wind Generators and Electric Cars to usage of Biomass. For chemicals, the options are more limited, mostly to Biomass [2].

The most researched (and already commercially applied) alternative chemicals are bioethanol and biodiesel, both used as component of conventional fuel in a range of 5-10%. However, these technologies only use the sugar or the fatty acids of the plant, while the rest is waste [3].

There are approaches for 2nd and 3rd generation fuels, which also use the rest of the plant, however these are still in the research phase and most of them are facing economic problems.

Biomass mostly consists of cellulose, hemicellulose and lignin in varying weight fractions. Normally, cellulose is most abundant [3].

In this paper, the conversion of Cellulose is discussed. The goal is not to produce fuel, but chemicals. Chemicals have a higher value than fuels, thus, it is easier to find an economically sound process [4]. Cellulose itself is water insoluble, thus,

it first needs to be broken down into monomers before it can be processed. Previous work focused mostly on conversion of cellulose towards EG using bifunctional catalysts [5]. Main products obtained were ethylene glycol and propylene glycol. Hydrogenation is mostly achieved by use of metals like ruthenium or nickel, while tungsten carbide, oxide or acid is used for C-C cleavage by retro-aldol condensations. [6]. Also amphoteric metal oxides like ZnO were tested for C-C cleavage [7]. The highest reported yield to date was 75,4% ethylene glycol using a Ni-W/SBA-15 catalyst [8]. During this work, new, basic catalysts were tested for C-C cleavage while copper is used as hydrogenation catalyst. Hydroxide ions are known to catalyze cellulose hydrolysis [9], but they also catalyze isomerization [10] and retro-aldol condensations [11]. Since ethylene glycol is produced from glucose, while propylene glycol is produced from fructose after isomerization of glucose, the use of basic supports should increase the yield of propylene glycol [7].

2 Literature Research

Conventional approaches to biomass conversion normally employ multiple steps to convert lignocellulosic biomass to products. Some of these use biological methods (e.g. fermentation) which have residence times in excess of a day [3]. Thus, a new approach using a catalytic one-step conversion would make a potential process simpler and, since no biological steps are involved, much faster. The first attempts were made 2006 [12], and until today more research has been done. This section will focus on the feedstock, degradation methods and the reaction network proposed for conversion to diols as well as previous research on catalystic systems.

2.1 The feedstock: Cellulose

While plants consist of Cellulose, Hemicellulose and Lignin, this work focuses on the conversion of Cellulose. It is a biopolymer consisting of glucose an-hydride units.

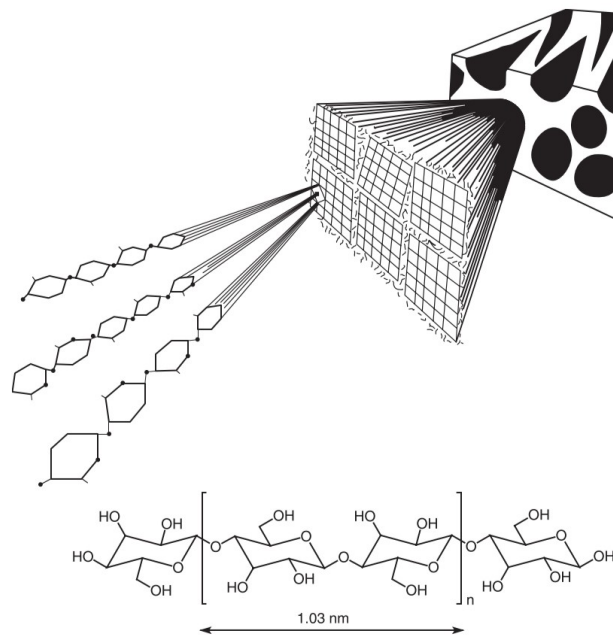As can be seen in figure 2.1, glucose an-hydride units are linked by beta-1,4-

Figure 2.1: Structure of a cellulose fiber [2].

glycosidic bonds. The glycosidic bonds are relatively stable, which makes cellulose

hard to process. For its conversion into chemicals, it needs to be broken down into monomers.

2.2 Hydrolysis of Cellulose

Common methods for breaking down cellulose are acid hydrolysis (with H_2SO_4, HCl or other acids), alkaline hydrolysis (with NaOH) or biological hydrolysis using enzymes. If acid treatment is used, high concentrations or severe reaction conditions are required in order to achieve full conversion to glucose monomers. If concentrated acid is used, it needs to be recovered after hydrolysis in order for the process to be economically sound. Process control is critical: If the residence time is too long, degradation products will be formed: 5-HMF (5-(hydroxymethyl)-2-furaldehyde) and furfural. The pathway for 5-HMF is depicted in figure 2.2. Depending on the following steps, 5-HMF and furfural are highly undesirable as they inhibit bacterial growth [13].
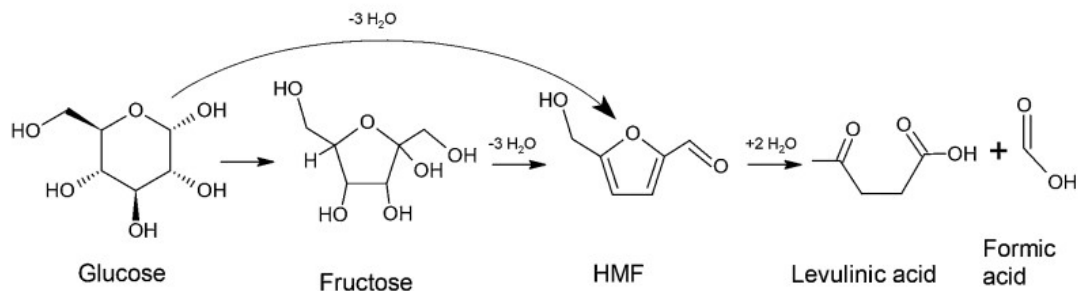
Figure 2.2: Degradation Mechanism of Glucose [14].

Enzymatic degradation does not yield 5-HMF or furfural, however, it requires enzymes which are expensive and need long residence times [3].

2.2.1 Mechanism of Acid Hydrolysis

Acid hydrolysis is a common method to convert cellulose into monomers. The acid attacks beta-glycosidic links between monomers, thereby reducing chain length and yielding hydrocellulose which has a reduced degree of polymerization. Given

a severe enough treatment, link cleavage continues until monomers are formed
[3].

2.2.2 Mechanism of Alkaline Hydrolysis

Instead of acids, bases can be used to hydrolyse cellulose. They use two different mechanisms: At high temperatures of 140-170°C and above, random glycosidic link cleavage occur. The second mechanism, peeling, already occurs at low temperatures. Single monomers starting from the reducing -OH end are liberated from the chain. The mechanism is shown in figure 2.3.
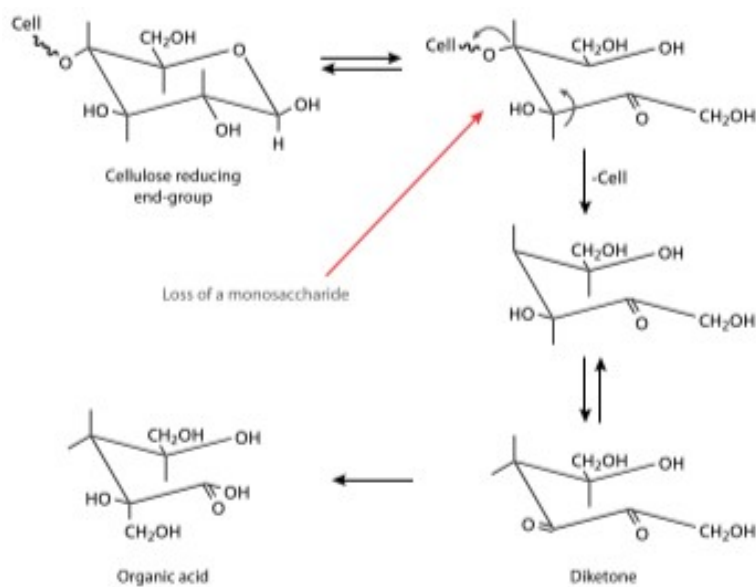
Figure 2.3: Peeling mechanism [3].

Different to acid hydrolysis, the result are diketones or organic acids of glucose and not glucose itself. As side reaction, elimination of a hydroxyl group might occur resulting in a stop of the peeling chain reaction [3].

2.2.3 Hydrothermolysis

During one-pot conversion, liquid hot water (or Hydrothermolysis) is used to depolymerise cellulose. Instead of acid or enzymes, hot compressed water (245°C, 50+ bar) is used. Under these conditions, the ion product of water is high, and H^+

ions formed by dissociation of water molecules attack the glycosidic bonds similar to the mechanism of acid hydrolysis. Also further degradation to 5-HMF and Furfural can occur [3]. The ion product is depicted in figure 2.4. As it can be seen,
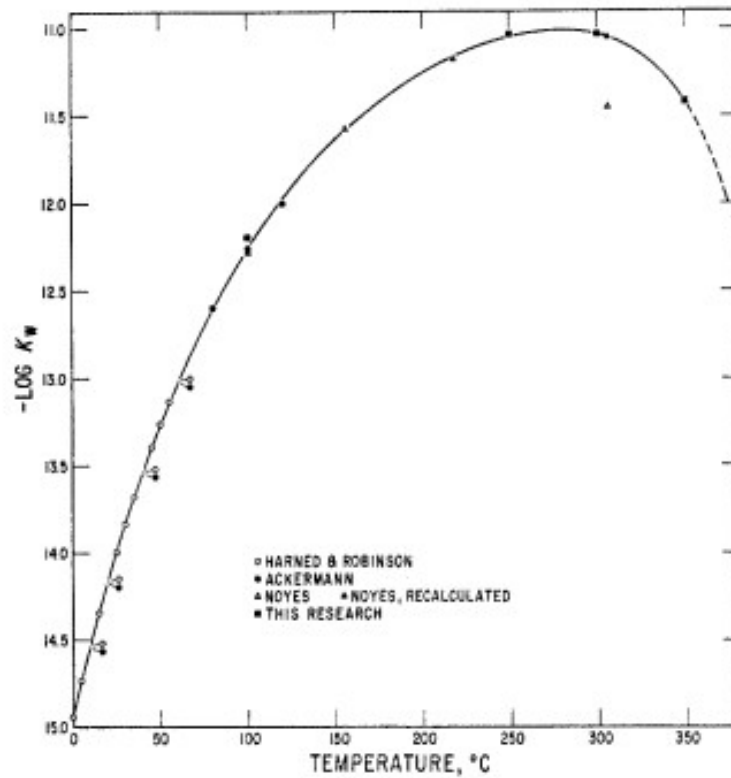
Figure 2.4: Molal ion product of water dependent on temperature [15].

between 240 and 300°C the ion product is at its maximum, a reaction temperature in this range was chosen to promote the decomposition of cellulose. In the special case of one-pot conversion, glucose and fructose are only intermediates, which react further as discussed in the next chapter. Therefore the formation of 5-HMF and furfural is largely dependent on the relative reaction rates of the different reactions.

2.3 Pathways and possible products

Once the cellulose is converted into monomers, it can be converted using appropriate catalysts.

6

Depending on the catalyst, different main products are possible. If catalysts which are only active for hydrogenation are used, the main products are sorbitol and mannitol. To obtain diols catalysts which are also active for C-C cleavage and retro-aldol-condensations are required as pictured in figure 2.5 [6].
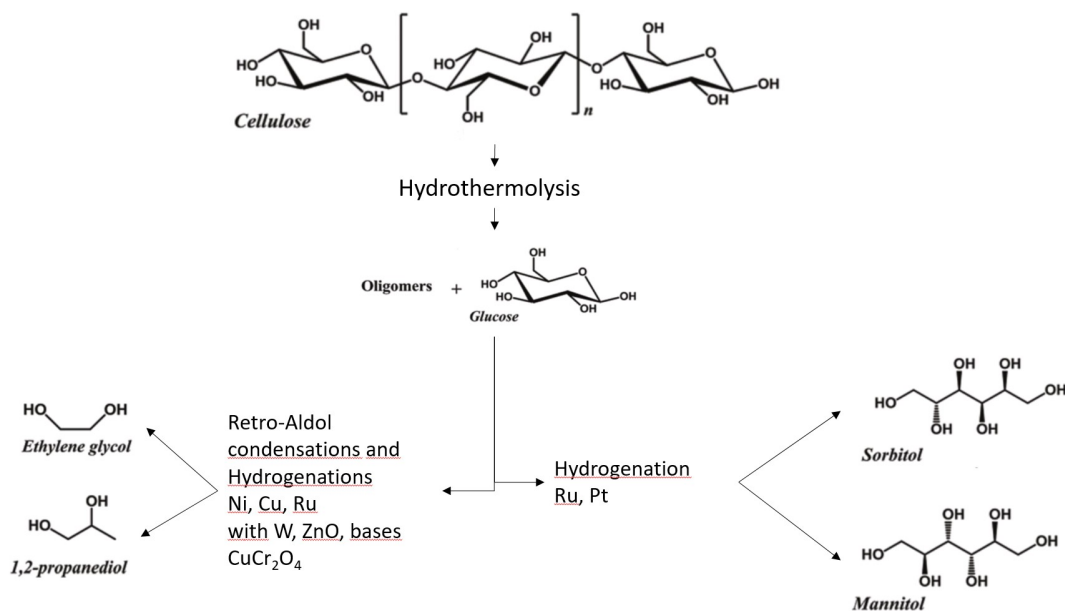
Figure 2.5: Products of cellulose hydrolysis and subsequent catalytic conversion. Adapted from [6]

The aim of this work was to produce ethylene glycol (EG) and 1,2-propylene glycol (PG) using Cu catalysts. The pathway for the route resulting in diols is depicted in more detail in figure 2.6.

Ethylene glycol and 1,2-propylene glycol are not the only possible products. Other products include glycerol, 1,2-butanediol, 1,2-pentanediol and 1,2-hexanediol as well as derivates of HMF. The first main pathway is the ethylene glycol branch. The glucose produced by the depolymerisation of cellulose reacts via retro aldol condensations (2) and hydrogenations (3) to form ethylene glycol.

Alternatively, the glucose can isomerise to form fructose. Then, it can react further via hydrogenation and retro-aldol condensations to propylene glycol, glycerol and ethylene glycol. Glycerol is in equilibrium with glyceraldehyde, thus, it is possible to reach full conversion towards ethylene glycol and 1,2 propylene glycol.
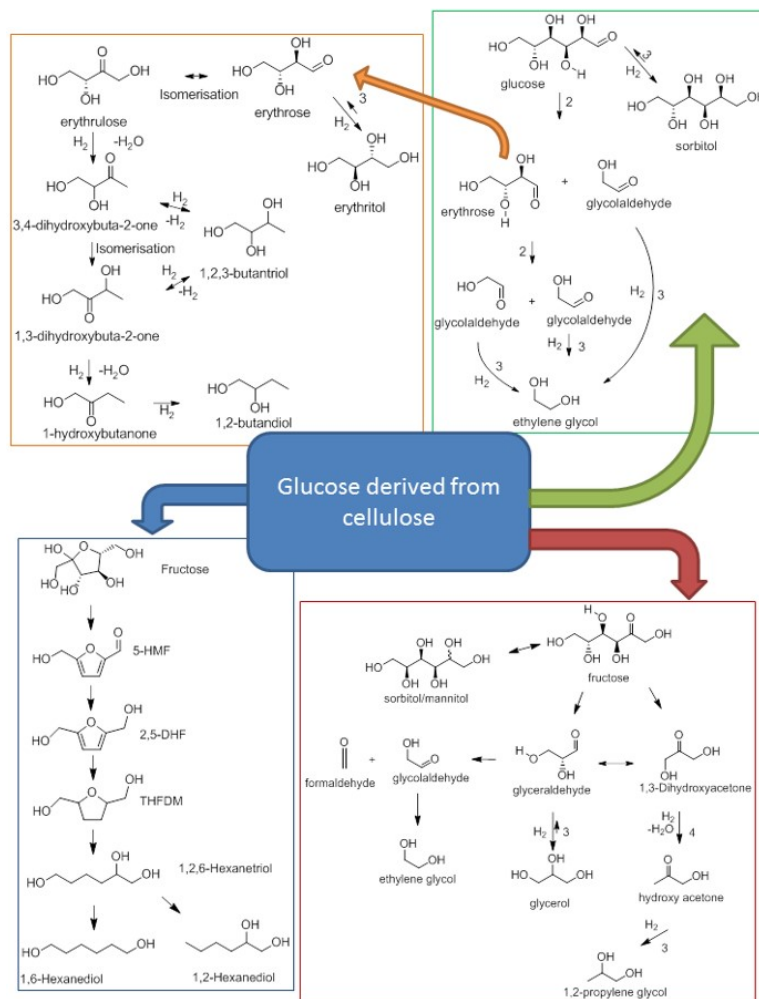
Figure 2.6: Reaction Network for cellulose hydrolysis and subsequent catalytic conversion [16]

A side reaction of both pathways is the hydrogenation of glucose and fructose towards sorbitol and mannitol, however, these reactions are reversible.

As described in the previous chapter Hydrolysis, glucose and fructose can react further to form 5-HMF. If this happens, 5-HMF can be hydrogenated to form 2,5-DHF, THFDM or after ring opening 1,2-hexanediol after intermediate formation of 1,2,6-hexanetriol and dehydrogenation thereof [17].

This pathway is described in more detail by Yao et al [18], but they propose a different pathway then van der Wijst as shown in figure 2.7. Van der Wijst assumed that THFDM is an intermediate of the pathway, while Yao et al assume it to be a side product. Yao et al used 5-HMF as feedstock, which was converted to 1,2,6-hexanetriol. They used milder reaction conditions, thus, further dehydrogenation towards 1,2-hexanediol was only observed at small yields. As first step, the 5-HMF aldehyde group is hydrogenated to form 2,5-DHF. Depending on the adsorption onto the catalyst, 2,5-DHF either is completly hydrogenated to form THFDM, or only partly hydrogenated and ring opened by cleavage of the C-O bond. The adsorption leading to ring opening was catalysed by basic metal oxide sites (here: CoO), while the hydrogenation was performed by Ni.
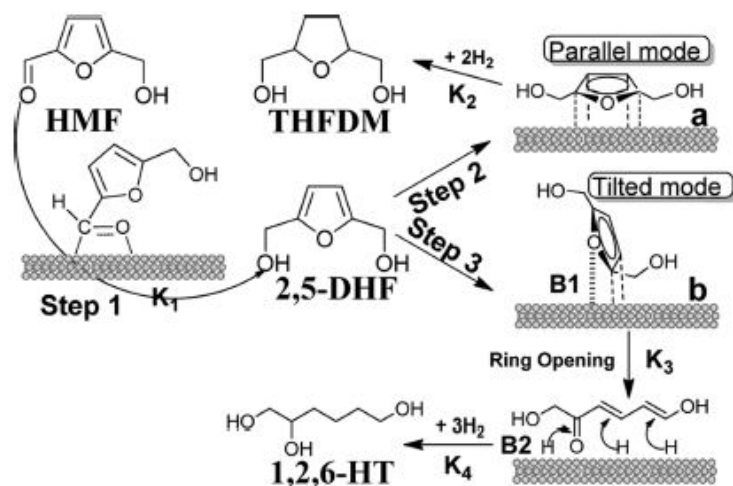
Figure 2.7: Reaction Mechanism for Conversion of HMF [18]

As last pathway, the erythrose formed by retro-aldol condensation of glucose can not only react to form EG, but can also undergo a secondary pathway with 1,2-butanediol as final product.

2.4 Hydrogenation catalyst

There are a range of different catalysts which can be used for different hydrogenation reactions involved in the conversion of cellulose. Traditional hydrogenation catalysts are expensive noble metals (Pt, Ru, Ir), but also other, cheaper metals

like Ni and Cu are possible [19]. If used as single catalyst, Pt, Ru and Ni lead to the formation of sorbitol and mannitol [20][5].

One of the challenges while designing the hydrogenation catalyst are possible degradation reactions, especially hydrogenation of ethylene glycol. As example, Tai et al showed that they obtain a maximum yield of 54,4% ethylene glycol with an Ru/C catalyst with 1,2% loading. Upon increasing loading, the yield decreased to 19,4% at 4,0% loading as shown in figure 2.8. Degradation products such as CO_2 and CH_4 could be detected in the gas phase [21]. Thus, balancing the activity of the hydrogenation catalyst - high enough to hydrogenate all compounds to EG and PG, but low enough to not cause degradation - is a major challenge.
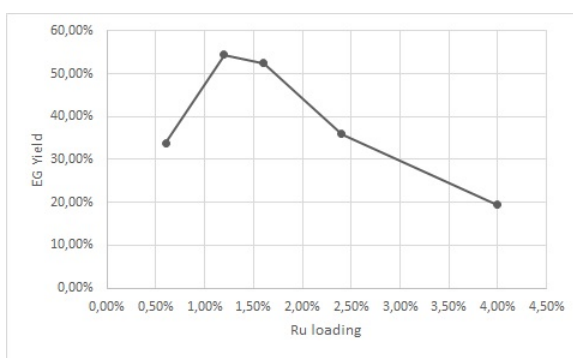
Figure 2.8: EG yield dependance on Ru Loading. Reaction Conditions: 0,15g Ru/C Catalyst, 0,05g H2WO4, 0,5g Cellulose in 50g H_2O, 518K, 6 MPa H_2, 30min [21]

2.5 Retro-Aldol Condensation catalysts

In order to produce EG and PG instead of mannitol and sorbitol, a catalyst active for C-C cleavage has to be added. The simplest way is the addition of H_2WO_4 to the reaction mixture. This approach also has the advantage of an easy way to optimize the ratio between hydrogenation and retro-aldol condensation catalyst [21]. Other possible catalysts include the use of ZnO, either as support [22] or as co-catalyst dispersed on carbon nanotubes (CNT) [7], WO3 (used as solid additive or dispersed on supports[23]).

Other basic or amphoteric metal oxides are also candidates for Retro-Aldol condensation catalysts. Additionally, alkali metal hydroxides [24] as well as solid bases are possible options [25].

2.6   Catalysts used by NTNU and their origin

First experiments for one-pot conversion of biomass were done 2006 by Fukuoka et al [12], using Pt or Ru on inorganic oxides. Lou et al [26] refined the process using a Ru on Carbon Catalyst and protonic acid to enhance reaction speed. Both reactions produced hexitols, however, they sparked interest in one pot conversion. Ji et al [27] used Ni promoted Cu catalysts, resulting in the production of ethylen glycol (1,2-Ethanediol). Ethylene glycol is a widely used polyol, thus would be an interesting product.

Wang et al [22] used a Ni on ZnO catalyst, which resulted in high total diol yields of 70,4%. They also tried addition of Cu to convert the glycerol byproduct to 1,2-propanediol (propylene glycol). ZnO as support has a low surface area, thus van der Wijst [7] used carbon nanotubes (CNT) as support for Ni-ZnO. The CNT-supported catalyst resulted in a higher yield due to the higher surface area.

Morken [28] used a Ni/Cu/ZnO on CNT and optimized reaction parameters.

Table 2.1: Catalysts used by NTNU

Catalyst	Conversion [%]	Selectivity (carbon-basis, %)				
		EG	PG	1,2-BG	Hexitols	2-Butanol
Ru/C[1]	100	5,0	0	4,5	39,3	0
Ni-ZnO[2]	100	19,1	34,4	10,1	0	0
Ni-ZnO/CNT[3]	100	32,8	15,2	2,9	0	0
Ni-Cu-ZnO/CNT[4]	100	10,8	17,5	5,9	0	7,2

[1] 30min, 6MPa H_2, 518K [26] [2] 2h, 6MPa H_2, 518K [22] [3] 2,5h, 6MPa H_2, 518K [7] [4] 5h, 6MPa H_2, 528K [28]

Metal content of her catalyst was around 45wt%. Morken reached a top conversion of 18% 1,2 propylen glycol, 11% ethylen glycol, up to 5% 1,2 butylenglycol and up to 10% 2-butanol. Depending on the ratio between copper and nickel, the amount of 1,2 butylenglycol increased (maximum with copper only). The yields of the other products was relatively stable. Reaction conditions were 6h, 255°C and 50bar H_2 pressure.

The yields of the different catalysts are summarized in table 2.1.

2.7 Work by other research groups

In general, the main focus was on improving the selectivity of ethylene glycol production. Much research was done, with different catalytic systems. The most sucessful approach to date is the use of tungstenic catalysts, were tungsten is employed either in the form of tungsten carbide, tungsten acid or tungsten oxide. In general, these catalysts reach a high EG yield with only low amounts of PG and hexitols. Their performance could be further improved by the addition of Ni in order to promote hydrogenation. A short summary of catalysts used can be found in table 2.2.

Table 2.2: Tungstenic Catalysts [25]

Catalyst	Conversion [%]	Selectivity (carbon-basis, %)		
		EG	PG	Hexitols
WC$_x$/MC[1]	100	72,9	5,1	2.6
Ni-WC$_x$/MC[1]	100	74,4	4,5	5,2
Ru/AC + H$_2$WO$_4$[2]	100	58,5	3,5	14,0
Raney Ni + H$_2$WO$_4$[3]	100	48,9	5,4	7,6

[1] 518 K, 6 MPa H$_2$, 30 min, 1.0 g cellulose, 0.30 g catalyst, 100 mL water [29] [2] 0,5g Cellulose, 6 MPa H$_2$, 518 K, 30min, 0.1 g 1,2%wt Ru/AC catalyst, 0,0524g H$_2$WO$_4$ [21] [3] 518 K, 6 MPa H$_2$, 0.5 h [30]

To further investigate the effects of transition metals, a catalyst with metallic tungsten (for c-c cleavage) and different transitions metals (for hydrogenation), Ru, Pt, Pd and Ir were prepared by Zheng et al [8]. They in general reached high conversions around 60%, the exact selectivities are shown in table 2.3. Using nickel on mesoporous silica (SBA-15), a EG yield of 75,4% was reached after optimization of the nickel/tungsten ratio. Until now, this is the highest selectivity reported. However, no Ni-W/AC catalyst for direct comparison with the other transition metals was prepared.

 A secondary approach are metals of group 8, 9 or 10 on basic or amphoteric supports (like ZnO which was used extensivly in NTNUs biomass conversion group) aswell as bases. In general, these have a higher selectivity towards PG then tungstenic catalysts [5]. These are discussed in more detail in the next chapters.

Table 2.3: Transition metal catalysts

Catalyst	Conversion [%]	Selectivity (carbon-basis, %)		
		EG	PG	Hexitols
Pd-W/AC	100	59,6	3,8	10,7
Pt-W/AC	97,0	56,9	3,3	3,6
Ru-W/AC	100	61,7	3,2	7,2
Ir-W/AC	100	50,6	2,5	0
Ni5-W25/SBA-15	100	75,4	4,1	4,4

[1] 518 K, 6 MPa H_2, 30 min, 1.0 g cellulose, 0.30 g catalyst, 100 mL water [8]

2.8 Tuning Selectivity: Glucose isomerization

Most research was done on producing high yields of EG. However, PG is another
important bulk chemical, thus it might be an interesting chemical to produce [19].
One possible way is to facilitate or inhibit the glucose-fructose isomerization. If
more fructose is formed, the yield of PG should increase. If no fructose is formed,
instead more (or only) ethylene glycol will be produced. The different pathways of
glucose-fructose isomerization are shown in figure 2.9. Lewis acids lead to a in-
tramolecular hydride shift, while solid bases can catalyse a proton transfer lead-
ing to the formation of fructose [10]. In this work, metal oxides (lanthanium oxide,
magnesium oxide and aluminium oxide) deposited on an support of carbon nano
tubes and nitrogen doped carbonspheres are used as basic (or amphoteric) cata-
lysts. Basic groups are also active for retro-aldol condensations, thus the basic
catalysts can also catalyze the retro-aldol condensation [24].

2.9 Alternative pathways caused by use of basic catalysts

If basic catalysts are used, considerable amounts of 1,2,5-pentanetriol can be
formed [25]. This product was only formed when cellulose was used as feedstock,
if any of the intermediates were used (eg glucose or sorbitol), none was detected.
This is a strong indicator that the pentanetriol is formed during depolymerisation
of the cellulose. As described in chapter 2.2, during alkaline hydrolysis a peeling
reaction occurs. As shown in figure 2.10, during that reaction 1,2,5-pentanetriol
might be formed. TianYin et al[25] used a 2%wt Ruthenium catalyst with differ-
ent basic supports and solid bases as shown in table 2.4. In addition to EG and
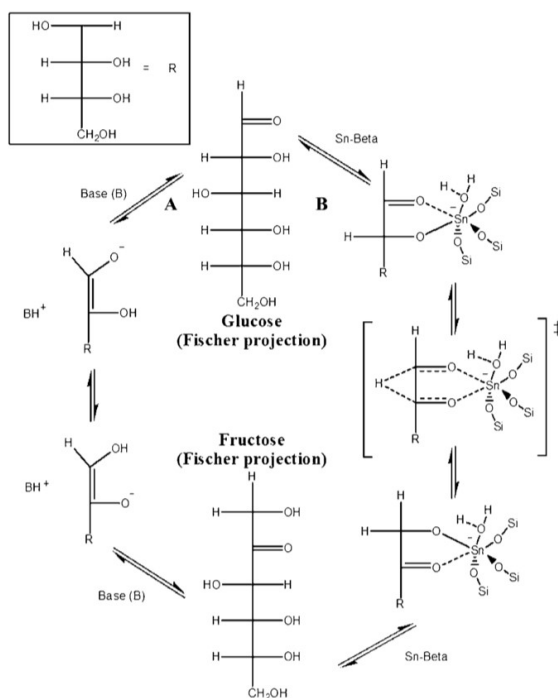
Figure 2.9: Glucose isomerization: A: proton transfer, B: intramolecular hydride shift [10]
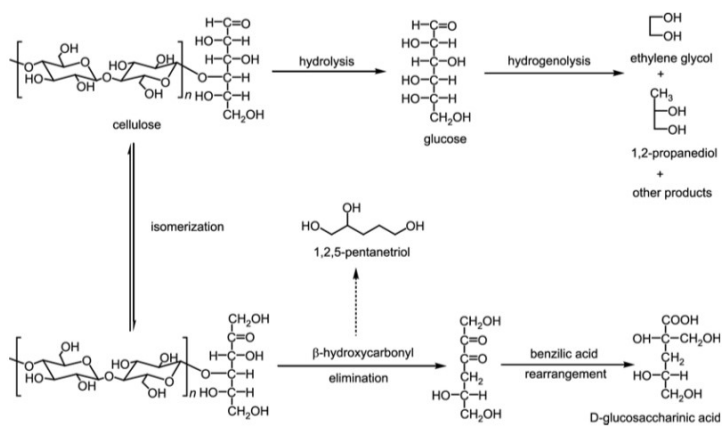

Figure 2.10: Cellulose degradation pathways with bases [25]

PG, they produced considerable amounts of 1,2,5-pentanetriol. They only run for short times, thus, their conversion is relativly low.

Sun et al used a Ni/AC catalyst with a number of metal compounds, including lanthanium oxide and hydroxide [19]. They did not detect 1,2,5 pentanetriol, however

they used longer reaction times and thus reached higher conversion. Also, the effect of lanthanium oxide and hydroxide on C-C cleavage can be observed.

Table 2.4: Yields using basic supports [25]

Catalyst	Conversion [%]	Selectivity (carbon-basis, %)			
		EG	PG	1,2,5-pentanetriol	Sorbitol
Ru/C + La$_2$O$_3$[1]	7,4	15,1	3,9	2,1	
Ru/C + Al(OH)$_3$[1]	6,8	13,8	9,3	13,1	
Ru/HZSM[2]	44,6	15,0	18,3	17,1	
Ru/C[2]	38,1	15,8	16,4	12,8	
Ru/ZrO$_2$[2]	38.0	15,3	13,9	22,1	
Ru/Mg-Al-O[2]	38,0	15,0	18,3	7,5	
Ru/Zeolite 13X[2]	32,6	11,7	15,4	18,2	
Ni/C[3]	87,8	9,5	9,8	-	16,6
Ni/C + La$_2$O$_3$[3]	95,6	36	14,7	-	3,5
Ni/C + La(OH)$_3$[3]	96,6	38,4	14,6	-	5,1

[1] 1g Cellulose, 6 MPa H$_2$, 498 K, 5 min, 0,2g Ru/C + 0,5g base [25] [2] 1g Cellulose, 6 MPa H$_2$, 498 K, 30min min, 0.25 g supported Ru catalysts (2 wt%) + 50 g 0.05 M phosphate buffer (pH 8)[25] [3] 0,15g 10% Ni/AC, 0,02mmol metal cation, 0,25g cellulose, 25ml Water, 5MPa H$_2$, 120min [19]

Xiao et al [6] tried a different catalyst to improve 1,2 PG yield. They used a CuCr catalyst which consist of two phases, a CuCr$_2$O$_4$ spinel and a CuO phase. Best results were obtained from a catalyst using about 1:1 ratio of both phases. With the pure catalyst, 36,3% yield of PG was achieved, but only 7,6% EG yield. Addition of Ca(OH)$_2$ as homogeneous co-catalyst increased yields further to 42,6% PG and 31,6% EG, showing potential of bases. Compared to other research, they used a higher cellulose loading, thereby demonstrating a way to reduce energy needs of a potential industrial process.

Table 2.5: Yields using CuCr$_2$O$_4$ and Base [6]

Catalyst	Conversion [%]	Selectivity (carbon-basis, %)		
		EG	PG	Total
CuCr$_2$O$_4$	100	7,6	36,3	72,5
CuCr$_2$O$_4$ + 0,06g Ca	100	31,6	42,6	76,5

Reaction conditions: 3g Cellulose, 30g water, 0,3g catalyst, 518 K, 6 MPa H$_2$

A third way to enhance PG yield was discovered by Liu et al [23]. To a mixture of Ru/C and WO_3, activated carbon (AC) was added. This greatly improved the selectivity towards PG, from 6,7 to 31,9%. The yield of PG was further increased by dispersing the WO_3 used onto a support of Al_2O_3 as shown in table 2.6. However, the reaction was run at lower temperatures, thus, only partial conversion was reached. Upon increasing temperature, full conversion was reached, but the selectivity decreased to 30,7% PG. An additional effect of the addition of AC was a reduction in hexitol yield. Thus, AC does not only affect the selectivity of EG and PG, but also catalyses C-C cleavage [23].

Table 2.6: Yields using AC

Catalyst	Conversion [%]	Selectivity (carbon-basis, %)		
		EG	PG	Hexitols
WO_3[1]	23,4	51,1	6,7	16,9
WO_3+ AC[1]	22,8	24,4	31,9	8,1
50%WO_3/Al_2O_3[2]	21,5	45,0	10,0	16,8
50%WO_3/Al_2O_3 + AC[2]	21,2	27,7	40,9	3,3
50%WO_3/Al_2O_3 + AC[3]	100	16,6	30,7	1,0

[1] 478K, 6 MPa H_2, 1,0g cellulose, 0,02g 3wt% Ru/C, 1g WO_3, 1g AC, 30min [2] 478K, 6 MPa H_2, 1,0g cellulose, 0,02g 3wt% Ru/C, 0,016g WO_3 on support, 1g AC, 30min [3] 518K, 6 MPa H_2, 1,0g cellulose, 0,02g 3wt% Ru/C, 0,016g WO_3 on support, 1g AC, 30min [23]

2.10   Properties of the basic supports used

As a new approach, three different metal oxides were used. Only MgO exhibits only basic sites, La_2O_3 and Al_2O_3 are amphoteric. They contain basic sites of different strength. To characterise basic site amount and strength, CO_2 desorption (TPD) can be used. In figure 2.11, the results of CO_2 TPD of various metal oxides are given. Al_2O_3, MgO and La_2O_3 were choosen because they cover a wide range of strength. Al_2O_3 contains weak, MgO medium and La_2O_3 strong basic sites [31].

As another support, carbon spheres were used. They are currently under research for a wide range of applications. CO_2 storage, energy storage, drug delivery carriers and catalyst support are possible applications. They exhibit a large surface area, high porosity as well as tuneable pore structures and the possibility to in-
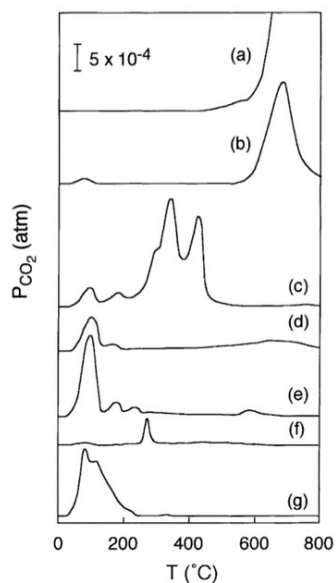
Figure 2.11: CO_2 TPD of (a) CaO, (b) La_2O_3, (c) MgO, (d) CeO_2, (e) ZrO_2, (f) ZnO, (g) Al_2O_3[31]

troduce nitrogen sites [32].

In general, two different kinds of basic nitrogen sites exists: Pyridinic nitrogen sites, where the nitrogen atom is bonded to two carbon atoms, and graphitic nitrogen, where nitrogen is bonded to three carbon atoms and substitutes a carbon atom [33]. Given these basic nitrogen sites, nitrogen doped carbon spheres can be used as a solid catalysts [34]. A CO_2-TPD profile from model catalysts containing only pyridinic or only graphitic nitrogen is given in figure 2.12. Only the pyridinic sites lead to adsorption of CO_2 which is an indication to Lewis basicity [33]. The graphitic sites do not adsorp CO_2, thus do not possess lewis basicity. Li et al have shown that only the pyridinic sites have relevant basic properties, while the graphitic nitrogen does not improve basicity [33].

Additionally, hydroxyapatite (HAP) was briefly tested. Hydroxyapatite, $Ca_5(PO_4)_3(OH)$ is a main constituent of bones and teeths. It consists of Ca_2^+ ions and PO_4^{3-} ions, thus has both weak acid and base sites. Given it insolubility and stability as well as its low toxicity, it received interest for many reactions both as catalyst and support [35].
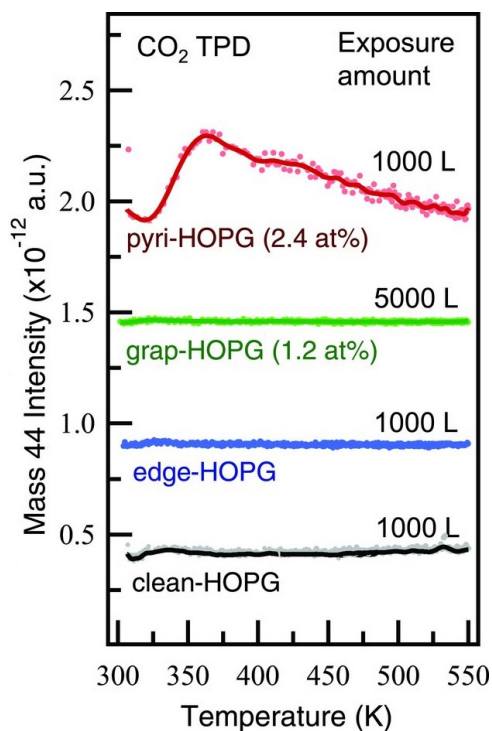
17

Figure 2.12: CO_2-TPD of nitrogen doped model catalysts, pyri-HOPG exhibit only pyridinic sites, grap-HOPG only graphitic sites [33].

2.11   Catalyst Preparation Methods

In general, there are two different ways to produce supported catalysts. Either the support and the active component is co-precipitated, or the support is synthesized first and the active component is loaded by impregnation, ion exchange or precipitation. The main difference is that in the case of co-precipitation the active sites are in the volume of the support, while after impregnation the active sites are located on the pore surfaces. Depending on the reaction mechanism, both methods may be advantageous [36].

There exist different ways of impregnation, the simplest one being incipient wetness impregnation. The active component is dissolved in water and the exact amount of solution to fully soak the pore volume of the support is added to the support [37].

An alternative is the pechini method, where a gel solution is formed as intermediate which is subsequently impregnated using the incipient wetness method. The

18

gel is formed by dissolution of metal salts in hydroxycarboxylic acids such as citric acid and addition of a polyhydroxylic alcohol (eg. ethylene glycol). Upon heating, these form a metal-citrate complex where the metals are chelated [38] [39].

If the support possesses suitable groups, ion exchange is also a possibility. Here, the support is added to a solution of the active component and stirred (normally for an extended period of time, eg. 24 hours) [37].

2.12 Catalyst Characterization Methods

2.12.1 CO_2 temperature programmed desorption

CO2-TPD can be used to identify the amount and the strength of basic sites. Also, characterisation of the nature of sites is possible. Commonly, desorption peaks at 100°C are attributed to OH^- groups, peaks at 150-200°C to M-O pairs, and peaks at 450°C to O^{2-} groups [18].

2.12.2 X-ray diffraction

X-ray diffraction is mostly used to identify crystallographic phases of each substance present in the catalyst. It can detect the structural parameters of crystals, thus crystal composition can be calculated using the Bragg relationship and comparing the obtained lattice spacing with possible compounds. Crystal size can be calculated using the Sherrer equation.

The method requires a certain crystal size, thus XRD cannot detect very small crystals, amorphous materials or highly dispersed active phases [36].

2.12.3 N_2 adsorption analysis

The surface area and the pore size distribution can be determined using N_2 adsorption analysis. N_2 is physisorbed on the surface of the catalyst and from the amount of N_2 adsorbed in order to form a monolayer, the surface characteristics can be calculated using the Brunauer Emmet and Teller method (BET) [36].

2.12.4 Scanning electron microscope

Electron microscopy is a picture generating method, thus it can be used to determine the shape and size of catalyst particles. Also active components might be visible, enabling further analysis. In general, the sample is exposed to an electron beam. Once the electrons hit the surface of the sample, a number of effects occur causing back scattering, creation of secondary electrons, auger electrons, x-rays and transmitted electrons. Scanning electron microscope (SEM) detects secondary electrons and uses the amount of secondary electrons detected to generate a greyscale picture [40].

2.13 High Performance Liquid Chromatography

HPLC or High Performance Liquid Chromatography uses a chromatography column to separate the different substances of a solution. The column consists of a fixed phase, where the different compounds of the solution bind to thereby increasing their retention time. The bonding strength depends on the compound, resulting in a separation of the compounds. After the HPLC, either a RID or a MS can be used to detect the compounds. Using an MS has the additional benefit of being able to identify the molar mass, which helps to confirm the compound. For calibration, external standards were used. Linearity of the response was confirmed by using three standards with different concentrations. However only the RID has a good enough linearity to be used for quantitative analysis, the MS was only used for qualitative analysis [36].

3 Experimental

3.1 Catalyst Preparation

Seven different catalysts as listed in table 3.1 were prepared. Loading is the amount of metal or metaloxide divided by the weight of the support.

Table 3.1: Prepared Catalyst

Name	Metal and Loading	Support
Cu/NCS	40wt% Cu	Nitrogen-doped Carbonspheres
La$_2$O$_3$-Cu/CNT	26wt% La2O3 + 40wt% Cu	Carbon Nanotubes
MgO-Cu/CNT	26wt% MgO + 40wt% Cu	Carbon Nanotubes
Al$_2$O$_3$-Cu/CNT	26wt% Al2O3 + 40wt% Cu	Carbon Nanotubes
Cu-NP/CNT	8wt% CuO / Cu(OH)$_3$	Carbon Nanotubes
CuMn$_2$O$_4$/CNT	38,6wt% MnO$_2$ / 7wt% Cu	Carbon Nanotubes
Ru/CNT	1wt% Ru	Carbon Nanotubes

3.1.1 Carbon Nanotubes

The carbon nanotubes had to be pretreated in order to remove growth catalysts. To do so, 20g were heated to 80 °C in 500ml nitric acid (65%) for one hour three times. After the third repetition, they were washed with distilled water until pH reached 7 in order to remove all acid.

3.1.2 La2O3, MgO and Al2O3-Cu/CNT

These catalysts were prepared in two steps. First, the metal oxide was added to the CNT using the pechini method. The pore volume of the support was determined by adding water to the support until it was completely wetted. The amount of water used per gram support was calculated and the appropriate amount of precursor solution prepared and mixed with the support. As precursor, the nitrate of the metal was used, mixed with ethylene glycol and citric acid in a molar ratio of 7:8:8 to form a pechini solution and mixed using an ultrasound bath for 10 minutes. The precursor was added to the support using the incipient wetness method and the catalysts were dried for 12 hours at room temperature and additional 12

21

hours in an drying oven at 105°C.

As next step, the pechini precursor got burned off. For that, the catalyst was heated to 400°C under nitrogen flow, calcinated with air for 10 min and cooled down in nitrogen. After calcination, Copper was added by impregnation with an copper nitrate solution. The catalyst was then reduced at 400°C in hydrogen flow for 5 hours and passivated for 30min using 1% O_2 in argon at room temperature.

3.1.3 Cu/NCS

The carbon spheres used for this project were made by Daniel Skodvin. They were synthesized from resorcinol and formaldehyde using ultrasonic irradiation to form spheres. The non carbon part was later burned by calcination, resulting in porous spheres. In order to add nitrogen sites, melanine was added to the resorcinol.
The used carbon spheres had a melanine / resorcinol ratio of 1:1 and the calcination temperature was 477°C.

As with the CNT, first, the pore volume was determined. Using the obtained volume, a pechini precursor of Cu-Nitrate, EG and citric acid was prepared (using the same 7:8:8 ratio) and introduced to the spheres. Afterwards, they got directly reduced using the same temperatures and times as described for the CNT.

3.1.4 Cu-NP/CNT

A second approach to produce a supported copper catalyst with a very high dispersion was done similar to an approach of d'Halluin et al [41]. 120ml of a 0,5mmol copper acetate in methanol solution was mixed with 1g CNT in a 300ml Parr autoclave (Model 4564), flushed with H_2 and stirred under low H_2 pressure for 16h. After filtration, the solid residue was washed with methanol, destilled water and acetone and then dried in an excavator at room temperature.

3.1.5 CuMn₂O₄/CNT

Xiea et al [6] had used a $CuCr_2O_4$ spinel catalyst with great success. An attempt to replace the toxic chromate with mangan was done. Mangan was introduced to the CNT using a method developed by Lou et al [42]. CNT were added to 100ml

of 0,1M KMnO$_4$, held at room temperature for 1 hour under stirring and then heated to 70°C and hold at that temperature for three more hours. Afterwards, they were washed with distilled water and dried in a drying oven over night. Loading was determined by weighing the catalyst before and after the treatment. According to Xiao et al, the best results were obtained using a molar ratio of 4:1, thus 7% Copper was introduced using the incipient wetness method. As last step, the catalyst was calcined in nitrogen flow at 500°C for 2 hours.

3.1.6 Ru/CNT

A Ruthenium on CNT catalyst was produced by Haakon Rui using incipient wetness impregnation. The catalyst was reduced at 280°C, using the same methods as previously mentioned.

3.2 Catalyst Characterisation

3.2.1 XRD

A Bruker D8 Advanca DaVinci X-Ray Diffractometer was used to perform the XRD. The instrument uses monochromatized radiation (CuKα, λ = 1.541 Å) and a LynxEye SuperSpeed detector. Analysis was performed in the range of 20-80°.

3.2.2 N$_2$ adsorption analysis

N$_2$ adsorption analysis were performed using a Micromeritics Tri Star 3020 Area and Porosity Analyzer. Sampling was done at 77K (using liquid nitrogen as cooling agent). As pretreatment, the samples were degased under vacuum. As first stage, degasing was performed at room temperature, followed by a second stage at 200°C. Once the pressure in the degas unit dropped to 100m Torr or less, the samples were ready for measurement. Typically, the samples were degased over night.

3.2.3 SEM

The catalysts were analyzed using a Apreo SEM from FEI. The samples were dispersed on carbon tabe. The work was carried out in the NTNU Nanolab by

Greg Rutkowski.

3.2.4 CO$_2$ temperature programmed desorption

CO$_2$ TPD was performed using a Netzsch STA 449 C TGA instrument connected to an Netzsch QMS Aerlos 403 C. The sample was first heated to 300°C to remove impurities, cooled down to 30°C and exposed to CO$_2$. After flushing for 2 hours with argon, it was heated from 30°C to 1000°C under argon flow.

3.3 Catalytic activity test

Two different activity tests were performed.

For the standard test, a 100ml autoclave reactor (Parr 4561) was used with 0.33g microcrystalline cellulose (or alternative feedstocks), 33ml water and 0,1g catalyst. The reactor was purged 7 times with nitrogen and 5 times with hydrogen before applying the starting pressure of 60bar H$_2$. The reactor was then heated to 245°C (taking approximately 30min) at low stirring, run at 245°C for the desired time at high stirring and then cooled down to 40°C at low stirring before releasing the pressure and filtration of the product. The solid residue was weighted and the filtrate analysed using the HPLC-RID and HPLC-MS to identify and quantify products. Given the dilution during filtration, the product solution was diluted by a factor of 3 to 5. This test is very similar to the ones performed by most other research groups.

For the second test, a 300ml autoclave reactor (Parr 4564) was used with three times the amount of all chemicals to maintain the ratio between the different components. Different to the small reactor, the large reactor was equipped with a liquid sampling mechanism, enabling sampling mid reaction. The reactor was run for 3 hours at 245°C, and samples were taken after heatup, 15min, 30min, 60min, 90min and 180min.

After sampling, the samples were filtered using a syringe filter and analyzed using the HPLC. Given the different filtering, the product mixture was not diluted. In table 3.2, the different tests performed are summarized.

Table 3.2: Activity tests

Catalyst	Feedstock	Time	Reactor type
Cu/NCS	Cellulose	90min	small
Cu/NCS	Cellulose	180min	small
Cu/NCS	Cellulose	180min	large
Cu/NCS + 0,1g Ru/CNT	Cellulose	180min	large
Cu/NCS + 0,05g H_2WO_4	Cellulose	180min	large
La_2O_3-Cu/CNT	Cellulose	90min	small
La_2O_3-Cu/CNT	Cellulose	180min	small
La_2O_3-Cu/CNT	Cellulose	180min	large
La_2O_3-Cu/CNT + 0,1g Ru/CNT	Cellulose	180min	large
MgO-Cu/CNT	Cellulose	90min	small
MgO-Cu/CNT	Cellulose	180min	small
MgO-Cu/CNT	Cellulose	180min	large
MgO-Cu/CNT + 0,1g Ru/CNT	Cellulose	180min	large
MgO-Cu/CNT	Fructose	90min	small
MgO-Cu/CNT	Glycerol	90min	small
MgO-Cu/CNT	PG	180min	small
MgO-Cu/CNT + 0,066g$Ca(OH)_2$	Cellulose	180min	small
Al_2O_3-Cu/CNT	Cellulose	90min	small
Al_2O_3-Cu/CNT	Cellulose	180min	small
Al_2O_3-Cu/CNT	Cellulose	180min	large
Cu-NP/CNT + HAP	Cellulose	180min	small

3.4   Product Analysis

The product solution was analysed with an Agilent Technologies 1260 Infinity HPLC with a Hi-Plex Ca (Duo) 300 x 6.5mm column with destilled water as mobile phase, using both a differential refractive index detector (Agilent 1260 Infinity RID) and mass spectroscropy (single quadrupole MS, Agilent 6120 Quadrupole LC/MS). RID was primarily used for quantification, while MS was used to confirm the product. The RID was calibrated using external standards. In order to ensure accuracy, 3 standards with varying concentrations from 0.02g/l to 2g/l were produced and the result checked for linearity. In all cases, the result were linear (R>=0.95). Thus, the use of a single response factor was possible. When MS was used, not the molar mass of the compound was detected. Instead, the molar mass + 23 was detected. This is most likely due to the column which contains Na, which apparently binds to the compounds thereby alters the molar mass detected. For

25

comparison, yield based on carbon was used. Therefore, the concentration was multiplied with the amount of solution produced and multiplied with the carbon content of the compound. Finally, it got divided by the initial carbon mass of the cellulose.

$$Yield[\%] = Area * F_R * V_{Sol} * \frac{C*12}{C*12+O*16+H} * \frac{1}{C_0 * Conversion} \quad (3.1)$$

F_R = Response Factor

C = Carbon Atoms per Molecule

O = Oxygen Atoms per Molecule

H = Hydrogen Atoms per Molecule

V_{Sol} = Volume of Solution

C_0 = Initial Carbon Content (of the cellulose)

Table 3.3: HPLC Calibration

Product	Retention Time [min]	Response Factor	M_m in MS [u]
Glucose	16.23	6,64E-06	203
Fructose	19.35	6,82E-06	203
Erythritol	21.12	7,93E-06	145
Glycerol	22.22	6,99E-06	115
Mannitol	22.38	6,62E-06	205
Sorbitol	26.27	6,92E-06	205
EG	23.48	9,96E-06	85
PG	24.27	8,84E-06	99
1,2-butanediol	29,75	4,17E-06	113
1,2-pentanediol	39,25	7,67E-06	119
1,2-hexanediol	58,16	7,43E-06	141
1,6-hexanediol	38.68	7,55E-06	141
1,2-cyclohexandiol	59.00	7,41E-06	139
5-HMF	43,94	5,64E-06	141
Furfural	57,67	5,59E-06	119
THFDM	31,7	8,50E-06	119
2,5-DHF	34+36	8,40E-06	155
Tetrahydrofurfuryl alcohol	37,7	8,07E-06	125
Void Volume Peak	9-11	6,41E-06	

The void volume peak detected between 9 to 11min contains different compounds. The peak was treated as levulinic acid in order to quantify the carbon content.

Another problematic peak is the glycerol and mannitol peak, since their peaks overlap. Theoretically, an approximation of the ratio is possible by using MS and comparing the peak areas of their ions. This ratio can then be applied to the peak area of the RID.

In general, the analysis was performed as follows: Both an HPLC analysis with RID and an HPLC analysis with MS was done. Using table 3.3, the suspected species was confirmed using the MS. After positive identification of the peak, the RID area was multiplied by the response factor in order to get the concentration of the compound in the solution.

1,2,5 pentanetriol and EG cannot be separated using the Hi-Plex Ca (Duo) column. According to TianYin et al [25], 1,2,5 pentanetriol might be a major product if using basic catalysts. Thus, a method with a different column, Agilent Zorbax SB-Aq, was developed. Different to the Hi-Plex Ca (Duo) column, a mobile phase consisting of 1% ACN + 99% of a buffer solution of 20mM HNa_2PO_4 was used. Using a flow rate of 0,7ml/min and 35°C column temperature, separation of both compounds was possible and the Zorbax column was used to quantify 1,2,5 pentanetriol and EG if both compounds were present.

4 Results and Discussion

In the following chapter, characterisation of the different catalysts used is performed and catalytic activity tests assessed.

4.1 Catalyst Characterisation

To confirm successful catalyst preparation, all catalysts were examined using XRD, SEM and N_2-Adsorption analysis as well as further methods if necessary..

4.1.1 XRD

The XRD was used to confirm phases and obtain particle size. Particle sizes were calculated using the Sherrer equation.

Table 4.1: Particle Sizes

	Cu/NCS	La_2O_3-Cu/CNT	MgO-Cu/CNT	Al_2O_3-Cu/CNT	Cu-NP/CNT
Cu_2O	not detected	not detected	4,5nm	7,5nm	-
Cu	20,1nm	23,8nm	10,6nm	30,6nm	-

XRD spectra of the catalysts are shown in picture 4.1. The metal oxide catalysts and the nitrogen doped carbonspheres exhibit large copper peaks. This is due to the large particle size as shown in table 4.1. The Al_2O_3-Cu/CNT and the MgO-Cu/CNT contain an additional Cu_2O phase, while Cu/NCS and La_2O_3-Cu/CNT contain only Cu phases. The metal oxides were impossible to be detected using XRD. As mentioned in the literature part, XRD cannot detect very small particles or amorphous compounds. Given the metal oxides are crystalline, this is a sign for high dispersion of the metal oxides. On the MgO-Cu/CNT, a considerable amount of Cu_2O was found, while the other catalysts show no or only very small amounts of it. This difference might be caused by the small particle size of copper on MgO-Cu/CNT, which results in a bigger surface to volume ratio and therefore favor oxidation. Also the different metal oxides might have an stabilizing effect on copper. The copper particles are relatively large with particle sizes between 10,6 and 30,6nm.
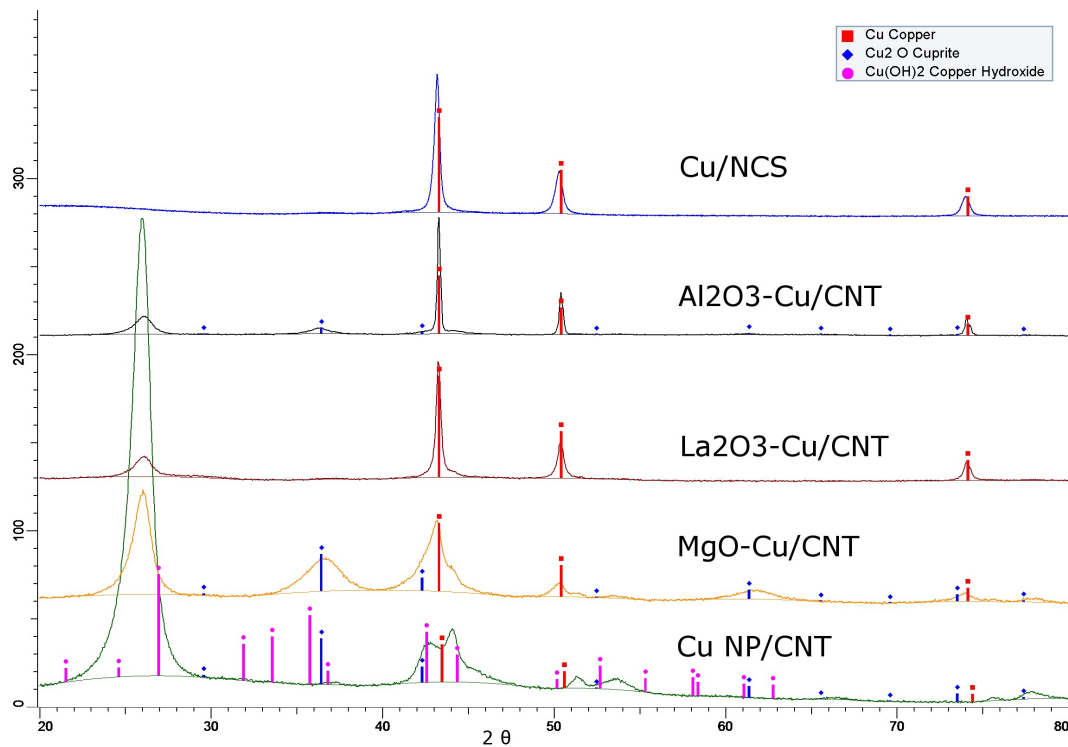This is a known problem as described by d'Halluin et al [41]. He developed a

Figure 4.1: XRD Spectra of finished catalysts

method to obtain smaller particle sizes on graphite support, where he obtained a mixture of copper hydroxide and copper oxide. Cu-NP/CNT were produced using his method and tested by XRD, figure 4.1. As with the metal oxides, the limitations of XRD become apparent with this catalyst. The peaks visible are most likly caused by the CNT, not by copper, as can be seen by the very bad match of the thereotical peaks to the actual peaks. Given the suggested particle size for this catalyst of around 2-5nm, this had to be expected.

Xiao et al[6] used a CuCr spinel for biomass conversion. Given the high toxicity of chromates, an alternative CuMn spinel catalyst was attempted to produce. The XRD analysis (figure 4.2) showed that the attempt was unsuccessful, instead of a CuCr spinel separate copper and manganoxide phases were found. Thus, this catalyst was not further tested.
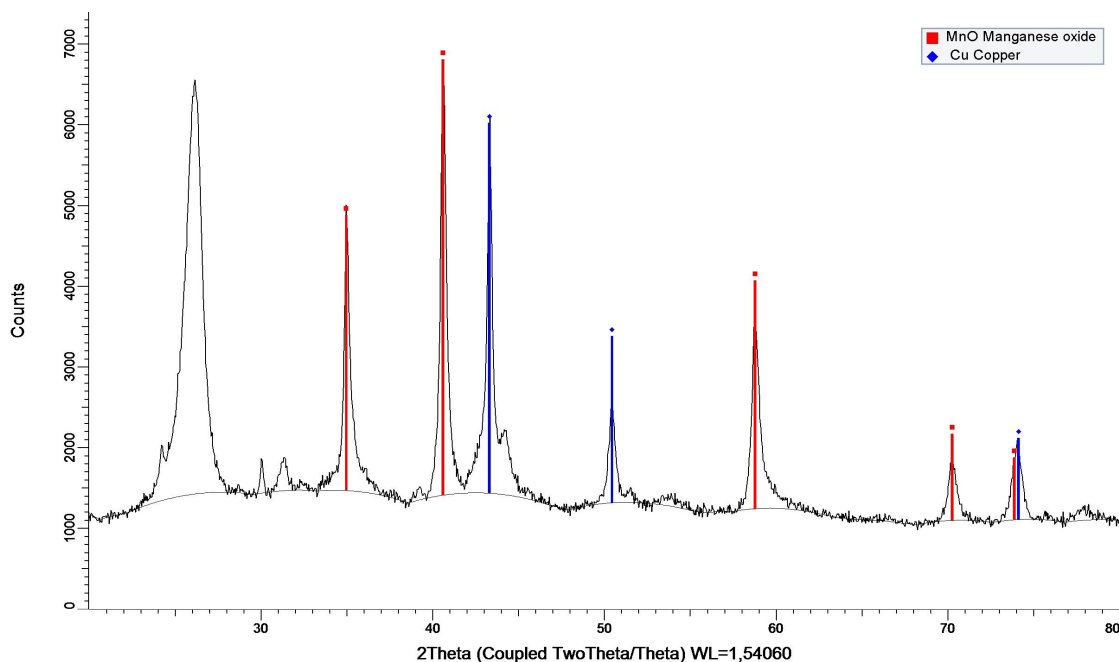
Figure 4.2: XRD Spectrum of Cu-MnO/CNT

4.1.2 SEM Analysis

The samples were examined using SEM to confirm particle sizes obtained from XRD. In figure 4.3, samples of the different supports, CNT and NCS, are displayed. They differ greatly, NCS are spheres with a diameter between 200-400nm, while CNT are long, thin fibers with a diameter of 20-30nm.

Copper is quickly charged which result in very bright particles. In figure 4.4, the different supports are displayed in more detail. The copper particles differ greatly between the individual catalysts. On NCS, they are deposited on the surface, forming spheres with diameters between 12 and 34nm. Some big particles can also be found in the range of 100nm. This fits to the XRD results of 20,1nm. The MgO-Cu/CNT are coated very evenly in small copper particles. Their size is around 10nm, with a very uniform distribution. On the La_2O_3-Cu/CNT, copper particles have a very wide distribution. The smallest are around 10nm, however, they tend to agglomerate. Some parts of the CNT are not covered with copper, while at other parts the particle form agglomerates exceeding 300nm.
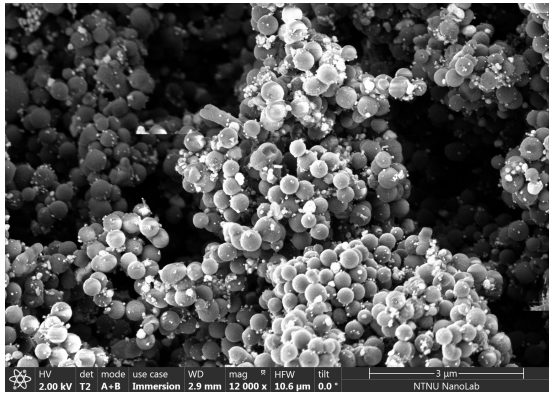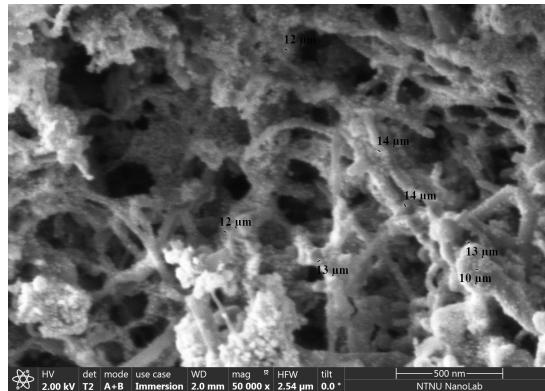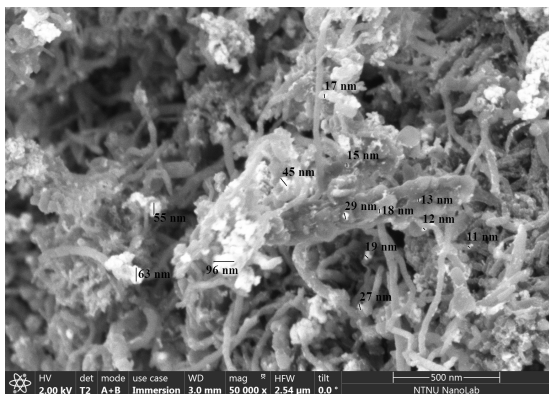
(a) Cu/NCS
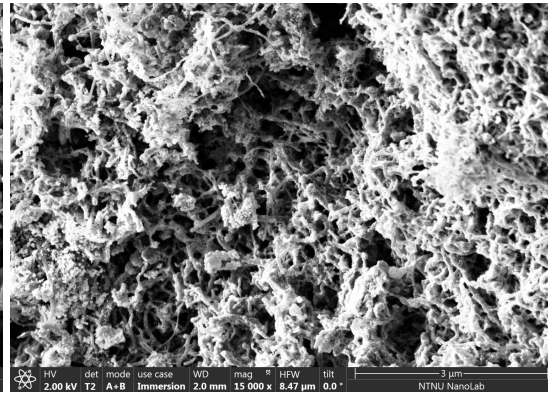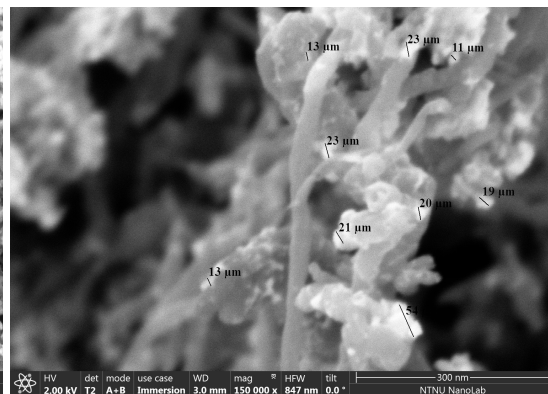

(b) MgO-Cu/CNT

Figure 4.3: SEM pictures of CNT and NCS
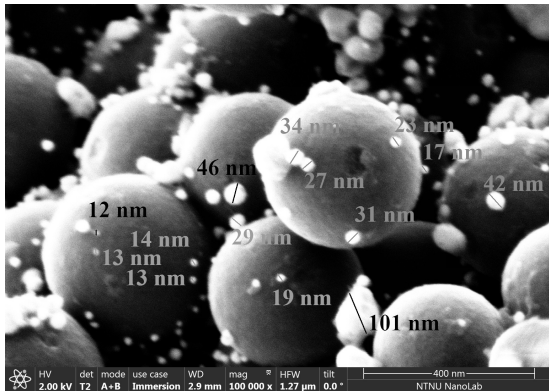
(a) Cu/NCS

(b) MgO-Cu/CNT

(c) La$_2$O$_3$-Cu/CNT

(d) La$_2$O$_3$-Cu/CNT

Figure 4.4: Particle Sizes of CNT and NCS

31

The big differences between the CNT catalysts show that the used oxide has a large influence on copper dispersion. This is a major issue if it is attempted to obtain data about the performance of different supports, as it is the goal of this thesis. With increasing particle size, the surface area diminishes squared. Since the reaction occur on the surface, the different particle sizes can have an drastic impact on the hydrogenation activity of copper which makes the catalysts hard to compare.

4.1.3 N_2-Adsorption Analysis

To confirm stability of the catalyst during impregnation, BET surface areas were obtained using N_2-Adsorption. The results are shown in table 4.2. The surface areas and the pore volumes are consistent within the CNT catalysts, thus the treatmeant did not damage the supports. La_2O_3-Cu/CNT show an lower surface area compared to the other catalysts, which might be caused by agglomeration of copper. NCS have a much higher surface area and lesser pore volume, which corresponds to literature [32].

Table 4.2: N_2-Adsorption Analysis

	Cu/NCS	La_2O_3-Cu/CNT	MgO-Cu/CNT	Al_2O_3-Cu/CNT	Ru/CNT	Cu-NP/CNT
S_{BET}	275,8 m2/g	52,5 m2/g	77,9 m2/g	85,9 m2/g	82,7m2/g	87,3 m2/g
Pore Volume	0,16 cm3/g	0,22 cm3/g	0,25 cm3/g	0,25 cm3/g	0,27 cm3/g	0,26 cm3/g

4.1.4 CO_2 temperature programmed desorption TPD

CO_2 TPD was done for the metal oxide and the carbon sphere catalysts in order to characterise basic sites. The CO_2-TPD profiles are shown in figure 4.5 in comparision to literature data.

As pure oxide, Lanthanoxide only exhibits one desorption peak at around 700°C. Supported on CNTs, La_2O_3 shows a peak at 675°C and an additional peak at 520°C. MgO has a peak at 600°C, while the pure oxide has two peaks at 380°C and 420°C. Al_2O_3, which has a peak at the very low temperature of around 100°C, only exhibits a broad, low peak which reaches its peak at 550°C but spans from 400 to 800°C. Nitrogen-doped carbonspheres have a low peak at 450°C, but keep desorbing CO_2 until 850°C.
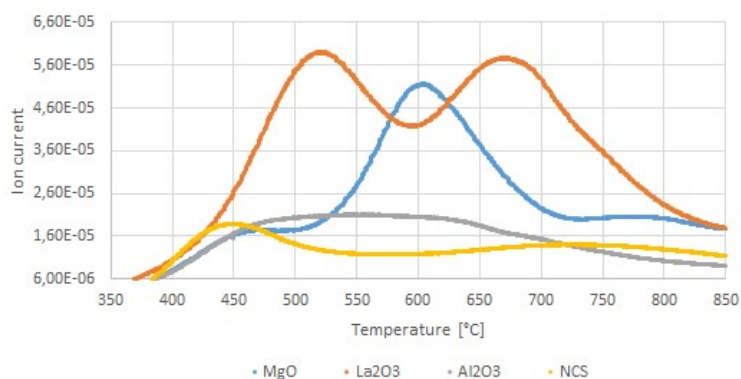
32

Figure 4.5: CO_2 TPD for La_2O_3-Cu/CNT, MgO-Cu/CNT, Al_2O_3-Cu/CNT

The shift in temperatures can be caused by interactions between the support and the metal oxide. Also, TPD was done in a TGA instrument, thus, there was no direct gas flow through the samples, only around the crucibles. This leads to inaccuracies and low resolution. Therefore, it is no surprise the double peak of MgO could not be detected.

Based on these results, La_2O_3 has most and strongest basic sites as shown by the high desorption temperature. MgO has sites with medium strength, while Al_2O_3 and NCS have only a low amount of basic sites with a broad distribution of strength. As mentioned in the Literature Research chapter, only pyridinic nitrogen sites add to the basicity of carbon materials. The detected peak of the NCS corresponds roughly to the TPD profile presented in the literature section, thus the active sites of NCS can be assumed to be pyridinic sites.

4.2 Product Analysis

The products from catalytic activity tests were analyzed using a HPLC with RID and MS. MS was primarily used to identify products, while RID was used for quantification once the peak was identified. Analysis was very complex, since the solution is composed of many different compounds. Some of these compounds have identical retention times, further increasing difficulty of analysis.

The baseline of the RID was unstable for the duration of the work. Thus, quantification of small concentration was problematic. This was mainly an issue when

running the small reactor, as the liquid was diluted 3:1 to 5:1 during the filtration process. The method for the large reactor was different, the samples taken using the sample valve were not diluted, instead, filtered by the use of a syringe filter and then analyzed maintaining the original concentration.

During the course of the thesis, the Ca Duo column showed shifts of retention time and eventually broke, thus had to be replaced which lead to a third shift of retention times.

As discussed,, MgO-Cu/CNT produced a new byproduct, 1,2,5-pentanetril which had the same retention time as EG. To enable quantification, a second column (Agilent Zorbax SB-Aq), was used. For the first experiment in the large reactor with MgO-Cu/CNT, EG and 1,2,5-pentanetriol were quantified using the Zorbax Acid column, while the other compounds were quantified using the Ca Duo column.

The Zorbax column showed rapid degradation, so it was not possible to use it for the run of MgO-Cu/CNT with added Ru/CNT. At this time, the Ca Duo column has been destroyed and replaced by a new Ca Duo column. The new Ca Duo column had shifted separation times, thus, 1,2,5-pentanetriol eluded earlier, during the same time as Glycerol and Mannitol. For quantification of the three different compounds, the amount of glycerol and mannitol was estimated by analysis using the MS. In general, the MS signal is nonlinear as shown in figure 4.6. The measured peak areas were very close to one of the standard, thus, a sufficient accuracy can be expected. The amount of glycerol and mannitol was then subtracted from the 1,2,5-pentanetriol area in order to obtain a concentration for 1,2,5-pentanetriol.
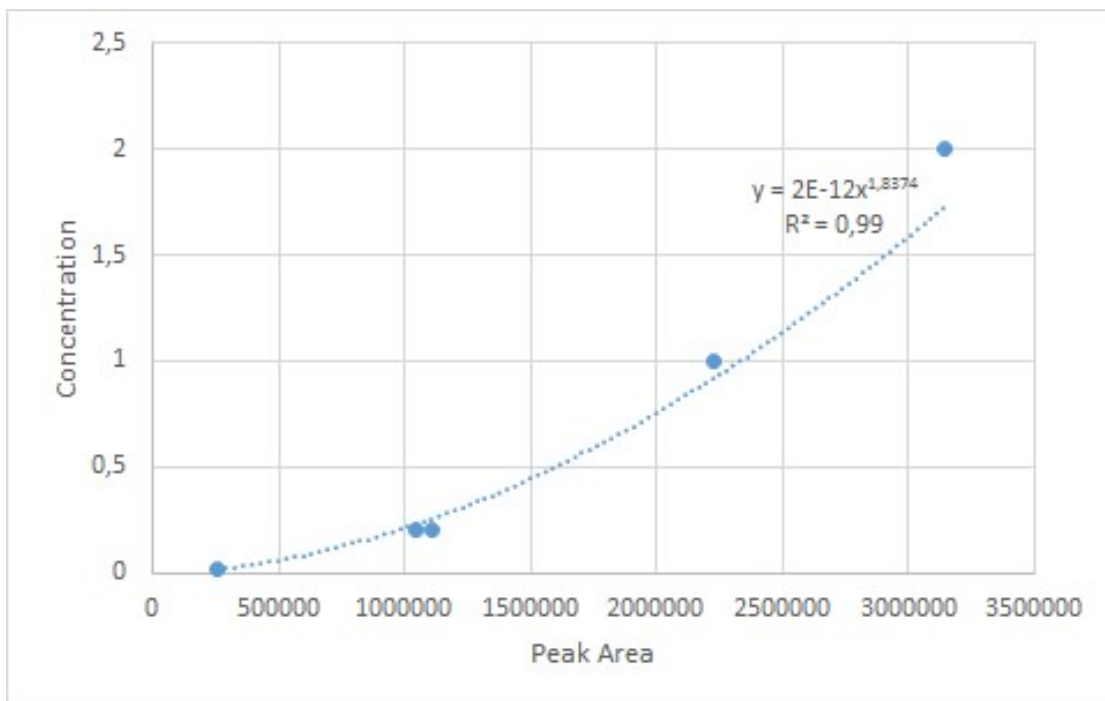
Figure 4.6: Linearity of the HPLC-MS

4.3 Catalytic activity test

4.3.1 Exploring the fructose pathway

The general idea of this project was to improve selectivity towards PG by improving isomerisation towards fructose.

To confirm this approach and also to confirm the reaction pathways, a reaction with fructose as feedstock was done. The result of the analysis can be found in table 4.3.

As expected, the selectivity towards PG is high. Also, Glycerol is formed which

Table 4.3: Selectivity using non-cellulosic feedstocks

Catalyst	Conversion [%]	Selectivity (carbon-basis, %)					
		EG	PG	Gly	BD	Therm. path.	Sor
MgO-Cu/CNT[1]	100	7,0	28,6	4,8	4,1	3,0	0,0
MgO-Cu/CNT[2]	53,1	0	32,76	-	0,0	0,0	0,0
MgO-Cu/CNT[3]	-	0	94,1	0,0	0,0	0,0	0,0

[1]0,33g Fructose, 6 MPa H_2, 518 K, 90 min, 0,1g MgO-Cu/CNT [2]0,33g Glycerol, 6 MPa H_2, 518 K, 90 min, 0,1g MgO-Cu/CNT [3]0,33g PG, 6 MPa H_2, 518 K, 3h, 0,1g MgO-Cu/CNT

is a byproduct of the pathway leading to PG. However, also some EG was formed. Given the isomerization between Glucose and Fructose is an equilibrium reaction, this had to be expected. The thermal pathway contains 5-HMF and all hydrogenation products of 5-HMF, THFDM, 1,2,6-hexanetriol, 1,2-cyclohexanedioland 1,2-hexanediol. Also THFA and 1,2-pentanediol are included. The integration of these C_5-compounds into the thermal pathway is discussed in chapter 4.3.7.

To further examine the pathways, another run was done with Glycerol. The reaction is slow with a conversion of 53,1% after 90min. Additionally, only 32,76% of the converted carbon was converted to PG. Since no further liquids were detected in the RID, the most probable byproducts are gases (CH_4, CO and CO_2). It is also worth noting that with the MgO-Cu/CNT catalyst, no formation of EG occured. Thus, retro-aldol condensation of glyceraldehyde to glycolaldehyde and formaldehyde does not occur with the catalyst. During earlier research by Morken et al [28] with an Ni-Cu-ZnO/CNT catalyst, retro-aldol condensations of glyceraldehyde occured and EG was formed. Based on the findings, for Cu-Catalysts the pathway

has to be altered as shown in picture 4.7.

To clarify the point of gas formation, a stability test with PG was performed. Af-
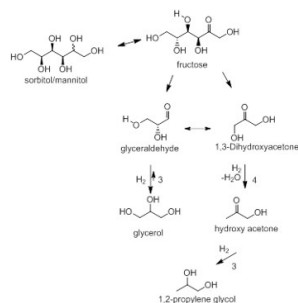

Figure 4.7: Modified fructose pathway for Copper catalysts

ter 3 hours, 94,1% of the PG employed was still present in the reactor. This means that PG is very stable under the reaction conditions, and the loss of carbon has to occur on earlier stages during the conversion from Glycerol to PG.

4.3.2 Catalytic activity tests

Examining the activity of the catalyst with the small reactor was problematic due to problems with the HPLC-RID. The baseline of the RID was unstable, making exact quantification of the products difficult and inaccurate. This is visible in the results from the runs, they are inconsistent. The conversion of all experiments was obtained by weighing the solid residue after the reaction, in all cases, it was found to be 100%.

Individual yields as depicted in table 4.4 are relativly low, with the highest yield being 17,8% PG after 180min with La_2O_3-Cu/CNT. Examining the side products provides some insight into the kinetics of the catalyst and shows possibilities to improve the catalysts.

In general, a good balance between the different reactions is required to obtain high yields. Depending on the imbalances, different side products are formed.

The first possible side reaction is the formation of sorbitol and mannitol. It occurs if the hydrogenation reaction is faster then the retro-aldol condensations. Given the reaction is reversible, production of sorbitol does not necessarily limit yields.

Table 4.4: Selectivity using the small reactor

Catalyst	Total	Yield (carbon-basis, %)								
	[%]	EG	PG	PT[1]	Gly[2]	BD[3]	Ery[4]	TP[5]	Sor[6]	VV[7]
Cu/NCS 90min	64,7	8,8	16,9	0,0	0,3	6,1	0,8	18,5	1,3	11,5
Cu/NCS 180min	52,4	14,5	11,7	0,0	0,4	6,4	0,0	12,3	1,0	5,8
La_2O_3 90min	47,8	9,2	13,6	0,0	0,3	1,2	0,0	4,2	0,8	18,5
La_2O_3 180min	61,7	16,9	17,8	0,0	0,3	4,7	0,6	10,0	0,0	10,3
MgO 90min	61,7	9,6[8]	12,4	-	1,9	1,7	2,5	11,6	2,3	14,5
MgO 180min	71,6	14,7[8]	14,3	-	0,0	2,9	0,7	17,9	3,8	14
Al_2O_3 90min	63,7	7,3	15,6	0,0	0,4	3,8	0,7	22,6	1,0	12,0
Al_2O_3 180min	47,0	5,2	14,6	0,0	0,0	3,1	0,0	13,8	0,0	9,1

[1] 1,2,5-Pentanetriol, [2] Glycerol, [3] 1,2-Butanediol, [4] Erythritol, [5] Thermal Pathway, [6] Sorbitol, [7] Void Volume Peak

0,33g Cellulose, 6 MPa H_2, 518 K, 0,1g CNT Catalyst [8] includes 1,2,5 pentanetriol

As can be seen by both Cu/NCS and La_2O_3-Cu/CNT, the amount of sorbitol decreases over time. Only in the case of MgO-Cu/CNT, it further increases. This is a sign that the hydrogenation ability of the catalyst is too strong and should be reduced in order to improve selectivity.

The thermal pathway occurs when the glucose and fructose are not converted into other products quickly, and instead degrade to 5-HMF. Thus it is a sign for too low activity of the catalyst. Here, large differences between the different catalysts exist. La_2O_3-Cu/CNT produces only small amounts of 5-HMF hydrogenation products, while Cu/NCS and Al_2O_3-Cu/CNT produce higher amounts. Exact quantification was difficult, since most intermediates and the final products are all present in rather low concentrations. Given the problems with the RID baseline during quantification, the possible summation of errors is quite high.

4.3.3 Testing Ca(OH)$_2$ as additive and a Ca based retro-aldol catalyst

Xiao et al [6] reported that $Ca(OH)_2$ addition lead to significant increase of his EG and PG yield. Thus, the same concentration of $Ca(OH)_2$ was added to the MgO-Cu/CNT catalyst and a 180min run performed. The change in EG and PG yield is displayed in table 4.5. As can be seen, the yield of EG and PG decreased instead of increasing. The catalyst used before with $Ca(OH)_2$ was $CuCr_2O_4$. Thus, addition

of Ca(OH)$_2$ lead to an addition of basic sites. With MgO-Cu/CNT the situation is different, as basic sites are already present in the form of MgO. Thus, no synergic effects as with the CuCr$_2$O$_4$ can be observed. The void volume peak after the addition of Ca(OH)$_2$ was unusual, it was bigger than normally and followed by a second, almost as large unidentificable peak.

A further test was done with HAP. For hydrogenation, Cu-NP/CNT was used.

Table 4.5: Addition of Ca(OH)$_2$ to MgO-Cu/CNT

Catalyst	Yield (carbon-basis, %)		
	EG	PG	VV
MgO-Cu/CNT	14,7	14,3	14
MgO-Cu/CNT with Ca(OH)$_2$[1]	12,0	10,5	20
delta	-2,7	-3,8	6
Cu-NP/CNT + HAP[2]	2,4	2,7	21,4

[1] 0,33g Cellulose, 0,1g MgO-Cu/CNT, 0,066g Ca(OH)$_2$, 3h [2] 0,33g Cellulose, 0,1g Cu-NP/CNT, 0,0012g HAP, 3h

The yield of EG and PG was very low, but the exact reason is unknown. It might be caused by insufficient activity of the Cu-NP/CNT catalyst.

To control the activity of the Cu-NP/CNT catalyst, a small amount was added to the La$_2$O$_3$-Cu/CNT catalyst, which lacking hydrogenation ability as discussed in the later chapters.

No significant increase in yield could be observed, so the hydrogenation ability of Cu-NP/CNT might be the main issue of the HAP testing. Since no other copper catalyst was available for testing and La$_2$O$_3$ looked promising, no further research on HAP was done.

4.3.4 Kinetic Studies

To get more insight into the kinetics of the reaction, activity tests with a larger reactor with an liquid sampling valve were done. The results are summarized in time plots for each of the catalysts. Compared to research done before by both NTNU's research group and extern groups, this method gives more detailed insight into the speed, order and reversibility of the reaction. Also since the reaction mixture is extracted without any dilution, it was easier to analyze and produced

consistent results.

The maximum yields of the products are presented in table 4.6.

La$_2$O$_3$-Cu/CNT has the highest total yield of desired products, with EG being

Table 4.6: Yields using the large reactor

Catalyst	Total	Yield (carbon-basis, %)								
	[%]	EG	PG	PT[1]	Gly[2]	BD[3]	Ery[4]	TP[5]	Sor[6]	VV[7]
Cu/NCS	62,2	9,9	12,1	0	2,3	4,6	0,0	25,3	4,9	3,1
La$_2$O$_3$-Cu/CNT	63,8	20,3	18,1	0	0,7	5,0	0,0	9,8	1,1	9,2
MgO-Cu/CNT	75,0	16,6	18,4	6	0,0	4,7	0,0	16,4	0	14,5
Al$_2$O$_3$-Cu/CNT	60,4	8,8	18	0	2,0	5,0	0,0	17,8	2,3	6,5

[1] 1,2,5-Pentanetriol, [2] Glycerol, [3] 1,2-Butanediol, [4] Erythritol, [5] Thermal Pathway, [6] Sorbitol, [7] Void Volume Peak

0,99g Cellulose, 6 MPa H$_2$, 518 K, 0,3g Catalyst

20,3%, PG 18,1%. Yields of MgO-Cu/CNT are good as well, with 16,6% EG and 18,3% PG. Al$_2$O$_3$-Cu/CNT has lower yields with 8,8% EG and 18% PG. Cu/NCS has the lowest yields with 9,9% and 12,1%, and high amounts of compounds from the thermal pathway. The main compound is 1,2 hexanediol, the final product of the pathway, with an yield of 10,2%. MgO-Cu/CNT produced a new product, 1,2,5-
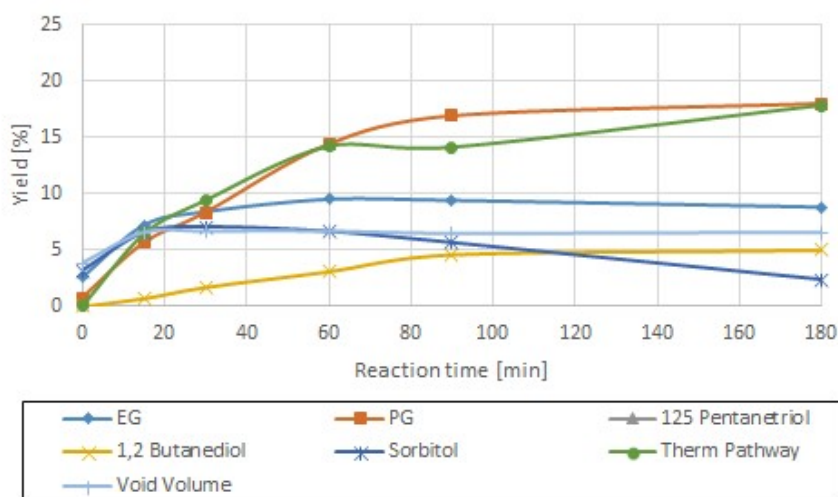
Figure 4.8: 0,99g Cellulose, 6 MPa H$_2$, 518 K, 0,3g MgO-Cu/CNT

pentanetriol, which was not found with the other catalysts. It was mentioned by

TianYin et al [25]. He suspected a formation during depolymerisation of cellulose (see literature review for more details). He detected it with all basic catalysts they used, including La_2O_3. The yield with La_2O_3 was quite low. Sun et al [19] did use La_2O_3 as well, without generating 1,2,5-pentanetriol. None was found with the La_2O_3-Cu/CNT catalyst, so it might be related to the differences in reaction conditions: TianYin used a short time of 5min and 498K instead of 518K.

La_2O_3 and Al_2O_3 are amphoteric while MgO exhibits only basic sites. The acid sites of La_2O_3 and Al_2O_3 might inhibit the formation of 1,2,5-pentanetriol, but that fails to explain the results of TianYing et al with La_2O_3. Another possibility might be the sensitivity of the used analysis method. With the column normally used for analysis, 1,2,5-pentanetriol cannot be detected since it eludes together with EG. Switching to a new column (including optimization and calibration) was necessary in order to detect the 1,2,5-pentanetriol. However, the elution of 1,2,5-pentanetriol occurs before a negative peak caused by water. The mobile phase used was 1%ACN in 20mM HNa_2PO_4. The sample is an aquaeous phase without ACN and buffer, resulting in large negative peaks of water. TianYing had a yield of up to 20% depending on the base, but with La_2O_3 his yield was quite low, 2,1%. Using the MgO-Cu/CNT, 6% 1,2,5-pentanetriol was found. If the La_2O_3-Cu/CNT also only produces a fraction of TianYings values, it might not be enough to detect. Given the low yield of 1,2,5-pentanetriol, it must be classified as unwanted byproduct instead of a possible product.

The activity of the catalysts differs greatly.

La_2O_3-Cu/CNT and Al_2O_3-Cu/CNT reach almost full conversion after 90 minutes, while yield of MgO-Cu/CNT still increases after 90min. Good benchmarks for problems of the catalysts are formation of sorbitol and of products from the thermal pathway. Sorbitol is produced when the hydrogenation function is too strong, while the thermal pathway only occurs when conversion of glucose and fructose into other products is too slow. La_2O_3-Cu/CNT shows a small peak of sorbitol in the beginning of the reaction, peaking after 15min at 5,5%. Over time, it decreases to 1,1%. This reinforces the assumption that the formation of sorbitol is a reversible reaction and produced sorbitol can be converted further to desired
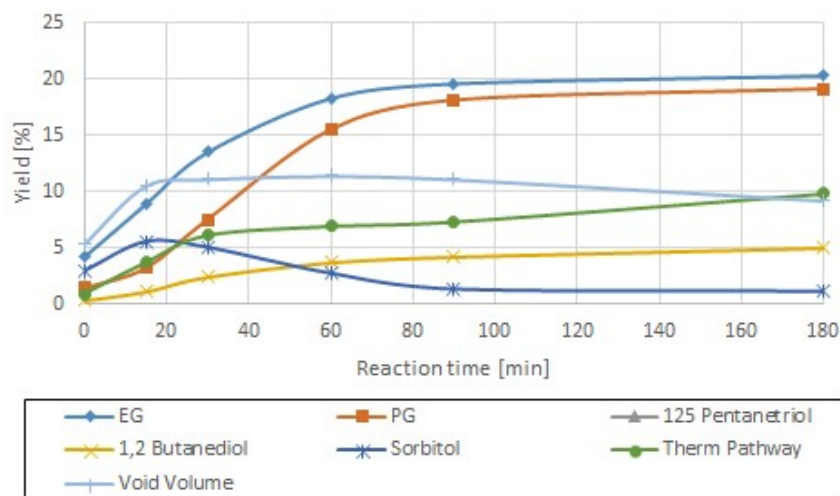
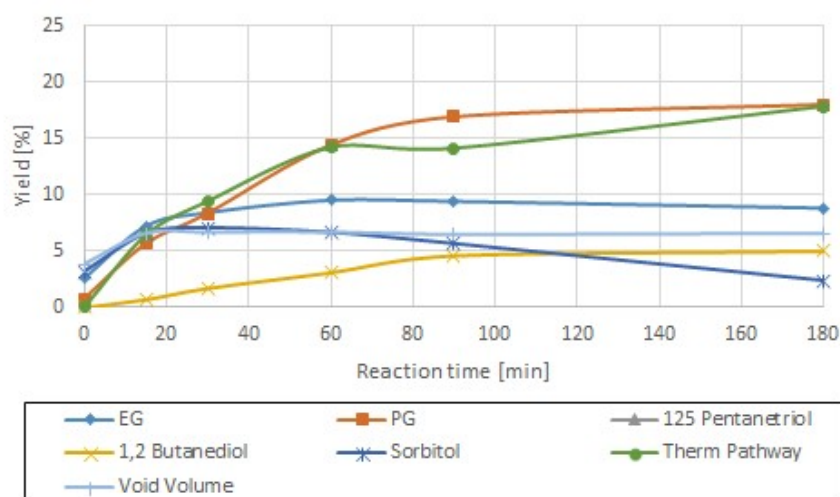**Figure 4.9:** 0,99g Cellulose, 6 MPa H_2, 518 K, 0,3g La_2O_3-Cu/CNT

Figure 4.10: 0,99g Cellulose, 6 MPa H_2, 518 K, 0,3g Al_2O_3-Cu/CNT

products. Al_2O_3-Cu/CNT produces more Sorbitol, peaking after 30min at 7%. Also it takes longer until it diminishes. This means that Al_2O_3 is not as active as the other metal oxide catalysts for C-C cleavage. Further reinforcing this conclusion is the high amount of 5-HMF degradation products.

Cu/NCS have similar problems. High sorbitol amounts and high amounts of 5-
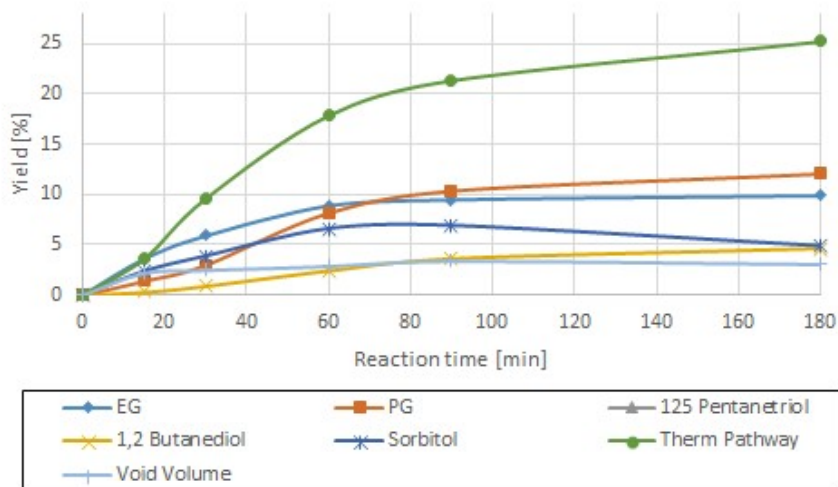
Figure 4.11: 0,99g Cellulose, 6 MPa H_2, 518 K, 0,3g Cu/NCS

HMF degradation products show that the catalyst is not very active for c-c cleavage, and a high amount of C_6 molecules are formed. Given the high yields of 5-HMF degradation products, it is worth taking a closer look into the distribution and time dependency of these.

As shown in figure 4.12, the main degradation products are 2,5-DHF and 1,2-
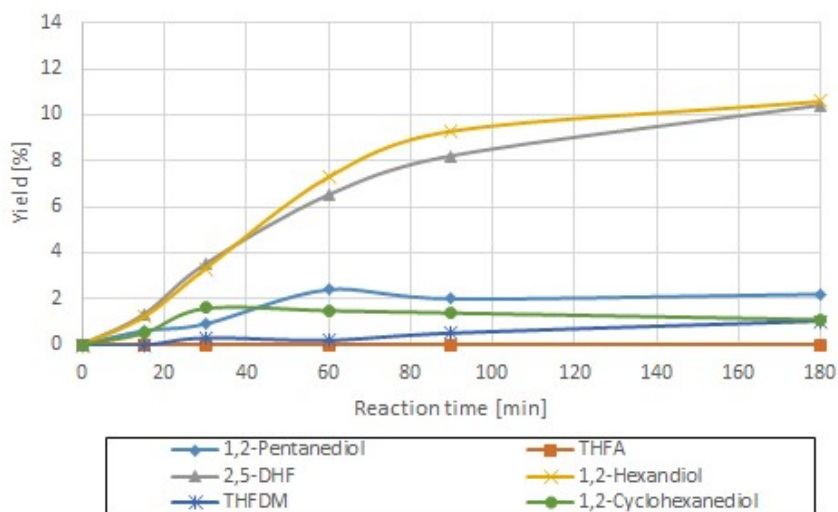
Figure 4.12: 5-HMF Degradation products formed by Cu/NCS

43

Hexanediol. Since it is impossible to find more than traces of the intermediates before 2,5-DHF, their hydrogenation is relativly fast. Ring-opening towards hexanes is much slower, leading to accumulation of 2,5-DHF. Ring opening forms 1,2,6 hexanetriol, which is further hydrogenated to form diols. This is another fast reaction, since only traces can be found. Selectivity of the hydrogenation is greatly in favor of 1,2-hexanediol, which accounts for 10,6% total yield. 1,6-hexanediol can be detected in traces by MS. Only small amounts of THFDM can be observed. This can mean two things: First, it is not part of the pathway and instead a side product as suggested by Yao et al [18] Second, the hydrogenation of the double bonds of 2,5-DHF is slower then the ring opening by cleavage of saturated C-C bonds. From a chemical point of view, this is unlikely, thus a modification of the pathway as suggested in figure 4.13 is necessary.

Yao et al [18] propose that the basic sites of CoO are responsible for cleavage of
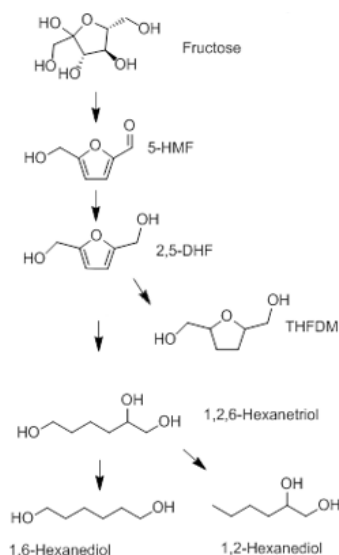
Figure 4.13: Modified degradation pathway

the C-O bond. With NCS, no metal oxides are present which could take over this function, instead, it is catalysed by the basic nitrogen sites.

MgO-Cu/CNT, La_2O_3-Cu/CNT and to an lesser extent Al_2O_3-Cu/CNT produce a large void volume peak in the early stages of the reaction. The suspected compounds for this peak are acids like levulinic acid and formic acid produced by decomposition of 5-HMF or polymerisated 5-HMF as shown by Morken [28]. This

is reinforced by the production at early stages of the reaction. Exact identification is impossible, as all these compounds have identical retention times. HPLC-MS was also not helpful, since a vast amount of different molar masses were detected. There is a direct connection between hydrogenation activity and formation of the void volume peak, the more sorbitol is formed, the smaller the void volume peak is. Given the reaction to sorbitol is reversible, aiming towards formation of a small amount of sorbitol might be beneficial towards total yield in order to limit the formation of polymerisated 5-HMF and 5-HMF degradation products.

4.3.5 Manipulating the Hydrogenation to Retro-Aldol condensation activity ratio

To further research the influence of the ratio of hydrogenation to C-C cleavage activity towards the obtained yields, additional hydrogenation catalyst was added. A Ru/CNT catalyst was chosen since it is known to solely catalyse hydrogenation, without adding to C-C cleavage [5]. Al_2O_3-Cu/CNT already produced a high amount of sorbitol, thus it was not further examined.

Adding Ru/CNT to La_2O_3-Cu/CNT greatly increased EG yield as shown in table 4.9. A time plot can be found in figure 4.14.

Table 4.7: Addition of Ru/CNT to La_2O_3-Cu/CNT

Catalyst	Total	Yield (carbon-basis, %)							
	[%]	EG	PG	PT[1]	Gly[2]	BD[3]	Ery[4]	TP[5]	Sor[6]	VV[7]
no Ru/CNT	65,2	20,3	19,1	0	0,7	5	0	9,8	1,1	9,2
with Ru/CNT	71,2	28,2	19,2	0	4,8	2,6	2,9	10,7	0,8	2
delta	6	7,9	0,1	0	4,1	-2,4	2,9	0,9	-0,3	-7,2

[1] 1,2,5-Pentanetriol, [2] Glycerol, [3] 1,2-Butanediol, [4] Erythritol, [5] Thermal Pathway, [6] Sorbitol, [6] Void Volume Peak
0,99g Cellulose, 6 MPa H_2, 518 K, 0,3g La_2O_3-Cu/CNT, 0,1g Ru/CNT

The additional hydrogenation ability of the ruthenium catalyst lead to hydrogenation of the sugars before they could degrade to 5-HMF and polymerisation products thereof, as shown in the decrease of the void volume peak. Given the carbon content of the void volume is only an arbitrary figure in order to enable
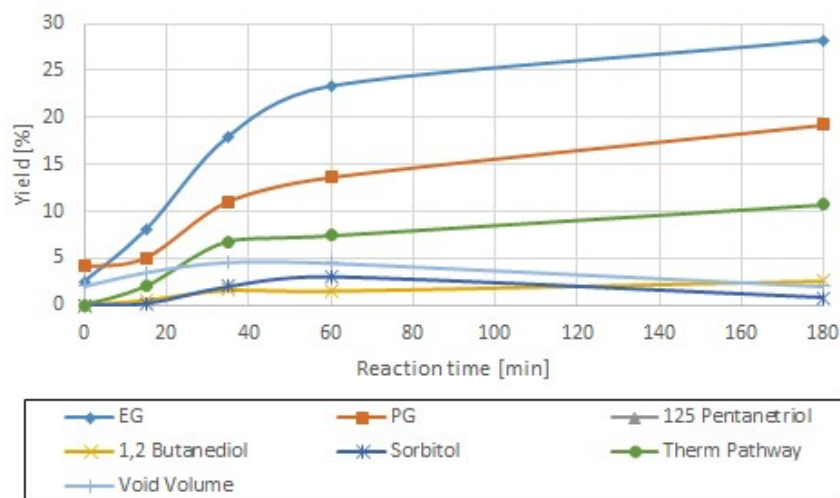
Figure 4.14: La_2O_3-Cu/CNT with added Ru/CNT

comparison, the "7,2%" decrease in void volume could amount to the 10% increase in EG yield.

Unexpectedly, the addition of hydrogenation catalyst did not lead to an increase in sorbitol amount. The maximum yield reduced from 5,5% at 15min to 3,1% after 60min. This might be a sign that further addition of hydrogenation catalyst might be possible. However, different than before, considerable amounts of glycerol and erythritol were formed. Erythritol is a side product during the formation of 1,2-butanediol, and the additional erythritol matches almost exactly the reduction in 1,2-butanediol yield. Given erythritol is, similar to sorbitol for ethylene glycol, a sideproduct of the 1,2-butanediol pathway caused by too strong hydrogenation, this shows that the 1,2-butanediol pathway is more sensitive to higher hydrogenation activities.

In total, the yield of desired products - ethylene glycol and propylene glycol - were high with a combined yield of 47,4%. It is noteworthy that only the yield of EG was improved, the yield of PG remained stable. This might be the effect of Ruthenium as hydrogenation catalyst, literature regarding Ruthenium showed in general high yields of EG but only low PG yields.

Addition of additional hydrogenation catalyst to the other catalysts was less successful, but further helped to understand the reaction mechanism.

To Cu/NCS, both Ru/CNT for improved hydrogenation and H_2WO_4 for improved
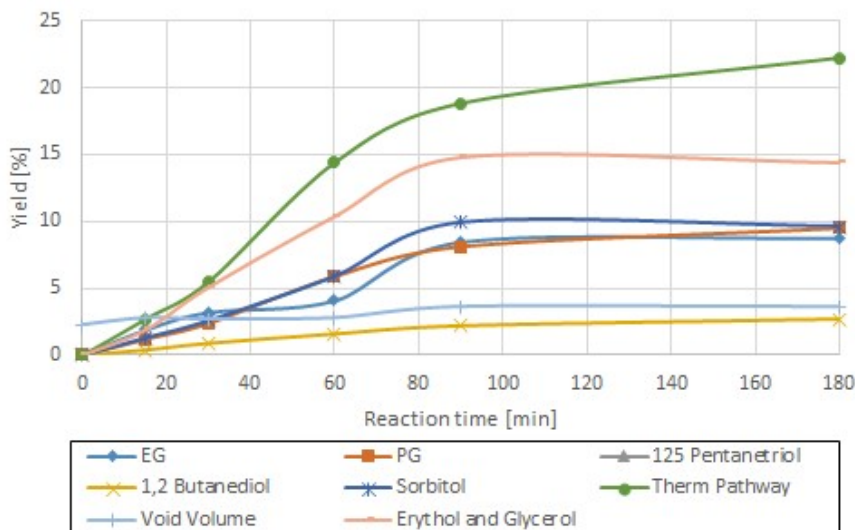
Figure 4.15: Cu/NCS with added Ru/CNT

C-C cleavage was added. The addition of Ruthenium catalyst lead to a slight decrease of EG and PG yields as shown in table 4.8 and figure 4.15 .

Instead, great amounts of sorbitol are formed. Also, a considerable amount of

Table 4.8: Addition of Ru/CNT and H_2WO_4 to Cu/NCS

Catalyst	Total	Yield (carbon-basis, %)								
	[%]	EG	PG	PT[1]	Gly[2]	BD[3]	Ery[4]	TP[5]	Sor[6]	VV[7]
no Ru/CNT	62,2	9,9	12,1	0	2,3	4,6	0	25,3	4,9	3,1
with Ru/CNT	70,8	8,8	9,5	0	6,7	2,7	7,7	22,2	9,6	3,6
delta	8,6	-1,1	-2,6	0	4,4	-1,9	7,7	-3,1	4,7	0,5
with H_2WO_4	34,7	6,7	2,4	0	0	1,4	0	7,7	0	16,5
delta	-27,5	-3,2	-9,7	0	-2,3	-3,2	0	-17,6	-4,9	13,4

[1] 1,2,5-Pentanetriol, [2] Glycerol, [3] 1,2-Butanediol, [4] Erythritol, [5] Thermal Pathway, [6] Sorbitol, [6] Void Volume Peak

0,99g Cellulose, 6 MPa H_2, 518 K, 0,3g Cu/NCS, 0,1g Ru/CNT or 0,05g H_2WO_4

erythritol and glycerol are formed, up to 14,8% combined. Without ruthenium, these were only produced in negligible amounts.

Interestingly, the void volume peak did not change much. Given the results from La$_2$O$_3$-Cu/CNT, a decrease would have been expected. The void volume peak of Cu-CNT is already small before addition of hydrogenation catalyst, and since the exact composition of the peak is unknown, the detected compounds might in fact be not produced by 5-HMF degradation.

The amount of compounds of the thermal pathway is still increasing after 3 hours, showing a slower reaction rate then before. The composition of the thermal pathway did change as well as shown in figure 4.16. While the main components are 1,2-hexanediol and 2,5-DHF as before, their concentration decreased to 6,7% and 6,9%. The amount of THFDM increased drastically, from 1% to 4,7%. That reinforces the assumption that THFDM is a side product and the pathway has to be changed as proposed in the earlier chapter. The increase in THFDM yield is caused by the additional hydrogenation ability of Ru/CNT, while the activity for C-O cleavage (catalyzed by the basic sites of NCS) remains constant, resulting in a loss of 1,2-hexanediol and 2,5-DHF yield.
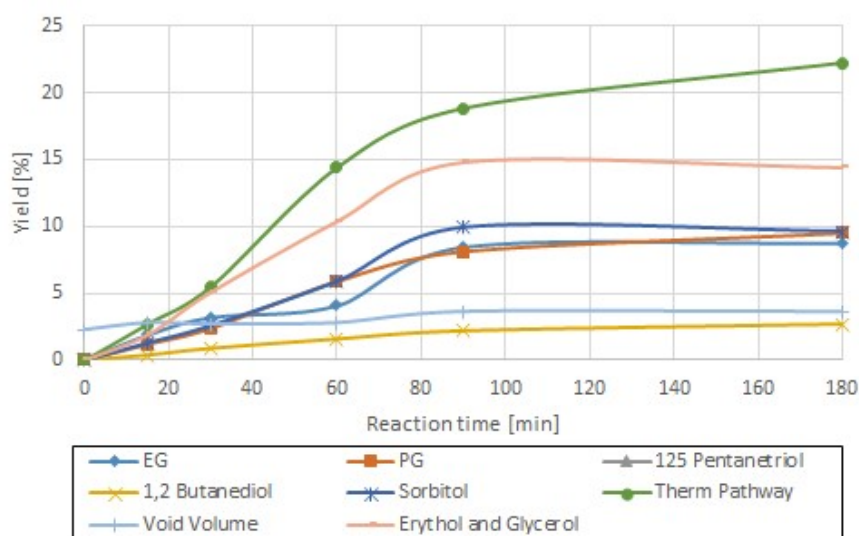
Figure 4.16: Degration products Cu/NCS with Ru/CNT

Since the addition of hydrogenation catalyst did not lead to an increase in yield, C-C cleavage activity was increased by the addition of H$_2$WO$_4$. As shown in figure 4.17, this did not improve yield either. Instead, the void volume peak was

increased considerably while yields of the products decreased drastically. The impact on the thermal pathway is quite interesting, while THFDM and 2,5-DHF are formed, no 1,2-Hexanediol can be found. Also, both THFDM and 2,5-DHF are formed very early in large quantities, and are degraded into undetectable compounds. Most likely, the additional C-C cleavage ability leads to complete degradation and formation of gases. The increase of the void volume peak can be attributed to 5-HMF formation and subsequent polymerization or degradation to acids. The samples were yellow and had a distinct smell after 5-HMF.

MgO-Cu/CNT also did not benefit from the addition of Ru/CNT as shown in figure
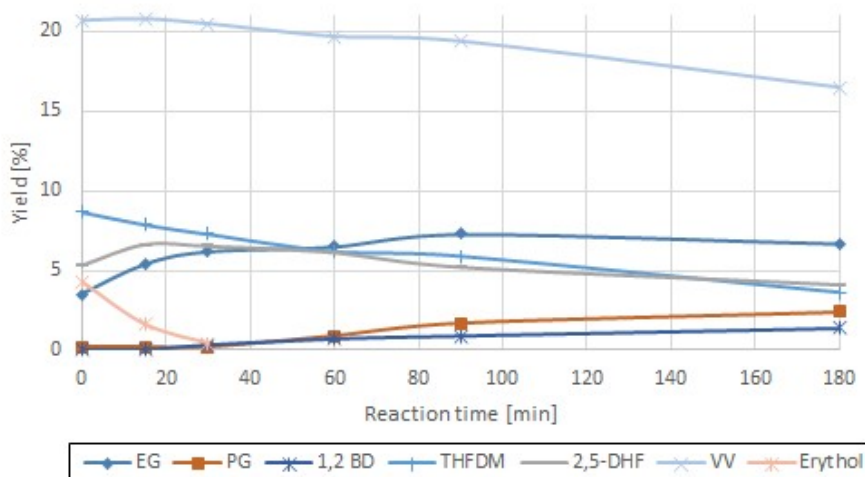
Figure 4.17: Cu/NCS with H_2WO_4

4.18 and table 4.9.

EG and PG yields decreased from 16,6% and 18,37% to 14,5% and 15,5%. However, the void volume peak decreased considerably, from 16,5% to 9%. Compared to the other catalysts, this is still high, but better than before. Yield of 1,2,5-Pentanetriol increased from 6% to 8%, but compared to the pure catalyst the analysis method is worse, as it involves an estimation of concentrations using the MS as described in the product analysis section.

As with NCS, a considerable amount of erythritol was formed, but only low amounts of sorbitol and glycerol. Thus, erythritol might be the most sensitive compound to
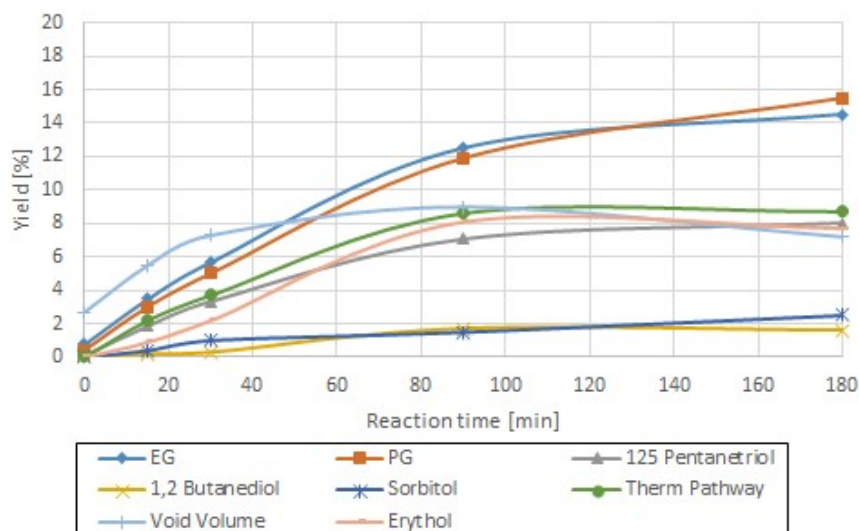
Figure 4.18: MgO-Cu/CNT with added Ru/CNT

Table 4.9: Addition of Ru/CNT to MgO-Cu/CNT

Catalyst	Total	Yield (carbon-basis, %)								
	[%]	EG	PG	PT[1]	Gly[2]	BD[3]	Ery[4]	TP[5]	Sor[6]	VV[7]
no Ru/CNT	76,6	16,6	18,4	6,0	0,0	4,7	0	16,4	0	14,5
with Ru/CNT	65,3	14,5	15,5	8,0	1,3	1,6	2,5	8,7	2,5	7,7
delta	-11,32	-2,1	-2,9	2,0	1,3	-3,1	2,5	-7,7	2,5	-7,3

[1] 1,2,5-Pentanetriol, [2] Glycerol, [3] 1,2-Butanediol, [4] Erythritol, [5] Thermal Pathway, [6] Sorbitol, [6] Void Volume Peak

0,99g Cellulose, 6 MPa H_2, 518 K, 0,3g La_2O_3-Cu/CNT, 0,1g Ru/CNT

detect too strong hydrogenation. Erythritol formation also seems to strongly depend on the used catalyst, using copper, erythritol was not formed in considerable quantities. This becomes especially apparent when looking back to the Al_2O_3-Cu/CNT catalyst, which formed extensive amounts of sorbitol and glycerol, but no erythritol.

4.3.6 Comparison of Reaction Rates for EG and PG formation

Based on the data obtained from the kinetic studies, reaction rates can be obtained. Reaction rates are given as $r = \frac{mg\,Product\,formed}{g\,Catalyst \cdot \Delta\,Time}$ and presented in table

4.10.

Table 4.10: Reaction Rates of EG and PG formation

Time	La_2O_3-Cu/CNT		MgO-Cu/CNT		Al_2O_3-Cu/CNT		NCS-Cu/CNT	
	EG	PG	EG	PG	EG	PG	EG	PG
0-15	11,40	3,57	6,30	6,94	11,15	9,71	8,73	2,77
15-30	11,15	8,52	3,39	2,58	2,91	5,35	5,58	3,17
30-60	5,82	7,93	3,52	3,57	1,33	6,04	3,64	5,15
60-90	1,58	2,58	2,67	1,98	-0,12	2,48	0,73	2,18
90-180	0,28	0,33	1,78	1,64	-0,24	0,36	0,16	0,56

Reaction rates are given in $\frac{mg}{g\,Cat \cdot min}$

As expected, La_2O_3-Cu/CNT show the highest reaction rates. Interestingly, Al_2O_3-Cu/CNT reach almost as high initial reaction rates, which rapidly level off. Cu/NCS is third, with MgO-Cu/CNT showing lowest reaction rates, but also the lowest decline in reaction rate. This was already possible to observe before, as the yields of EG and PG still increase after 3 hours.

More interesting is the time difference between formation of EG and PG as shown in figure 4.19. EG is formed very early in during the reaction, with a rapid de-
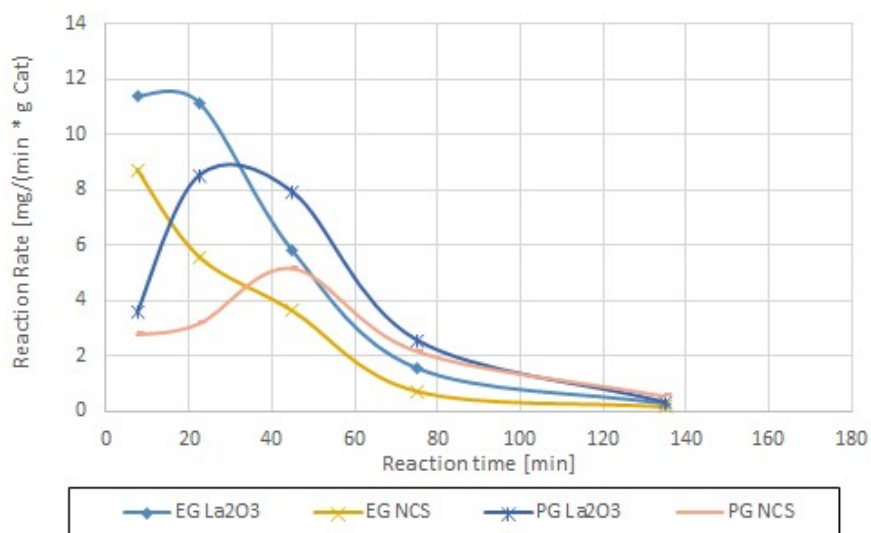
Figure 4.19: Comparison of Reaction Rates for EG and PG formation. Used catalysts: La_2O_3-Cu/CNT and Cu/NCS

crease in reaction rate. In contrast, the formation rate of PG increases in the

51

beginning, and only starts to decrease drastically after the first hour.

A possible explanation of this could be the different pathways of their formation. While EG is produced directly from glucose, glucose first has to isomerize to fructose before PG can be produced. This also has very interesting implications for how to increase PG yield. A slow reaction might be necessary to enable production of high amounts of PG. However, stability of the sugar intermediates is a challenge, as they tend to degrade towards 5-HMF.

4.3.7 C_5 Species - Suggestion for an Pathway

In addition to the compounds for which a pathway was already created, C5 species were detected during product analysis. Tetrahydrofurfuryl alcohol and 1,2-pentanediol were detected in nearly all of the samples, with individual concentrations up to 3,9%. Thus, finding a pathway for these compounds was considered important.

Using the MS, trace amounts of components can be found. The most interesting question is which molecule is the first C_5. The most probable pathway for generation of C_5s is the degradation of 5-HMF. There are two possible ways, removal of the alcohol group, or removal of the carbonyl group. Removal of the alcohol group results in furfural, while removal of the carbonyl group results in furfuryl alcohol. Both compounds can be found in very low concentrations using the MS, so both ways are possible. If furfural is formed, it is hydrogenated to form furfuryl alcohol. Furfuryl alcohol is very similar to 2,5-DHF, with a missing alcohol group.

Thus, its further reactions are in line with 2,5-DHF - it either becomes fully hydrogenated to form tetrahydrofurfuryl alcohol or the ring is opened and 1,2-pentanediol is formed. No 1,5-pentanetriol was found, which can be explained easily by steric hindrance due to the alcohol group, greatly favoring C-O cleavage between the 5th C-atom and the oxygen of the furan ring. Thus, the thermal pathway has to be altered a second time as shown in figure 4.20.
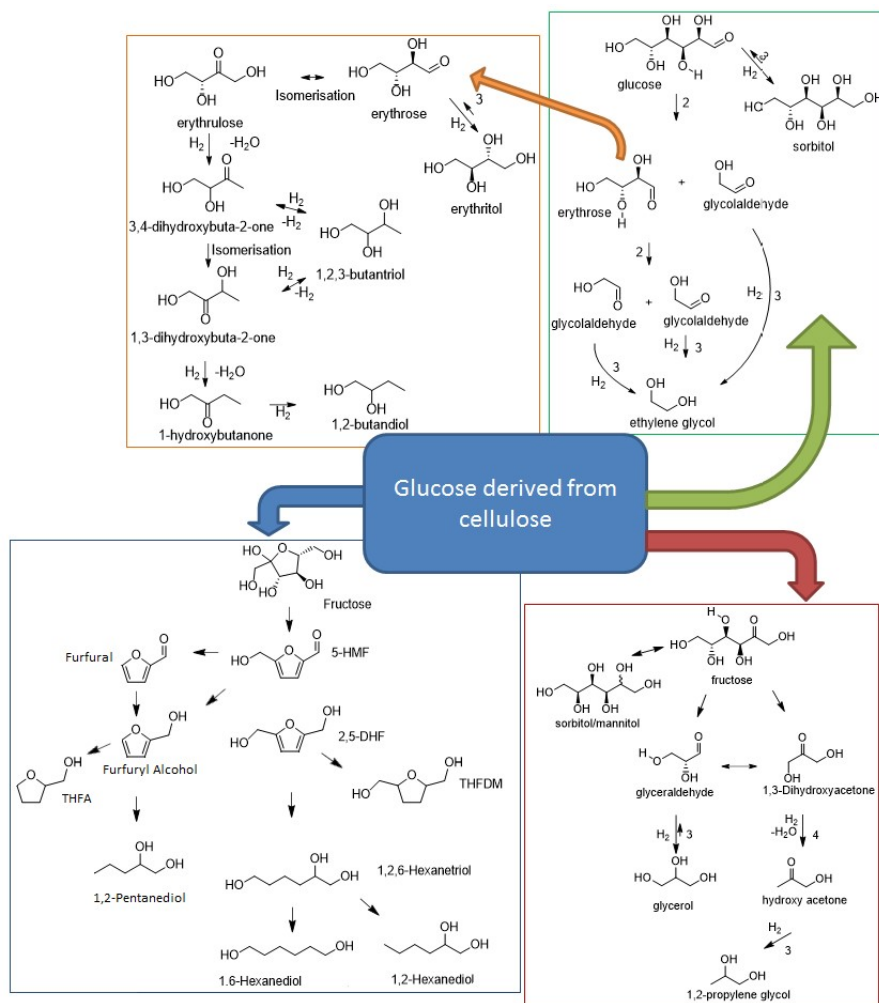
Figure 4.20: Modified pathway for copper catalysts

5 Conclusions

Testing of new, basic metal oxides and supports for one-pot conversion of cellulose as well as further investigation into the reaction mechanisms was performed. The ability to take many samples during one experiment greatly helped with understanding of the reaction mechanisms involved during the one-pot conversion of cellulose.

With the data obtained, it was possible to propose a reaction network for all products and intermediates found as shown in chapter 4.3.7.

Also, certain products can be related to imbalances in the ratio between hydrogenation activity and retro-aldol condensation activity. The void volume peak is caused by insufficient hydrogenation of the products, resulting in polymerisation of 5-HMF and / or degradation to acids.

Sorbitol is a sign for insufficient retro-aldol condensation. If sorbitol is only produced in the early stages of reaction but subsequently reacts to form EG or PG, formation of small amounts are no issue. However, if large quantities of sorbitol are formed, yield of EG and PG decrease and the ratio between the catalysts has to be optimized.

Testing of the basic supports was carried out using a fixed, nonoptimized ratio between the hydrogenation catalyst (copper) and the basic oxide or support. This resulted in only mediocre yields, the best result were 20,3% EG and 19,1% PG with La_2O_3-Cu/CNT. Given the sensitivity of the yields regarding the optimal ratio between the catalysts, additional hydrogenation ability was introduced by the use of a Ru/CNT catalyst. In case of La_2O_3-Cu/CNT, this further increased the yield to 28,2% EG and 19,2% PG. For the other catalysts, instead, more hydrogenated byproducts were formed, indicating a smaller activity for retro-aldol condensation of these catalysts.

In general, La_2O_3-Cu/CNT showed the best results, with high selectivity towards desired diols and very high retro-aldol condensation activity, requiring additional hydrogenation catalyst for improving yield. NCS-Cu produced high amounts of C_6 molecules, indicating lower C-C cleavage activity. Addition of C-C cleavage catalyst did not lead to improvement nor did addition of hydrogenation catalyst, however the amounts of each additive might have been too high.

MgO-Cu/CNT produced a new byproduct, 1,2,5-pentanetriol. Thus, the yield of EG and PG is reduced, to 16,6% EG, 18,4% PG and 6% 1,2,5-pentanetriol. Even though the copper on the catalyst was dispersed better and thus should be more active, the reaction was slower compared to the other catalysts. Based on these two observations, MgO-Cu/CNT is not a promising catalyst. Al_2O_3-Cu/CNT showed poor performance, with 8,8% EG and 18% PG and 6,5% sorbitol produced. Possibly, the hydrogenation activity is too strong in comparison with the retro-aldol condensation activity.

Comparison of the different supports and metaloxides is difficult. The metal oxides themselves appear to have very good dispersion on the catalysts. No metal oxide phases could be found by XRD, indicating a very small particle size.

Dispersion of copper is an issue, the smallest copper particle sizes are obtained on MgO-Cu/CNT with around 10nm. La_2O_3-Cu/CNT and NCS-Cu have particle sizes of 20 and 23nm, while Al_2O_3-Cu/CNT have the biggest particle size of around 30,6nm. Given this, the hydrogenation ability of the catalysts are different, with MgO having highest activity, followed by La_2O_3-Cu/CNT and NCS-Cu, and with lowest activity Al_2O_3-Cu/CNT. Given the properties of the supports and not the hydrogenation catalyst is supposed to be investigated, the difference in activity is undesired.

6 Future Studies

Of the catalysts tested, La_2O_3 proved to be the most active for retro-aldol condensations. Thus, further research in this area should be done. Even with the very low amount of optimization done, combined diol yield of 49,4% was reached.

During this thesis, copper dispersion was a big issue. Copper has some advantages compared to other hydrogenation catalysts, it is cheap and it does not cause degradation of the products. Additionally, it produces considerable amounts of PG. When used together with La_2O_3, copper reached its limits. Further increase of the amount of copper seems impracticable, as the loading was already very high. A possible solution would be improved dispersion. If that is impossible, addition of other, more active hydrogenation catalysts might be helpful, for example nickel or ruthenium.

Thus, optimization of the La_2O_3 catalyst should be done, both in regards of which hydrogenation catalyst and how much of the hydrogenation catalyst should be used.

The benchmark compounds as described in this thesis should prove very helpful in finding the right catalyst ratio.

Additionally, important lessons can be learned from this thesis. If screening of new catalyst candidates (eg HAP) should be attempted again, it should be done in a different way. Instead of preparing a bifunctional catalyst from the start,two independent catalysts should be prepared, one for hydrogenation, one for retro-aldol condensation. That way, interactions between the different components can be avoided, and comparison between the different candidates is much easier. Also, optimization of the ratio between the catalysts is possible by simply adding more of one catalyst. Once this is complete and the most promising candidate with an approximate ratio is found, bifunctional catalysts should be prepared and optimized for a second time to find optimal conditions.

References

[1] ExxonMobil, "The outlook for energy: A view to 2040," 2016.

[2] M. Belgacem and A. Gandini, *Monomers, Polymers and Composites from Renewable Resources*. Elsevier Science, 2008.

[3] O. Bédué, "Enzymatic and non-biological degradation of cellulose," in *Lignocellulosic Biorefineries*, pp. 129–138, 2006.

[4] E. K. Pye, "Industrial lignin production and applications," in *Biorefineries - Industrial Processes and Products. Vol. 2*, pp. 165–200, 2006.

[5] M. Zheng, J. Pang, A. Wang, and T. Zhang, "One-pot catalytic conversion of cellulose to ethylene glycol and other chemicals: From fundamental discovery to potential commercialization," *Chinese Journal of Catalysis*, no. 35, pp. 602–613, 2014.

[6] Z. Xiao, S. Jin, M. Pang, and C. Liang, "Conversion of highly concentrated cellulose to 1,2-propanediol and ethylene glycol over highly efficient cucr catalysts," *Green Chemistry*, no. 15, p. 891, 2013.

[7] C. van der Wijst, X. Duan, I. S. Liland, J. C. Walmsley, J. Zhu, A. Wang, T. Zhang, and D. Chen, "Zno–carbon-nanotube composite supported nickel catalysts for selective conversion of cellulose into vicinal diols," *ChemCatChem*, 2015.

[8] M.-Y. Zheng, A.-Q. Wang, N. Ji, J.-F. Pang, X.-D. Wang, and T. Zhang, "Transition metal–tungsten bimetallic catalysts for the conversion of cellulose into ethylene glycol," *ChemSusChem*, no. 3, pp. 63–66, 2010.

[9] K. Yen-Ning and J. Hong, "Investigation of solubility of microcrystalline cellulose in aqueous naoh," *Polym Adv Technol*, no. 16, pp. 425–428, 2005.

[10] Y. Roman-Leshkov, M. Moliner, J. A. Labinger, and M. E. Davis, "Mechanism of glucose isomerization using a solid lewis acid catalyst in water," *Angewandte Chemie Internation Edition*, no. 49, pp. 8954–8957, 2010.

[11] K. Yen-Ning and J. Hong, "Hydrogenolysis of glycerol over carbon-supported ru and pt catalysts," *Journal of Catalysis*, no. 249 (2), pp. 328–337, 2007.

[12] C. Luo, S. Wang, and H. Liu, "Cellulose conversion into polyols catalyzed by reversibly formed acids and supported ruthenium clusters in hot water," *Angewandte Chemie International Edition*, no. 46, p. 7636–7639, 2007.

[13] R. Katzen and D. J. Schell, "Lignocellulosic feedstock biorefinery: History and plant development for biomass hydrolysis," in *Biorefineries - Industrial Processes and Products*, pp. 129–138, 2006.

[14] L. A. H. Nogueria and R. S. C. Capaz, "Insights into the solvation of glucose in water, dimethyl sulfoxide (dmso), tetrahydrofuran (thf) and n,n-dimethylformamide (dmf) and its possible implications on the conversion of glucose to platform chemicals," *RSC Advances*, 2015.

[15] J. R. Fisher and H. L. Barnes, "Ion-product constant of water to 350.deg," *J. Phys. Chem*, no. 76, p. 90–99, 1972.

[16] C. van der Wijst, "Paper proposal," *Department of Chemical Engineering, NTNU*, 2017.

[17] T. J. Connolly, J. L. Considine, Z. Ding, B. Forsatz, M. N. Jennings, M. F. MacEwan, K. M. McCoy, D. W. Place, A. Sharma, and K. Sutherland, "Efficient synthesis of 8-oxa-3-aza-bicyclo[3.2.1]octane hydrochloride," *Org. Process Res. Dev.*, no. 14 (2), pp. 459–465, 2010.

[18] S. Yao, X. Wang, Y. Jiang, F. Wu, X. Chen, and X. Mu, "One-step conversion of biomass-derived 5-hydroxymethylfurfural to 1,2,6-hexanetriol over ni-co-al mixed oxide catalysts under mild conditions," *ACS Sustainable Chem. Eng*, no. 2, pp. 173–180, 2014.

[19] R. Sun, T. Wang, M. Zheng, W. Deng, J. Pang, A. Wang, X. Wang, and T. Zhang, "Versatile nickel-lanthanum(iii) catalyst for direct conversion of cellulose to glycols," *ACS Catal.*, no. 5, pp. 874–883, 2015.

[20] M. Besson, P. Gallezot, and C. Pinel, "Conversion of biomass into chemicals over metal catalysts," *Angewandte Chemie*, no. 124, pp. 3303–3307, 2014.

[21] Z. Tai, J. Zhang, A. Wang, M. Zhenga, and T. Zhang, "Temperature-controlled phase-transfer catalysis for ethylene glycol production from cellulose," *Chem. Commun.*, no. 48, pp. 7052–7054, 2012.

[22] X.Wang, L.Meng, F.Wu, Y. Jiang, L.Wang, and X.Mu, "Efficient conversion of microcrystalline cellulose to 1,2-alkanediols over supported ni catalysts," *Green Chem*, no. 14, p. 758–765, 2012.

[23] Y. Liu, C. Luo, and H. Liu, "Tungsten trioxide promoted selective conversion of cellulose into propylene glycol and ethylene glycol on a ruthenium catalyst," *Chemical Reviews*, no. 114, pp. 1827–1870, 2012.

[24] J. Feng, W. Xiong, H. Ding, and B. He, "Hydrogenolysis of glycerol over pt/c catalyst in combination with alkali metal hydroxides," *Open Chem.*, no. 14, pp. 279–286, 2016.

[25] D. TianYin, S. JiYing, and L. HaiChao, "Cellulose conversion to polyols on supported ru catalysts in aqueous basic solution," *SCIENCE CHINA Chemistry*, no. 53, p. 1476–1480, 2010.

[26] C. Luo, S. Wang, and H. Liu, "Cellulose conversion into polyols catalyzed by reversibly formed acids and supported ruthenium clusters in hot water," *Angewandte Chemie International Edition*, no. 46, p. 7636–7639, 2007.

[27] N. Ji, T. Zhang, M. Zheng, A. Wang, H. Wang, X. Wang, and J. Chen, "Direct catalytic conversion of cellulose into ethylene glycol using nickel-promoted tungsten carbide catalysts," *Angewandte Chemie International Edition*, no. 47, p. 8321–8321, 2008.

[28] S. F. Morken, "One-pot conversion of biomass to chemicals on ni-cu/zno based catalysts," 2015.

[29] Y. Zhang, A. Wanga, and T. Zhang, "A new 3d mesoporous carbon replicated from commercial silica as a catalyst support for direct conversion of cellulose into ethylene glycol," *Chemical Communication*, no. 46, pp. 862–864, 2010.

[30] Z. Tai, J. Zhang, P. A. Wang, D. J. Pang, D. M. Zheng, and P. T. Zhang, "Catalytic conversion of cellulose to ethylene glycol over a low-cost binary catalyst of raney ni and tungstic acid," *ChemSusChem*, no. 6 (4), p. 652–658, 2013.

[31] B. M. Bhanagea, S. ichiro Fujitaa, Y. Ikushimab, and M. Araia, "Synthesis of dimethyl carbonate and glycols from carbon dioxide, epoxides, and methanol using heterogeneous basic metal oxide catalysts with high activity and selectivity," *Applied Catalysis A: General*, no. 219 (1-2), p. 259–266, 2001.

[32] D. Skodvin, "Carbon nanomaterials for low temperature co2 capture. summer project," 2016.

[33] D. Guo, R. Shibuya, C. Akiba, S. Saji, T. Kondo1, and J. Nakamura, "Active sites of nitrogen-doped carbon materials for oxygen reduction reaction clarified using model catalysts," *Science*, no. 351 (6271), pp. 416–365, 2016.

[34] G.-P. Hao, W.-C. Li, D. Qian, and A.-H. Lu, "Rapid synthesis of nitrogen-doped porous carbon monolith for co2 capture," *Advanced Materials*, no. 22, p. 853–857, 2010.

[35] G. Xu, J. Guo, Y. Zhang, YaoFu, J. Chen, and Q. Guo, "Selective hydrogenation of phenol to cyclohexanone over pd–hap catalyst in aqueous media," *ChemCatChem*, no. 7, pp. 2485–2492, 2015.

[36] I. Chorkendorff and J. Niemantsverdriet, *Concepts of Modern Catalysis and Kinetics*. Wiley-VCH Verlag GmbH Co, 2003.

[37] D. J. Ostgard, L. Kustov, K. Poeppelmeier, and W. M. H. Sachtler, "Comparison of pt/kl catalysts prepared by ion exchange or incipient wetness impregnation," *Journal of Catalysis*, no. 133, pp. 342–357, 1991.

[38] J. Niemantsverdriet, *Spectroscopy in Catalysis: An Introduction*. Wiley-VCH Verlag GmbH Co, 2007.

[39] S. Sakka, *Handbook of Sol-gel Science and Technology - Processing Characterization and Application*. Wiley-VCH Verlag GmbH Co, 2007.

[40] I. Chorkendorff and J. Niemantsverdriet, *Spectroscopy in Catalysis: An Introduction*. Wiley-VCH Verlag GmbH Co, 2007.

[41] M. d'Halluin, T. Mabit, N. Fairley, V. Fernandez, M. B. Gawande, E. L. Grognec, and F.-X. Felpin, "Graphite-supported ultra-small copper nanoparticles – preparation, characterization and catalysis applications," *Carbon*, no. 93, pp. 974–983, 2015.

[42] F. Lou, H. Zhou, F. Huang, F. Vullum-Bruer, T. D. Tranc, and D. Chen, "Facile synthesis of manganese oxide/aligned carbon nanotubes over aluminium foil as 3d binder free cathodes for lithium ion batteries," *Journal of Materials Chemistry A*, no. 1, p. 3757–3767, 2013.

A   Catalyst Preparation

The catalysts were prepared as discussed in the experimental section. Here, more detail will be given.

For the metal oxide catalysts, 2g of CNT were used. NCS was not available in that quantity, instead, only 0,95g were used. The supports were pretreated as described before impregnation.

Table A.1: Amount of chemicals used for impregnation

	Cu/NCS	La_2O_3-Cu/CNT	MgO-Cu/CNT	Al_2O_3-Cu/CNT
Support	0,95g	2,00g	2,00g	2,00g
$La(NO_3)_3\,6\,H_2O$	0,00g	1,382g	0,00g	0,00g
$Mg(NO_3)_2\,6\,H_{20}$	0,00g	0,00g	3,308g	0,00g
$Al(NO_3)_3$	0,00g	0,00g	0,00g	1,086g
Citric Acid	1,177g	0,701g	2,479g	1,120g
Ethylene Glycol	0,380g	0,226g	0,801g	0,362g
$Cu(NO_3)_2\,3\,H_2O$	1,481g	3,117g	3,117g	3,117g

The amounts of chemicals used for impregnation are given in table A.1. These correspond to a loading of 40,9% copper and (if applicable) 26% metal oxide. Loading is defined as mass of the metal divided by mass of the support.

B   Catalyst Characterisation

B.1   Adsorption Isotherms
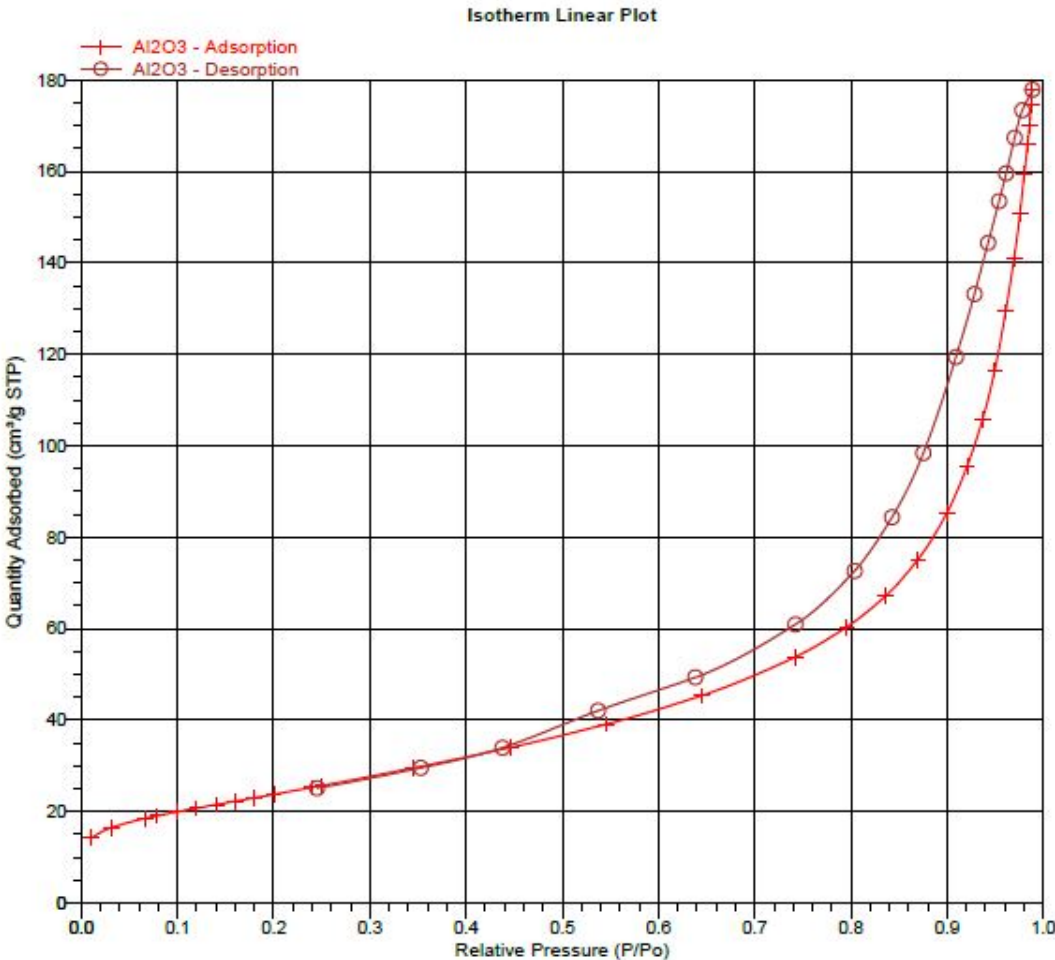
Figure B.1: Adsorption Isotherm for Al_2O_3-Cu/CNT
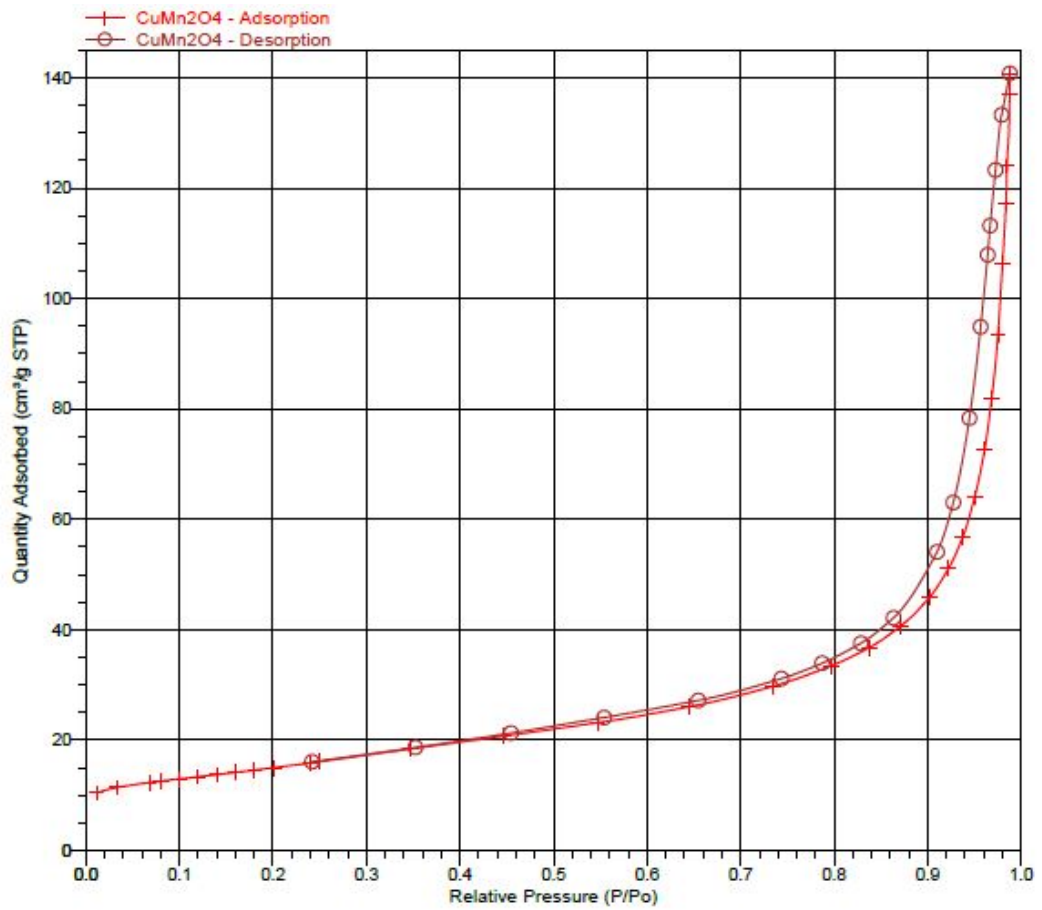
Figure B.2: Adsorption Isotherm for $CuMn_2O_4/CNT$
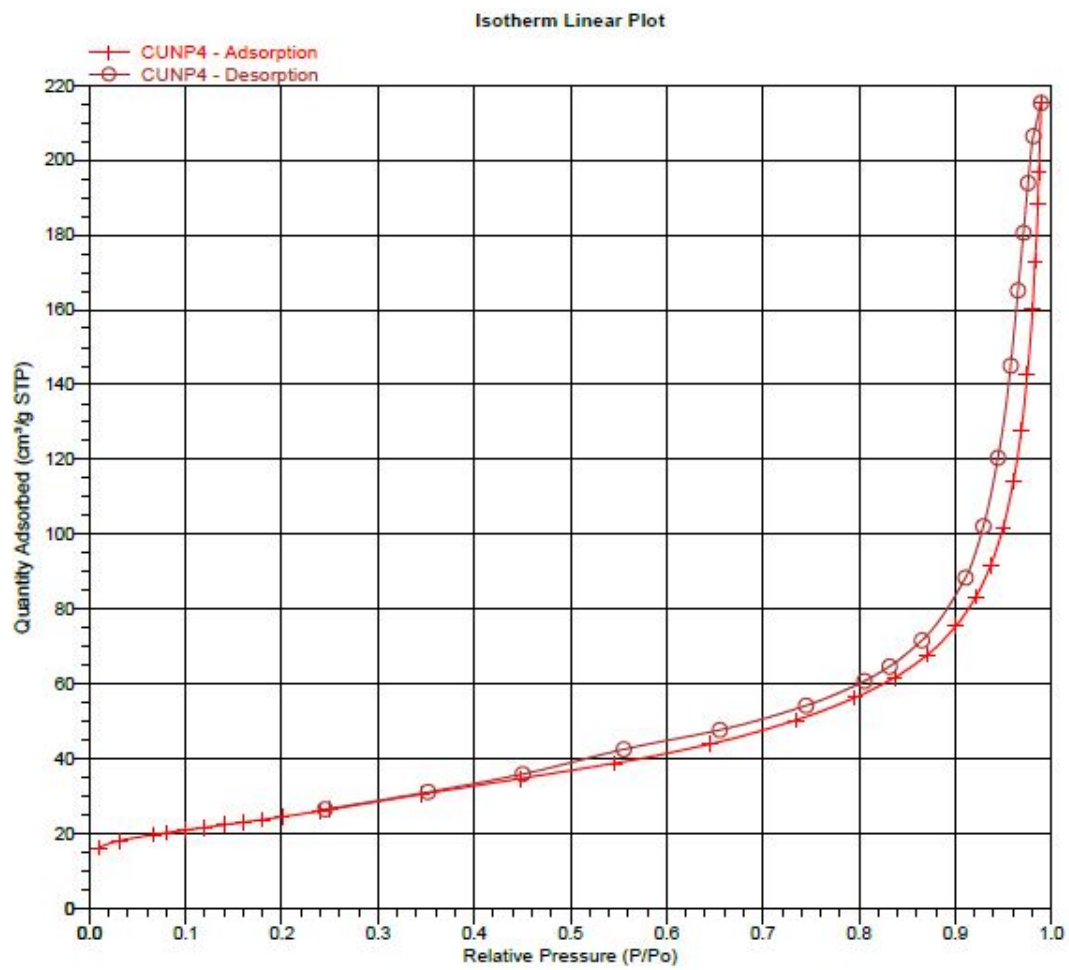
Figure B.3: Adsorption Isotherm for Cu-NP/CNT
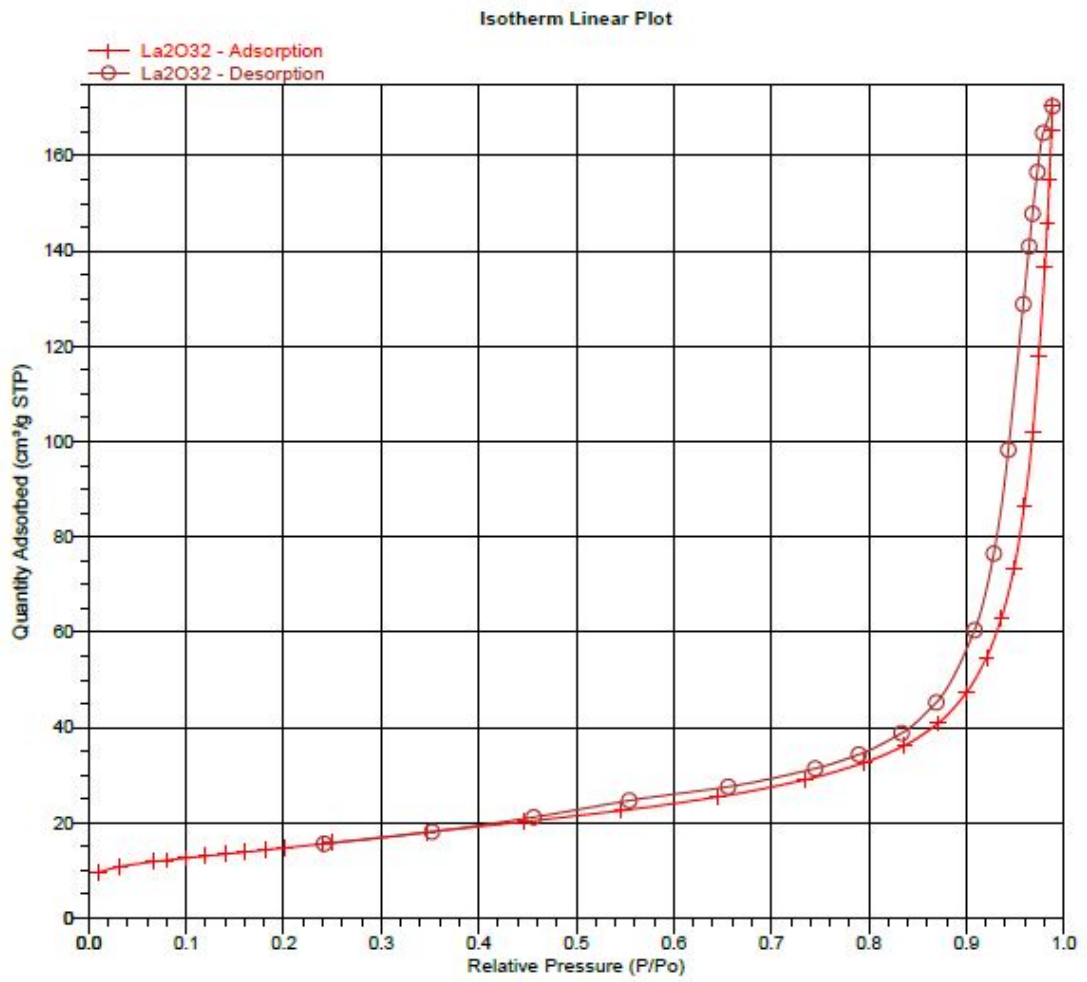
Figure B.4: Adsorption Isotherm for La_2O_3-Cu/CNT
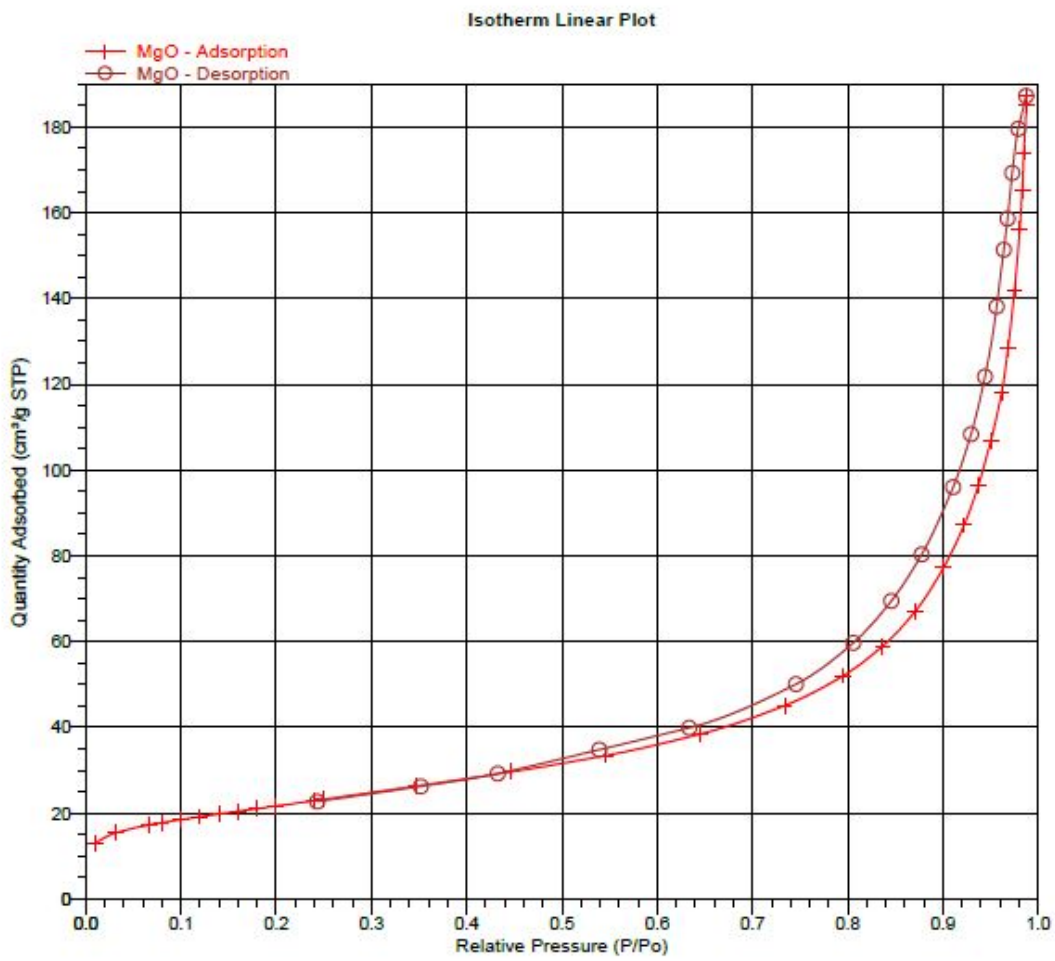
Figure B.5: Adsorption Isotherm for MgO-Cu/CNT
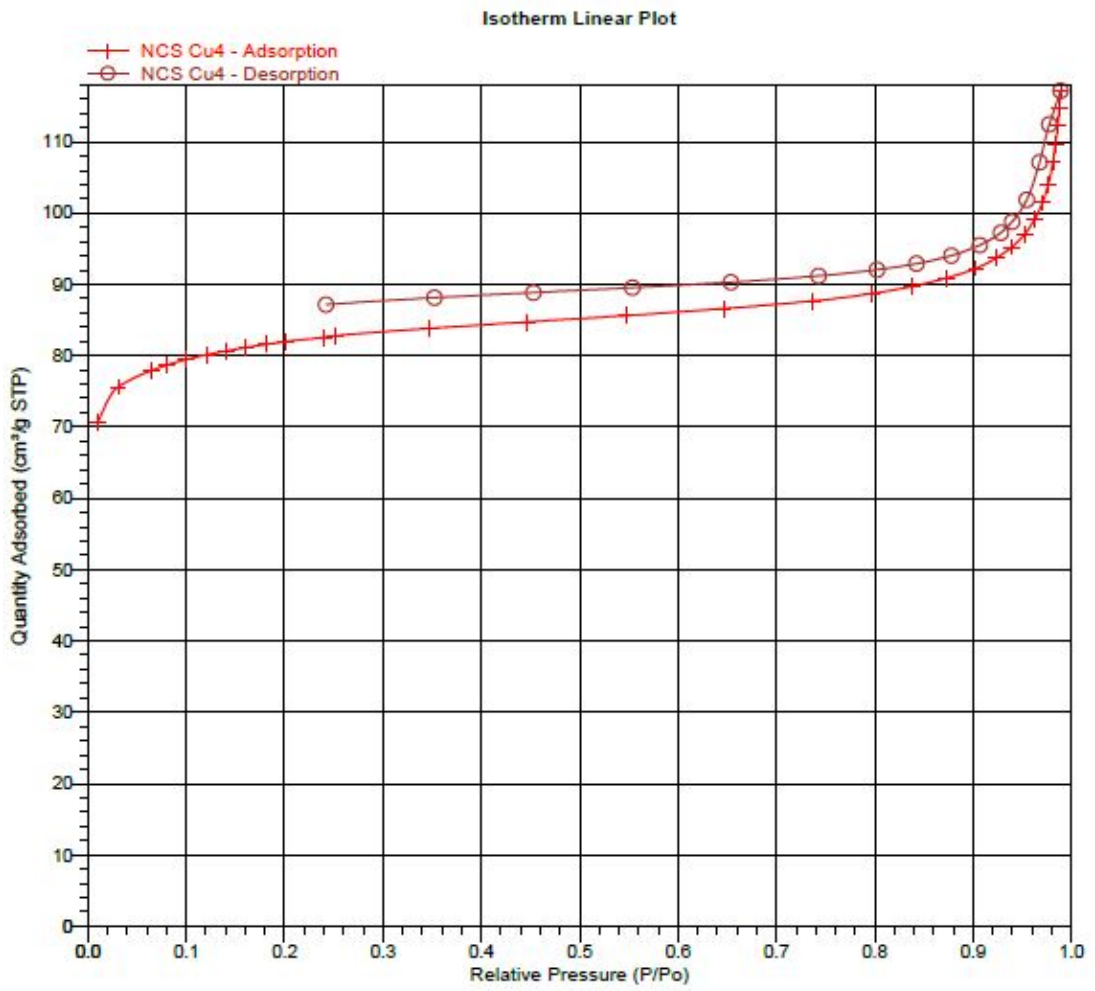
Figure B.6: Adsorption Isotherm for Cu/NCS
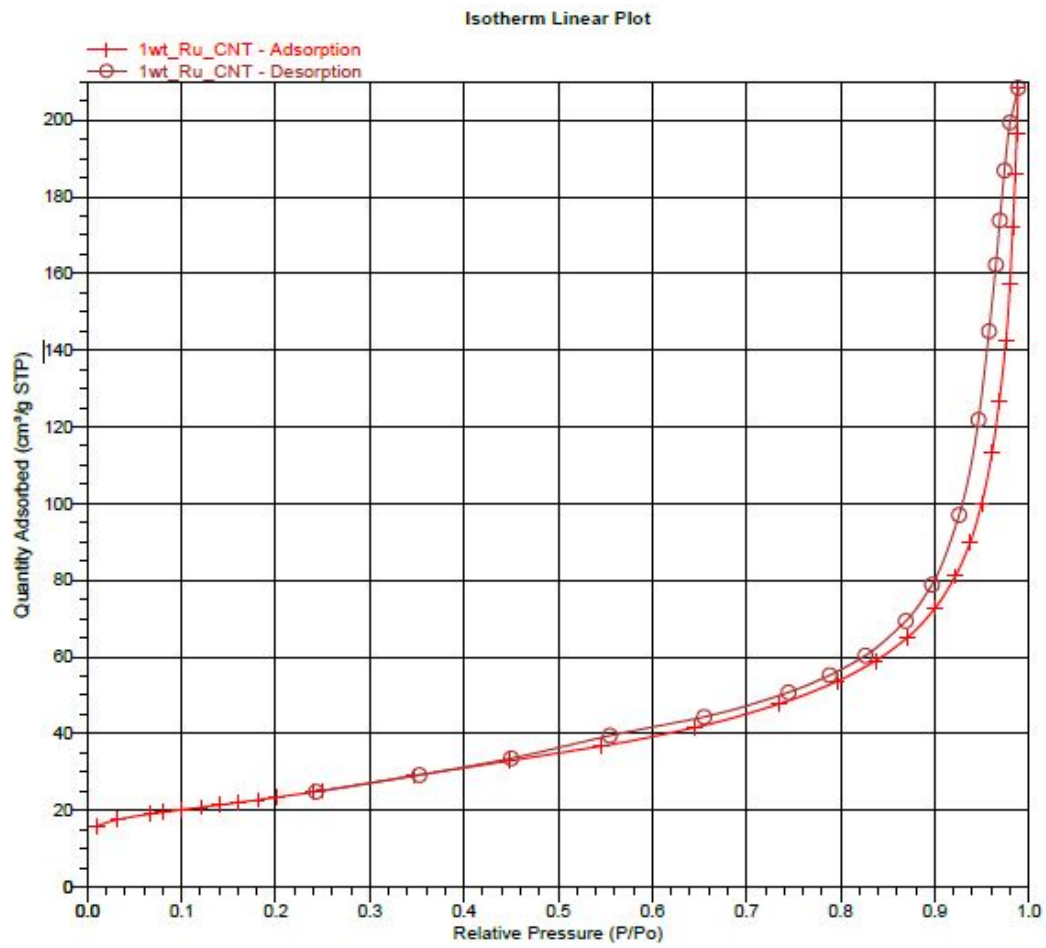
Figure B.7: Adsorption Isotherm for Ru/CNT

B.2 SEM pictures
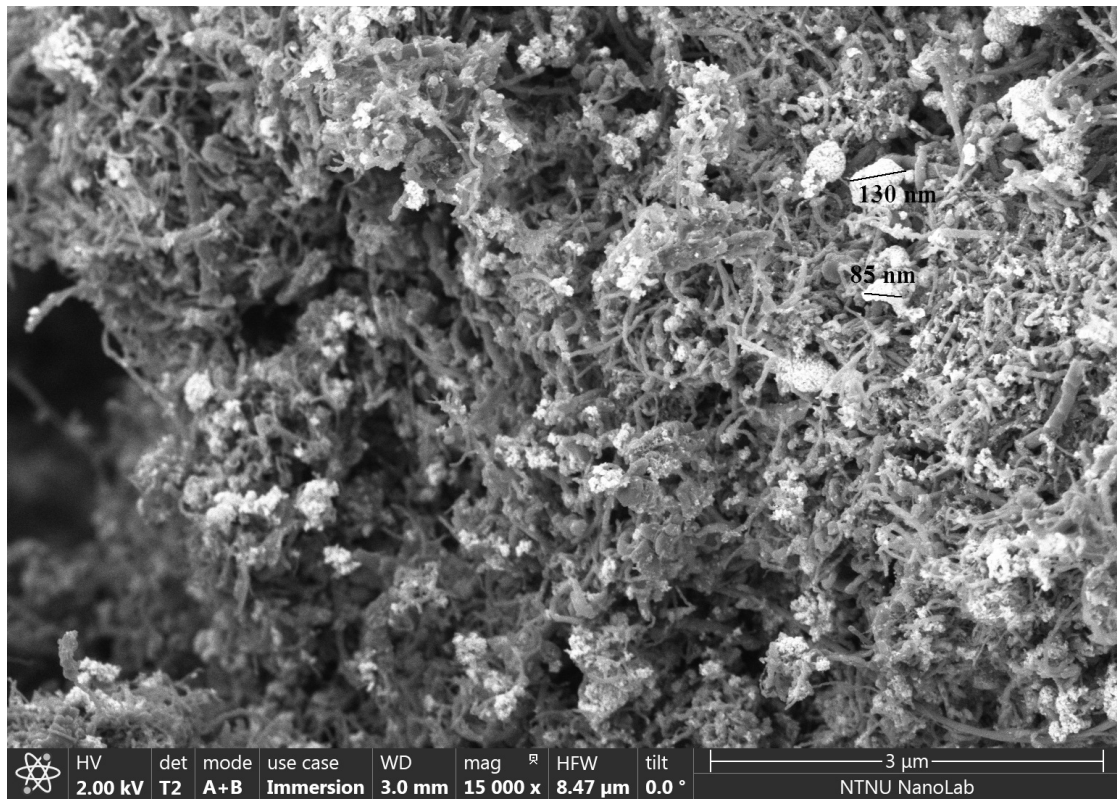
Figure B.8: SEM Picture of La_2O_3-Cu/CNT
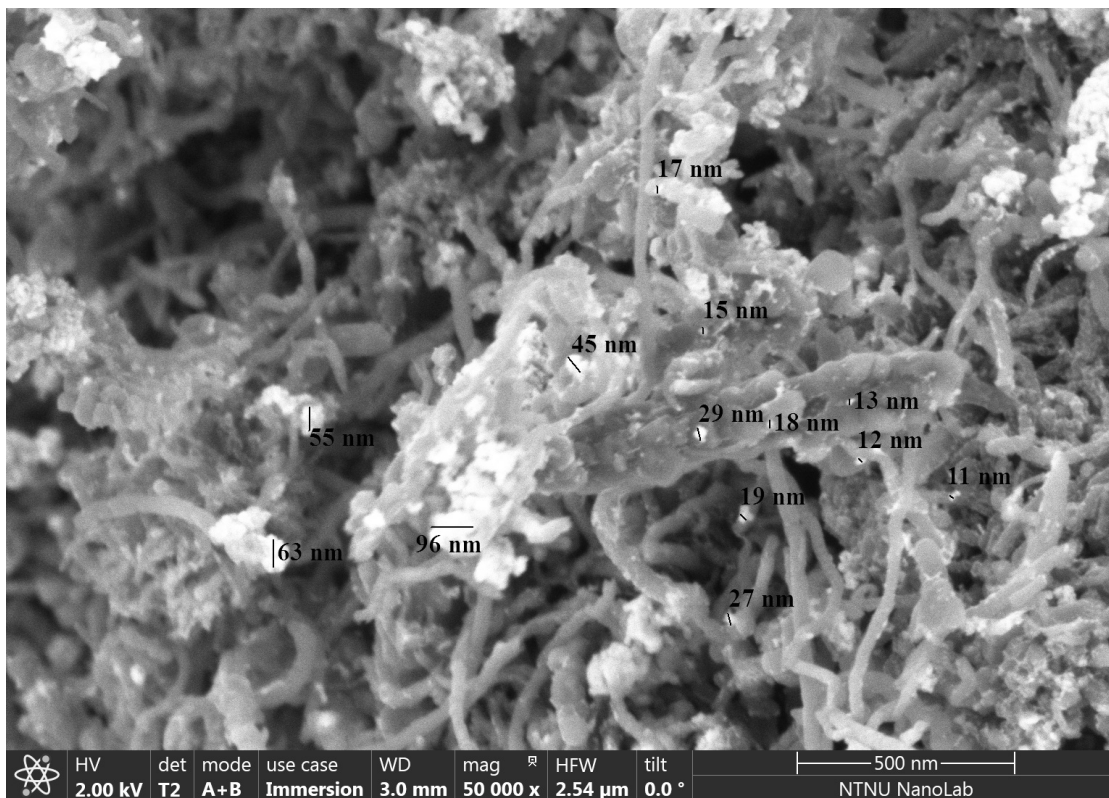
Figure B.9: SEM Picture of La$_2$O$_3$-Cu/CNT
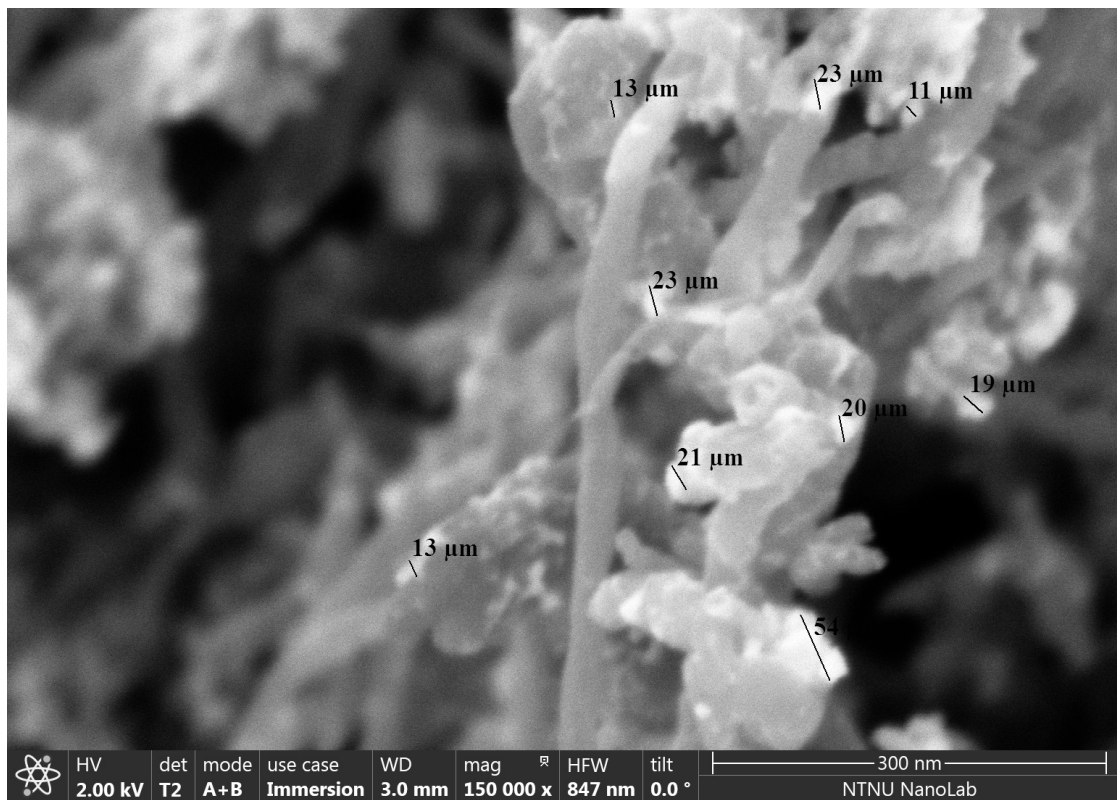
Figure B.10: SEM Picture of La_2O_3-Cu/CNT
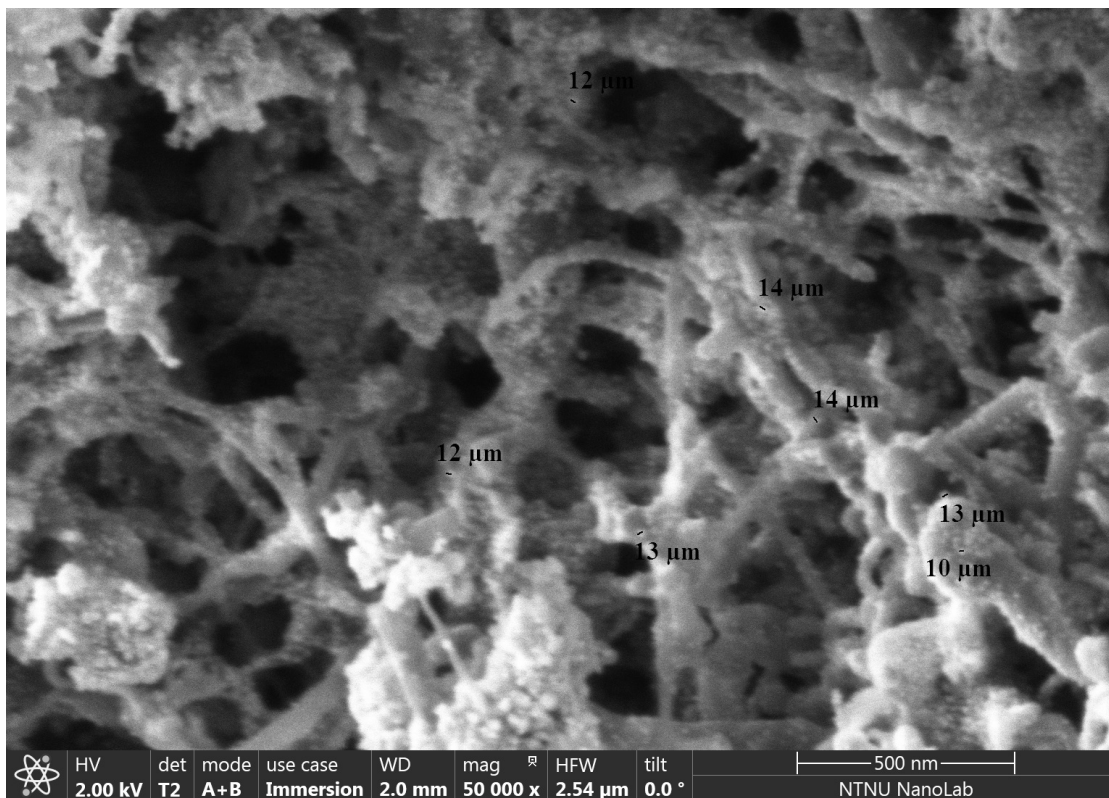
Figure B.11: SEM Picture of MgO-Cu/CNT

HV	det	mode	use case	WD	mag ㅁ	HFW	tilt	⊢————— 3 μm —————⊣
2.00 kV	T2	A+B	Immersion	2.0 mm	15 000 x	8.47 μm	0.0 °	NTNU NanoLab
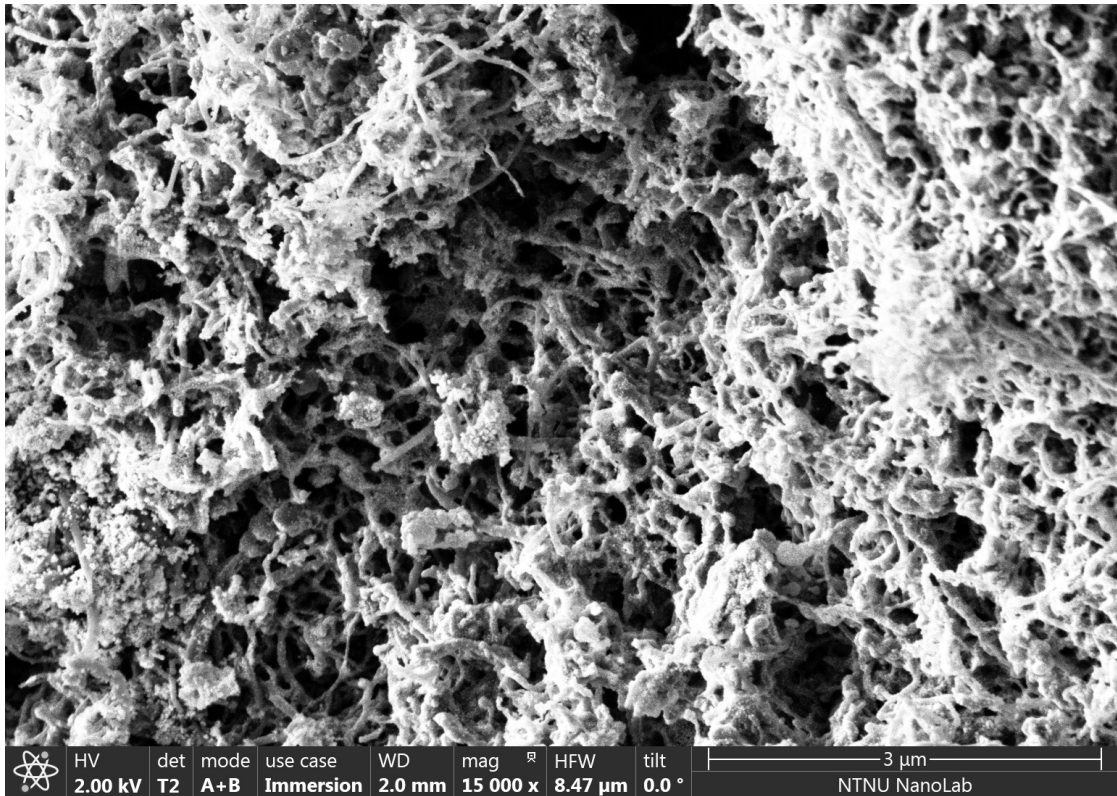
Figure B.12: SEM Picture of MgO-Cu/CNT

HV	det	mode	use case	WD	mag 인	HFW	tilt	3 μm
2.00 kV	T2	A+B	Immersion	2.9 mm	12 000 x	10.6 μm	0.0 °	NTNU NanoLab
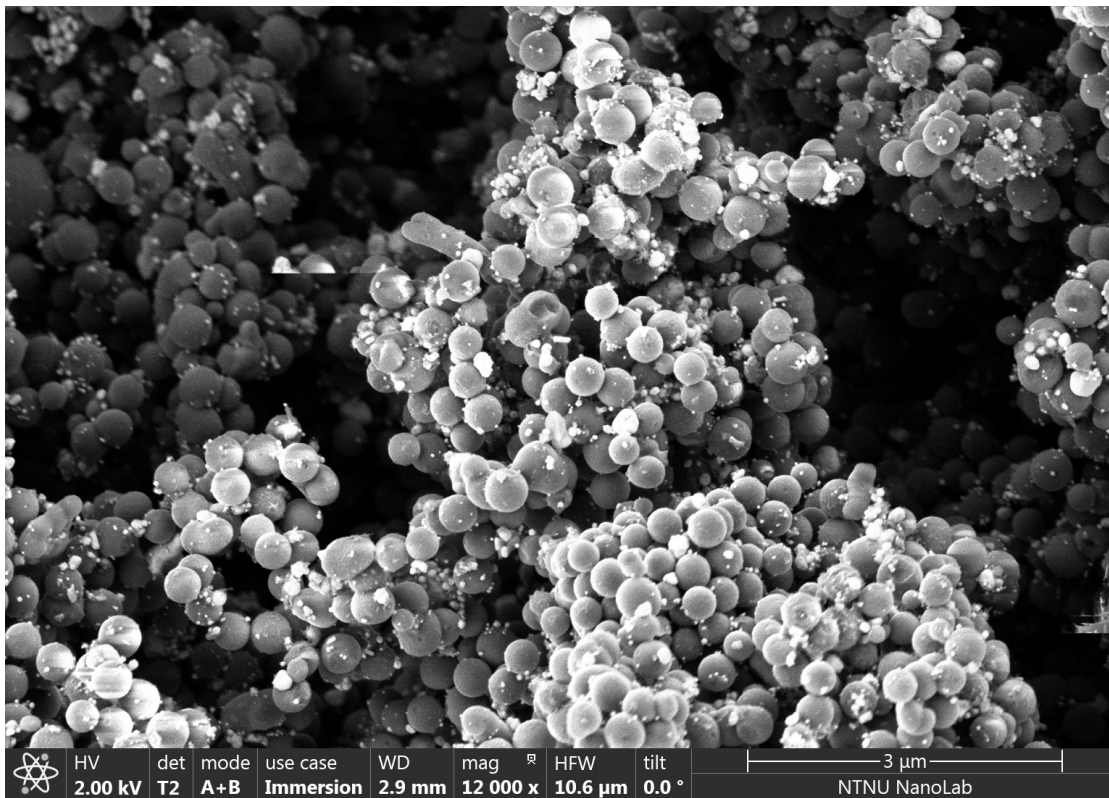
Figure B.13: SEM Picture of Cu/NCS
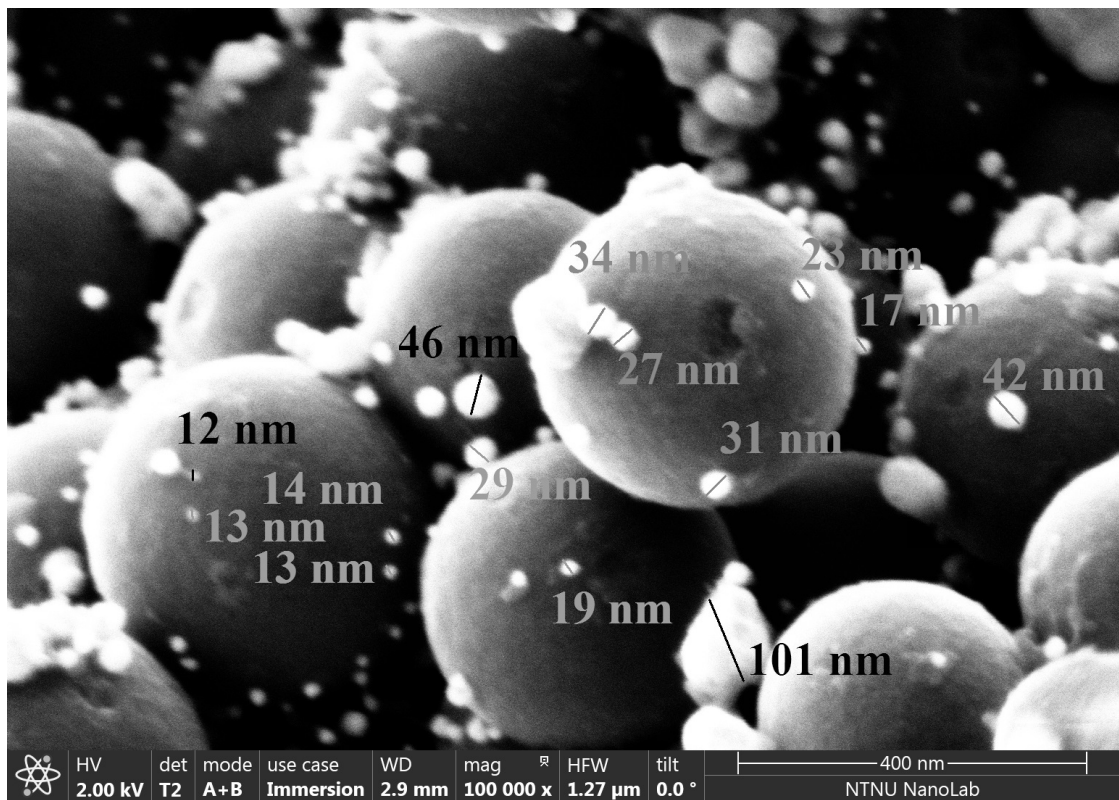
Figure B.14: SEM Picture of Cu/NCS

C Complete Yield Tables

During the thesis, on multiple occasion results were summarized into one entry to avoid overload. These are the detailed results. As described during the experimental, a factor to correct for wetness of the cellulose was used. The dry matter content of the cellulose was found to be 96%. It was determined by drying cellulose in a drying oven for two days.

Table C.1: Small reactor: 90min

| | 90min | | | |
	NCS	La	Mg	Al
Glucose	0,0%	0,0%	0,8%	0,0%
Fructose	0,0%	0,0%	1,9%	0,0%
Erythritol	0,8%	0,0%	2,5%	0,7%
Glycerol	0,3%	0,3%	1,9%	0,4%
Mannitol	0,4%	0,0%	2,7%	0,5%
EG	8,8%	9,2%	9,6%	7,3%
PG	16,9%	13,6%	12,3%	15,6%
Sorbitol	1,3%	0,8%	2,3%	1,0%
1,2 butanediol	6,1%	1,2%	1,7%	3,8%
2,5-DHF	2,6%	0,8%	3,1%	6,6%
THFDM	3,9%	0,6%	0,0%	3,9%
THFA	2,3%	1,5%	1,2%	3,5%
1,2-pentanediol	2,7%	0,0%	3,0%	1,4%
1,2-cyclohexanediol	1,5%	1,2%	2,4%	2,7%
1,2-hexanediol	5,6%	0,9%	0,9%	4,2%
Void Volume	11,5%	18,5%	14,5%	12,0%
Total	64,7%	48,6%	60,7%	63,6%

Table C.2: Small reactor: 180min

	3h			
	NCS	La	Mg	Al
Glucose	0,0%	0,0%	0,0%	0,0%
Fructose	0,0%	0,0%	1,1%	0,0%
Erythritol	0,0%	0,6%	0,7%	0,0%
Glycerol	0,4%	0,3%	0,0%	0,0%
Mannitol	0,0%	0,4%	2,3%	0,0%
EG	14,5%	16,9%	14,7%	5,2%
PG	11,7%	17,8%	14,3%	14,6%
Sorbitol	1,0%	0,0%	3,8%	0,0%
1,2 butanediol	6,4%	4,7%	2,9%	3,1%
2,5-DHF	3,1%	0,5%	7,0%	5,9%
THFDM	2,5%	1,1%	1,5%	1,4%
THFA	1,5%	1,3%	0,9%	2,1%
1,2-pentanediol	0,0%	2,0%	4,2%	1,3%
1,2-cyclohexanediol	1,1%	2,8%	3,0%	1,9%
1,2-hexanediol	4,2%	2,4%	1,4%	2,6%
Void Volume	5,8%	10,3%	14,0%	9,1%
Total	52,1%	61,0%	71,7%	47,1%

Table C.3: Small reactor: Runs with noncellulosic feedstock

	Fructose Mg	Glycerol Mg	PG Mg
Glucose	0,0%	0,0%	0,0%
Fructose	0,9%	0,0%	0,0%
Erythritol	0,0%	0,0%	0,0%
Glycerol	4,8%	46,9%	0,0%
Mannitol	6,9%	0,0%	0,0%
EG	7,0%	0,0%	0,0%
PG	28,6%	17,4%	94,1%
Sorbitol	0,0%	0,0%	0,0%
1,2 butanediol	4,1%	0,0%	0,0%
2,5-DHF	0,0%	0,0%	0,0%
THFDM	2,4%	0,0%	0,0%
THFA	0,0%	0,0%	0,0%
1,2-pentanediol	0,3%	0,0%	0,0%
1,2-cyclohexanediol	0,0%	0,0%	0,0%
1,2-hexanediol	0,6%	0,0%	0,0%
Void Volume	0,0%	0,0%	0,0%
Total	55,6%	64,3%	94,1%

Table C.4: MgO-Cu/CNT over time

MgO

Time	EG	PG	PT	BD	Sor	THFDM	PD	2,5-DHF	Hex	THFA	CHD	VV	Ery	Gly	Tot
0	3,1	3	0,1	1,2	0,7	1	0,9	0,2	0,4	0	0	9,1			19,3
15	5,7	6,5	0,2	2,3	0	1,6	1,6	0,6	0,6	0,1	1,1	12			32,1
30	7,1	7,8	0,5	2,4	0	1,5	2,6	0,8	0,6	0,3	1,6	15,1			40,3
60	10	11,4	1	3,1	0	2,6	2,7	0,9	0,8	0,5	1,7	16			50,7
90	12,2	13,4	1,6	2,8	0	2,4	3,2	1,6	1,1	0,5	2,1	16,5			57,4
180	16,6	18,37	6	4,7	0	3,4	3,6	2,4	1,6	1,4	4	14,5			76,57

Table C.5: Al_2O_3-Cu/CNT over time

Al2O3

Time	EG	PG	PT	BD	Sor	THFDM	PD	2,5-DHF	Hex	THFA	CHD	VV	Ery	Gly	Tot
0	2,6	0,7			3,1							3,8			10,2
15	7,2	5,6	0,7		6,5		1	4,7	0,7			6,5		1,5	34,4
30	8,4	8,3	1,7		7		1,8	6	1,6			6,6		2,1	43,5
60	9,5	14,4	3,1		6,6		2,9	8,2	3,1			6,6		2,4	56,8
90	9,4	16,9	4,6		5,6		2,8	7,3	4			6,4		2,2	59,2
180	8,8	18	5		2,3	0,9	3,1	8	5,8			6,5		2	60,4

Table C.6: La$_2$O$_3$-Cu/CNT over time

La2O3

Time	EG	PG	PT	BD	Sor	THFDM	PD	2,5-DHF	Hex	THFA	CHD	VV	Ery	Gly	Tot
0	4,2	1,4		0,3	2,9			0,9	0		0	5,3			15
15	8,9	3,2		1,1	5,5		1,1	1,8			0,8	10,5		0,3	33,2
30	13,5	7,5		2,4	5		1,3	3	0,7		1,1	11,1		0,5	46,1
60	18,3	15,5		3,7	2,7		2,3	2,1	1,3	0,2	1	11,4		0,7	59,2
90	19,6	18,1		4,2	1,3		2,4	2	1,7	0,4	0,8	11,1		0,7	62,3
180	20,3	19,1		5	1,1		2,5	2,6	3,1	0,7	0,9	9,2		0,7	65,2

Table C.7: Cu/NCS over time

Cu/NCS

Time	EG	PG	PT	BD	Sor	THFDM	PD	2,5-DHF	Hex	THFA	CHD	VV	Ery	Gly	Tot
0	0	0		0	0			0	0		0	0		0	0
15	3,6	1,4		0,3	2,4		0,6	1,3	1,2		0,5	2,2		0,4	13,9
30	5,9	3		0,9	3,9	0,3	0,9	3,5	3,3		1,6	2,5		1	26,8
60	8,9	8,2		2,4	6,6	0,2	2,4	6,5	7,3		1,5	2,9		2,1	49
90	9,5	10,4		3,6	6,9	0,5	2	8,2	9,3		1,4	3,4		2,6	57,8
180	9,9	12,1		4,6	4,9	1	2,2	10,4	10,6		1,1	3,1		2,3	62,2

Table C.8: La$_2$O$_3$-Cu/CNT with Ru/CNT over time

La2O3 Ru

Time	EG	PG	PT	BD	Sor	THFDM	PD	2,5-DHF	Hex	THFA	CHD	VV	Ery	Gly	Tot
0	2,5	4,1	0	0	0	0	0	0	0	0	0	2	0,6	0,1	9,3
15	8	5	0,5	0,1	0	0,4	0,6	0,7	0	0,3	0	3,5	1,1	1,2	21,4
35	17,9	11	1,6	2	0,1	2,1	1,9	1,2	0,8	0,8	0	4,6	2,8	3,5	50,2
60	23,3	13,6	1,5	3,1	0	1,5	2,2	1,4	1,6	0,7	0	4,5	3,6	4,6	61,6
180	28,2	19,2	2,6	0,8	0	1,6	3	2,3	2,3	1,5	0	2	2,9	4,8	71,2

Table C.9: Cu/NCS with Ru/CNT over time

NCS Ru

Time	EG	PG	PT	BD	Sor	THFDM	PD	2,5-DHF	Hex	THFA	CHD	VV	Ery	Gly	Tot
0	0	0	0	0	0	0	0	0	0	0	0	2,3	0	0	2,3
15	1,9	1,2	0	0,4	1,3	0,5	0,8	0,7	0,5	0,2	0	2,8	0,9	1	12,2
30	3,2	2,4	0	0,9	2,6	0,9	1,1	1,2	1,7	0,6	0	2,7	2,2	2,9	22,4
60	4,1	5,9	0	1,6	5,9	3,2	2,2	3	5	1	0	2,8	5,6	4,8	45,1
90	8,5	8,12	0	2,2	9,9	3,8	2,9	5,3	5,9	0,9	0	3,6	8,1	6,7	65,92
180	8,8	9,5	0	2,7	9,6	4,7	2,8	6,9	6,7	0,7	0,4	3,6	7,7	6,7	70,8

Table C.10: MgO-Cu/CNT with Ru/CNT over time

MgO Cu Ru

Time	EG	PG	PT	BD	Sor	THFDM	PD	2,5-DHF	Hex	THFA	CHD	VV	Ery	Gly	Tot
0	0,8	0,4	0,2									2,7			4,1
15	3,5	3	2,7	0,2	0,4	0,1	1	0,5	0,2		0,4	5,5	1		18,5
30	5,7	5	4,8	0,3	1	0,2	1,7	0,8	0,5		0,5	7,3	1,6		29,4
60	6,3	7,8	6,3	0,4	1,5	0,6	2,6	1,3	0,6		0,6	7,8	2,9		38,7
90	12,5	11,9	10,1	1,7	1,5	2	3,1	1,5	1,1		0,9	9	3		58,3
180	14,5	15,5	11,45	1,6	2,5	1,4	3,9	0,9	1,5		1	7,2	3,8		65,25

Table C.11: Cu/NCS with H_2WO_4 over time

NCS H2WO4

Time	EG	PG	PT	BD	Sor	THFDM	PD	2,5-DHF	Hex	THFA	CHD	VV	Ery	Gly	Tot
0	3,5	0,2		0		8,7		5,3				20,7	4,3		42,7
15	5,4	0,2		0		7,9		6,6				20,8	1,6		42,5
30	6,2	0,2		0,3		7,3		6,5				20,5	0,4		41,4
60	6,5	0,9		0,7		6,2		6,1				19,7			40,1
90	7,3	1,7		0,9		5,9		5,2				19,4			40,4
180	6,7	2,4		1,4		3,6		4,1				16,5			34,7

D HPLC Diagrams

D.1 100ml Reactor
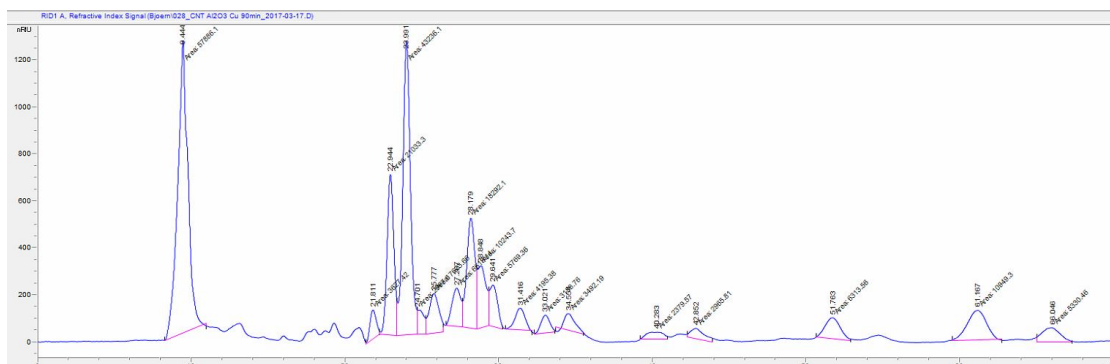
Figure D.1: 0,33g Cellulose, 0,1g Al_2O_3-Cu/CNT, 90min

Figure D.2: 0,33g Cellulose, 0,1g Al_2O_3-Cu/CNT, 3h
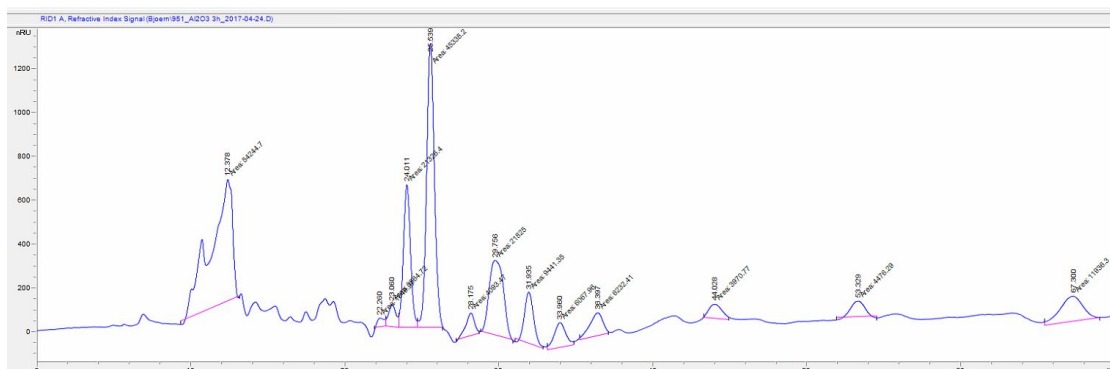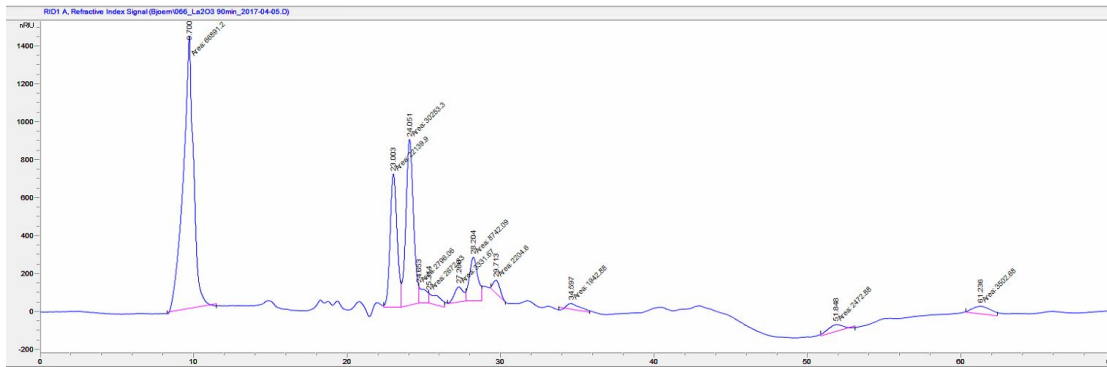
Figure D.3: 0,33g Cellulose, 0,1g La$_2$O$_3$-Cu/CNT, 90min
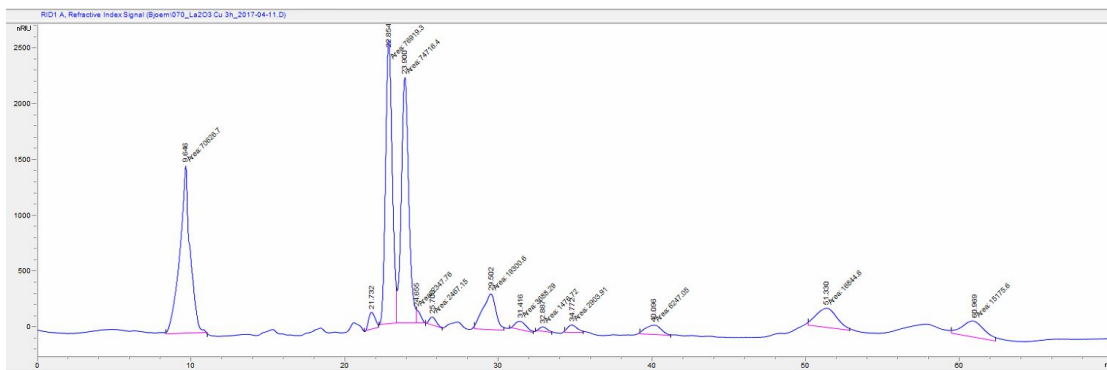
Figure D.4: 0,33g Cellulose, 0,1g La$_2$O$_3$-Cu/CNT, 3h
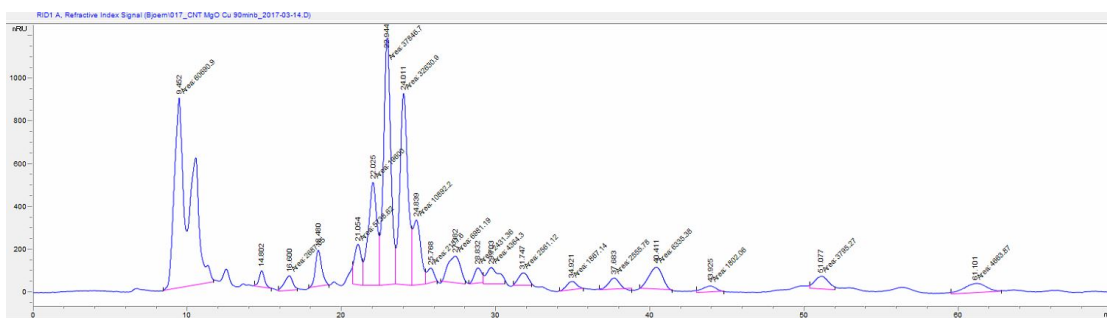
Figure D.5: 0,33g Cellulose, 0,1g MgO-Cu/CNT, 90min

85
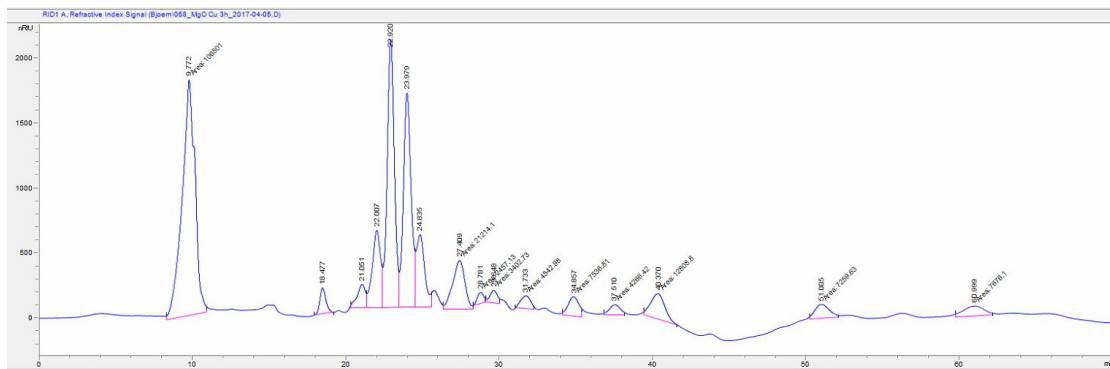
Figure D.6: 0,33g Cellulose, 0,1g MgO-Cu/CNT, 3h
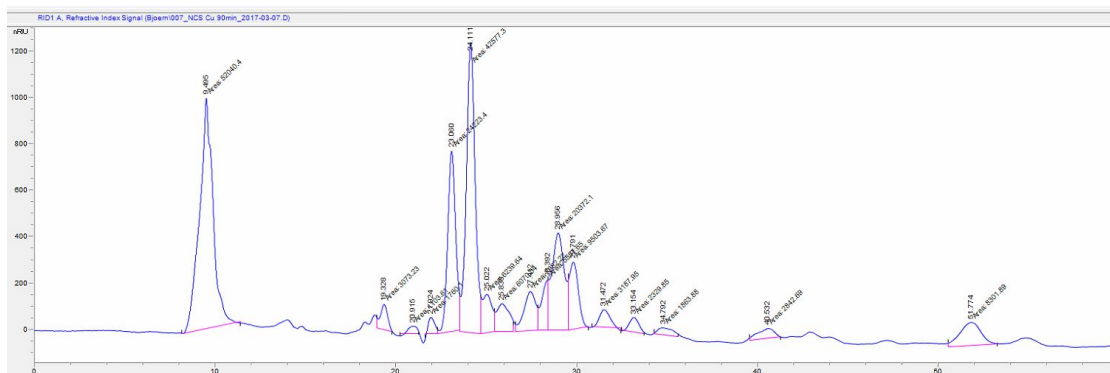
Figure D.7: 0,33g Cellulose, 0,1g Cu/NCS, 90min
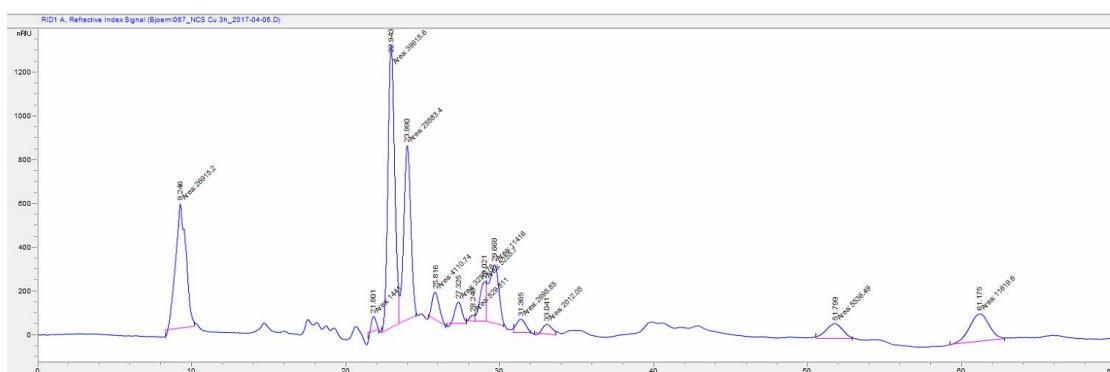
Figure D.8: 0,33g Cellulose, 0,1g Cu/NCS, 3h
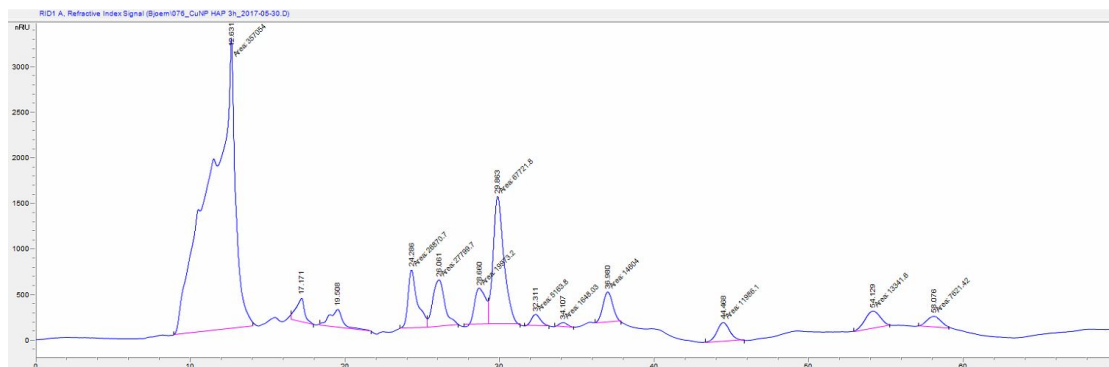
Figure D.9: 0,33g Cellulose, 0,1g Cu-NP/CNT, 0,01g HAP, 3h
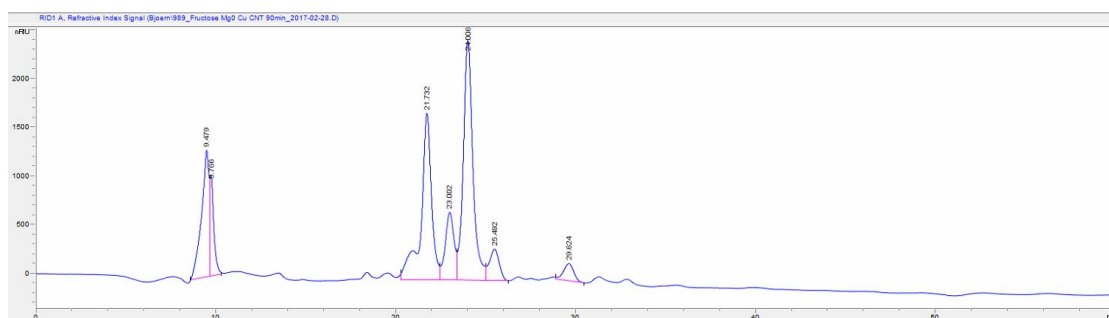
Figure D.10: 0,33g Fructose, 0,1g MgO-Cu/CNT, 90min
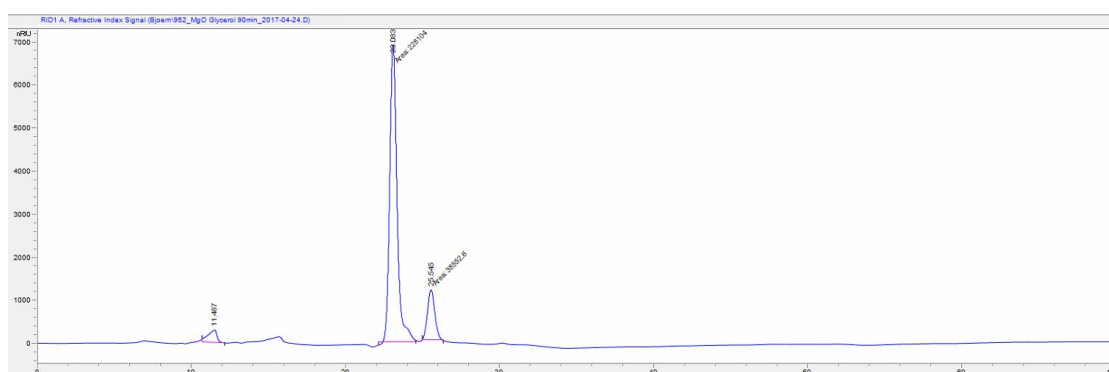
Figure D.11: 0,33g Glycerol, 0,1g MgO-Cu/CNT, 90min

D.2 300ml Reactor

Figure D.12: 0,99g Cellulose, 0,3g La_2O_3-Cu/CNT, Sampling after 0min

Figure D.13: 0,99g Cellulose, 0,3g La_2O_3-Cu/CNT, Sampling after 15min

Figure D.14: 0,99g Cellulose, 0,3g La_2O_3-Cu/CNT, Sampling after 30min
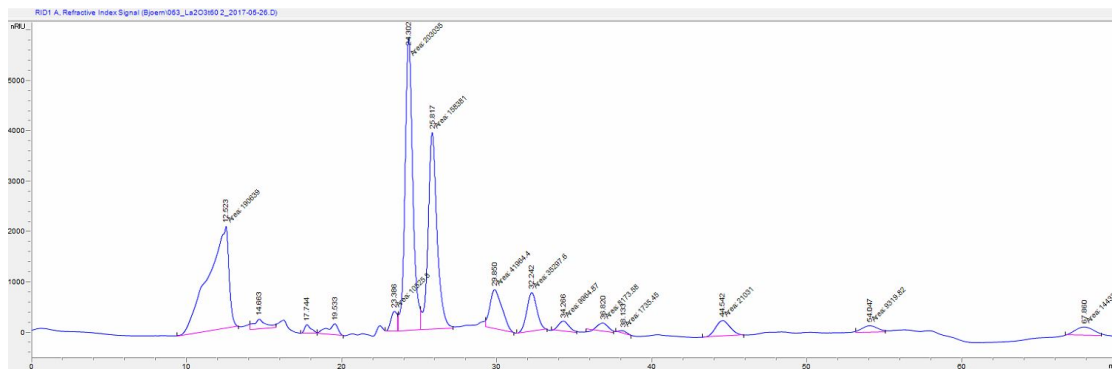
Figure D.15: 0,99g Cellulose, 0,3g La$_2$O$_3$-Cu/CNT, Sampling after 60min
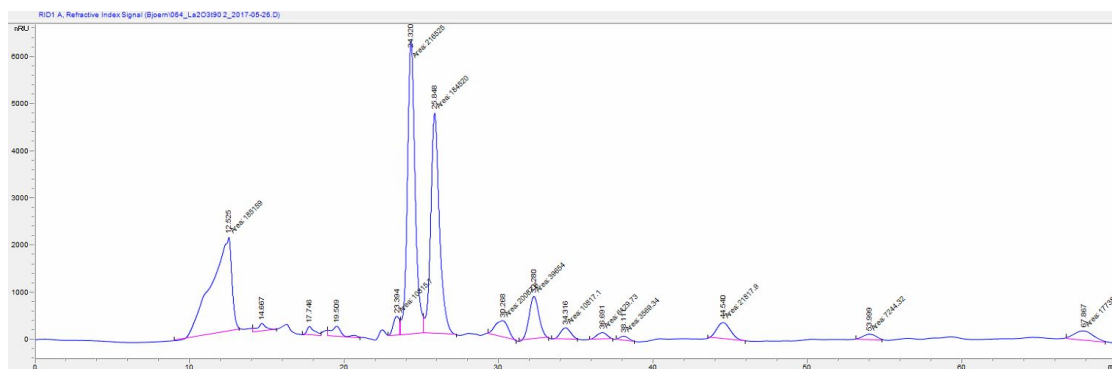
Figure D.16: 0,99g Cellulose, 0,3g La$_2$O$_3$-Cu/CNT, Sampling after 90min
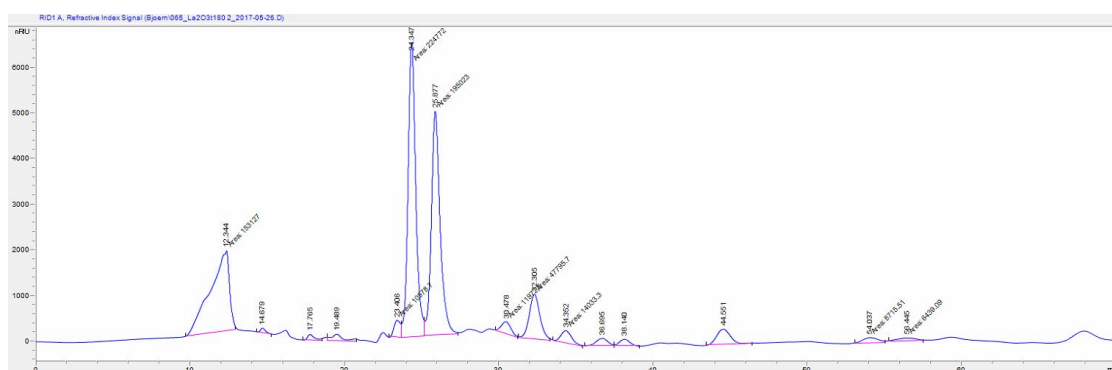
Figure D.17: 0,99g Cellulose, 0,3g La$_2$O$_3$-Cu/CNT, Sampling after 180min

Figure D.18: 0,99g Cellulose, 0,3g La$_2$O$_3$-Cu/CNT + 0,1g Ru/CNT, Sampling after 0min

Figure D.19: 0,99g Cellulose, 0,3g La$_2$O$_3$-Cu/CNT + 0,1g Ru/CNT, Sampling after 15min

Figure D.20: 0,99g Cellulose, 0,3g La$_2$O$_3$-Cu/CNT + 0,1g Ru/CNT, Sampling after 35min
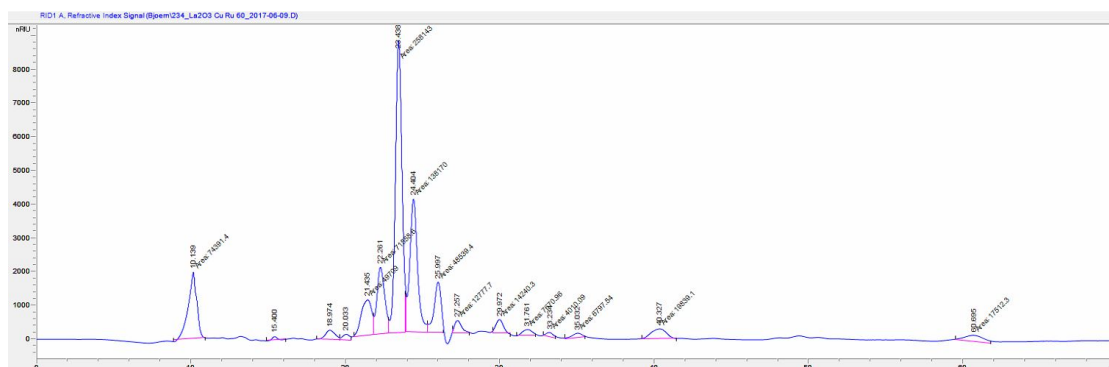
Figure D.21: 0,99g Cellulose, 0,3g La$_2$O$_3$-Cu/CNT + 0,1g Ru/CNT, Sampling after 60min
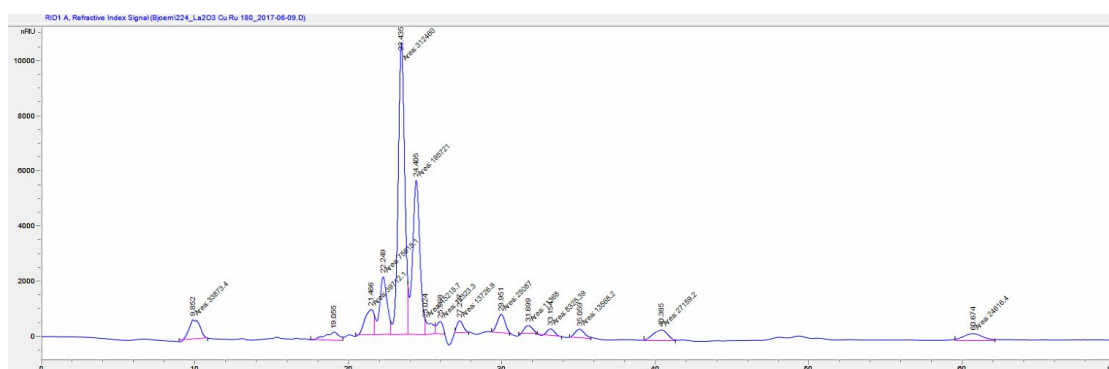
Figure D.22: 0,99g Cellulose, 0,3g La$_2$O$_3$-Cu/CNT + 0,1g Ru/CNT, Sampling after 180min
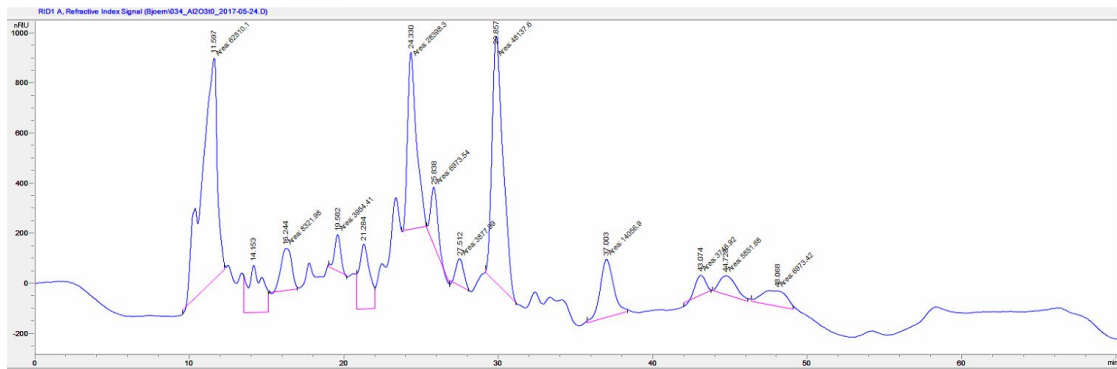
Figure D.23: 0,99g Cellulose, 0,3g Al$_2$O$_3$-Cu/CNT, Sampling after 0min
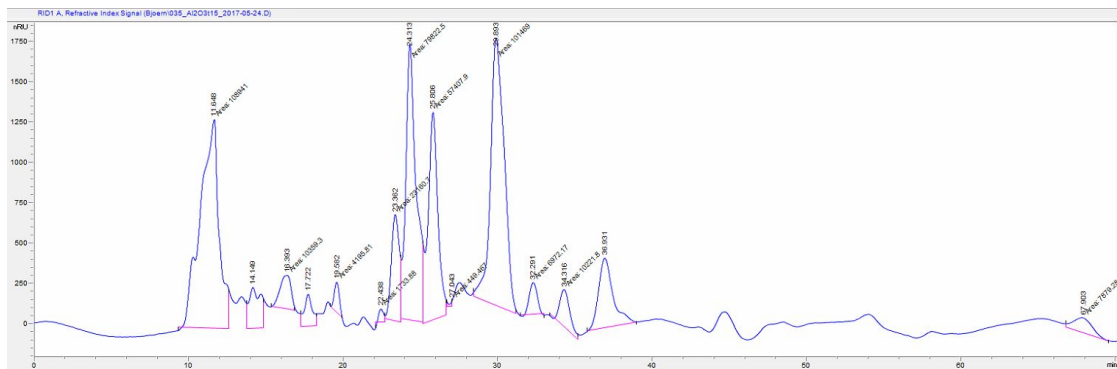
Figure D.24: 0,99g Cellulose, 0,3g Al$_2$O$_3$-Cu/CNT, Sampling after 15min
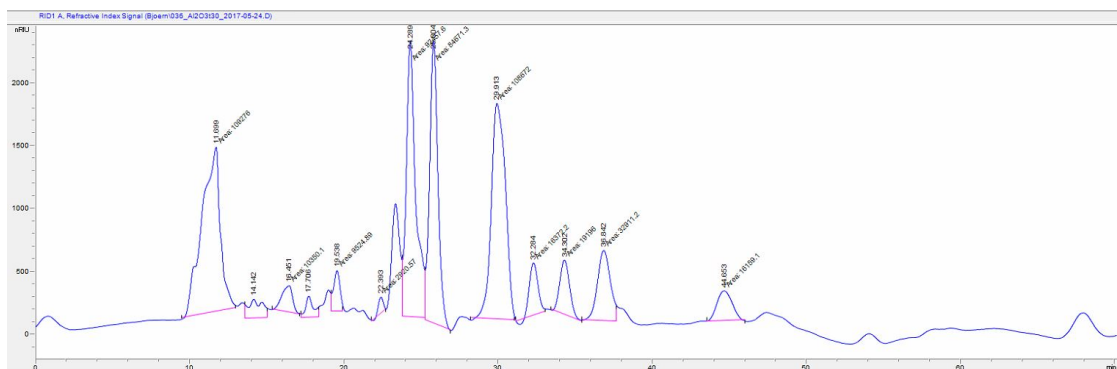
Figure D.25: 0,99g Cellulose, 0,3g Al$_2$O$_3$-Cu/CNT, Sampling after 30min
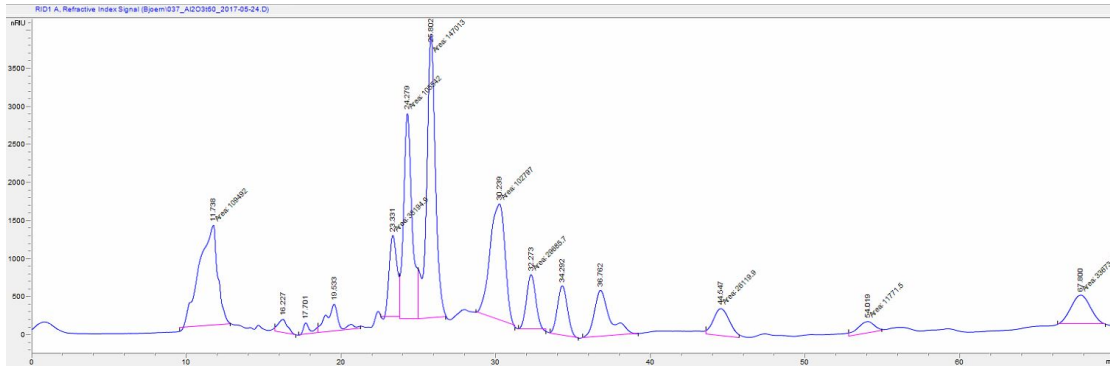
Figure D.26: 0,99g Cellulose, 0,3g Al$_2$O$_3$-Cu/CNT, Sampling after 60min
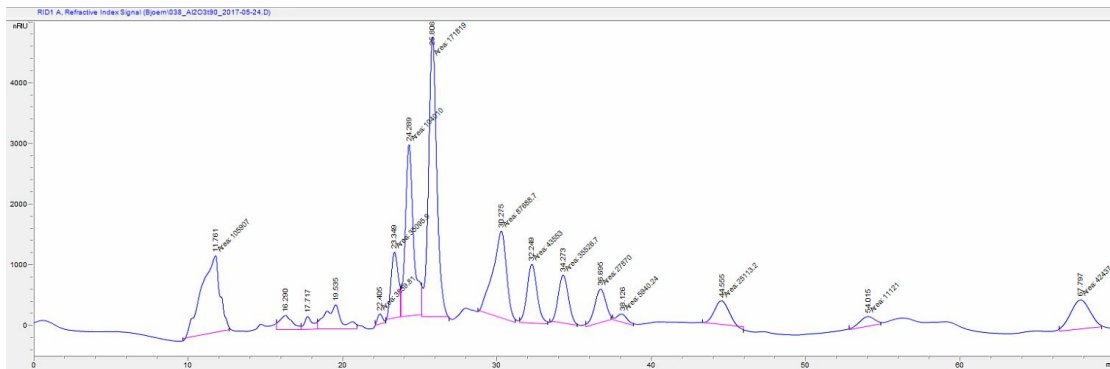
Figure D.27: 0,99g Cellulose, 0,3g Al$_2$O$_3$-Cu/CNT, Sampling after 90min
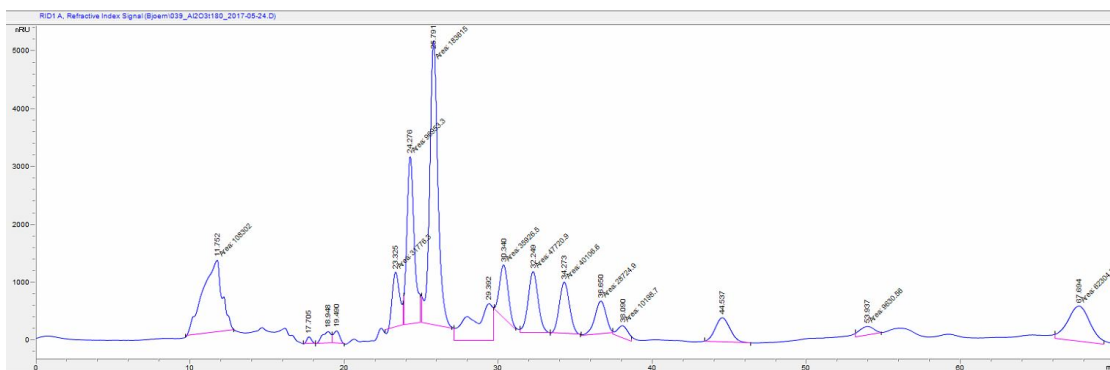
Figure D.28: 0,99g Cellulose, 0,3g Al$_2$O$_3$-Cu/CNT, Sampling after 180min
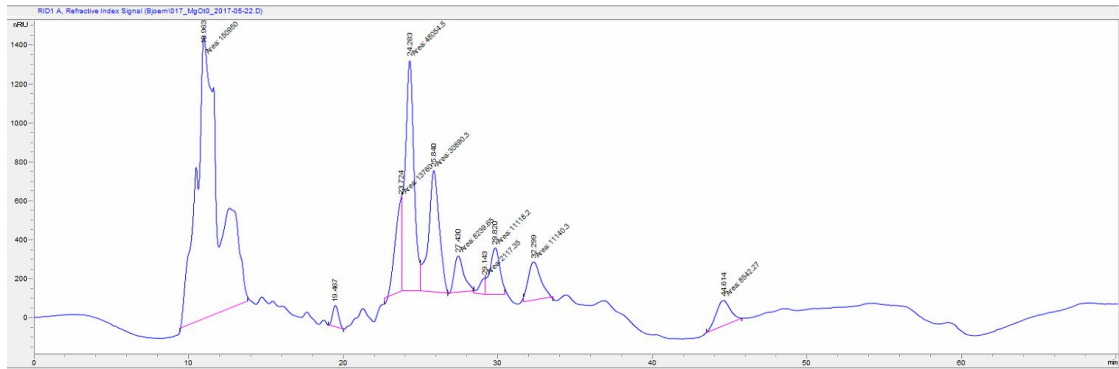
Figure D.29: 0,99g Cellulose, 0,3g MgO-Cu/CNT, Sampling after 0min
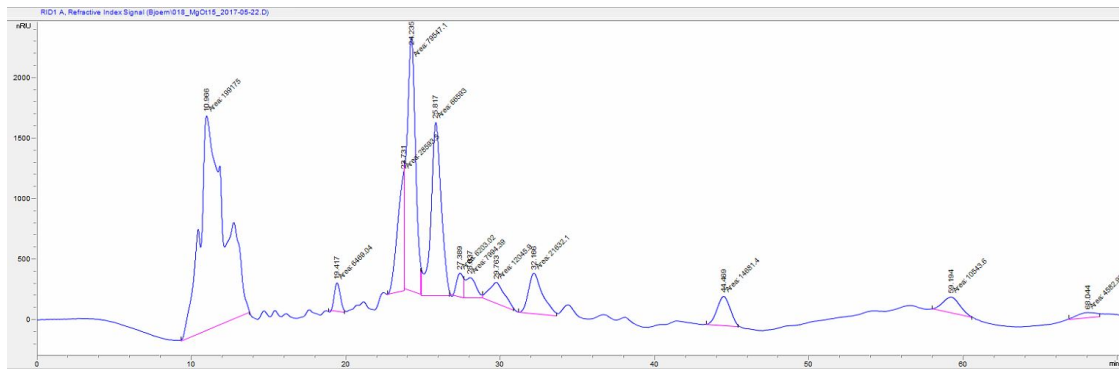
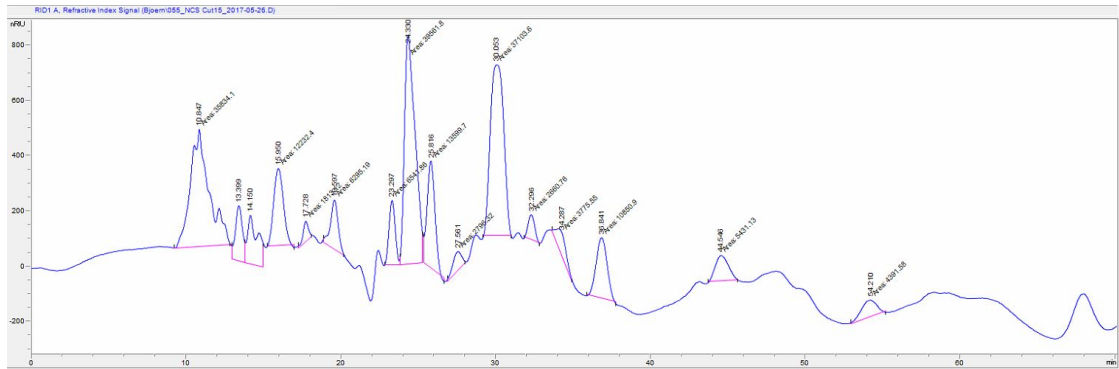**Figure D.30:** 0,99g Cellulose, 0,3g MgO-Cu/CNT, Sampling after 15min
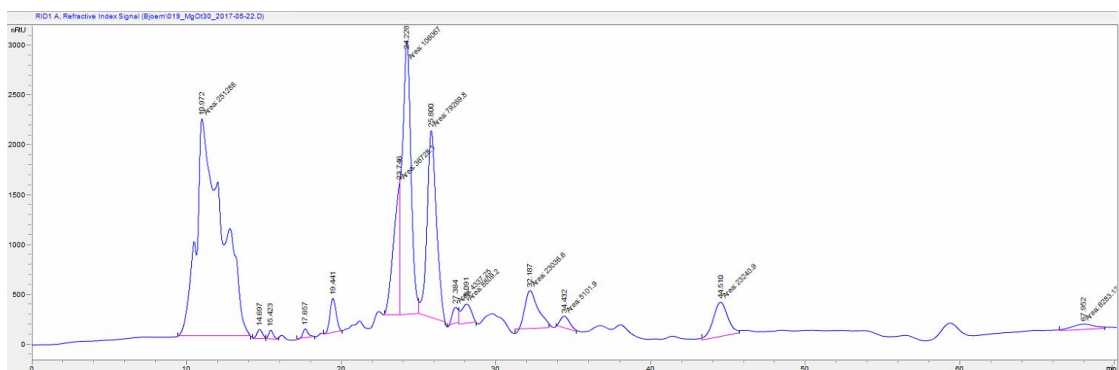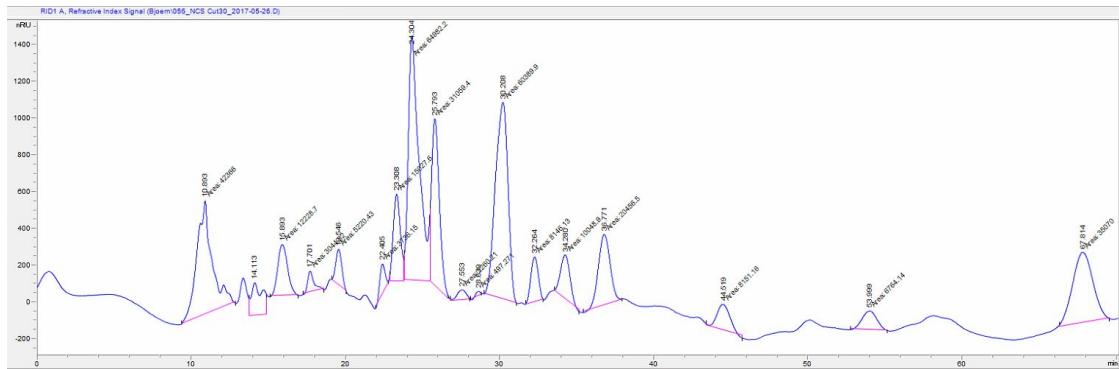

Figure D.31: 0,99g Cellulose, 0,3g MgO-Cu/CNT, Sampling after 30min
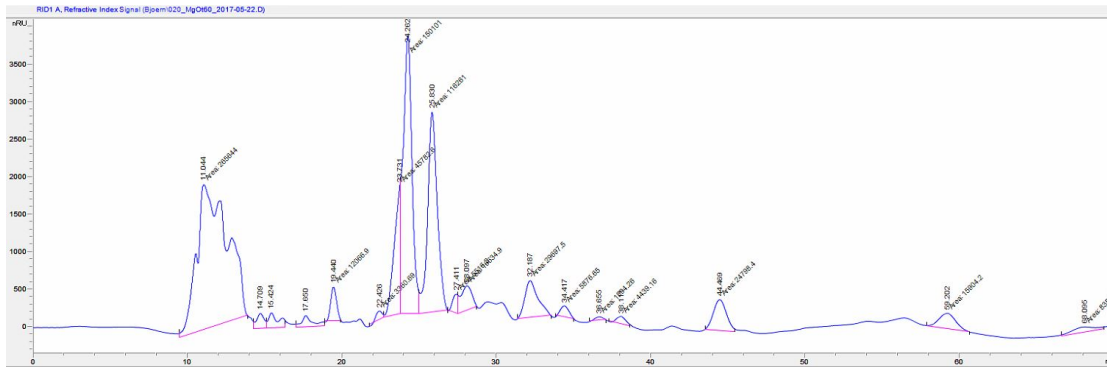
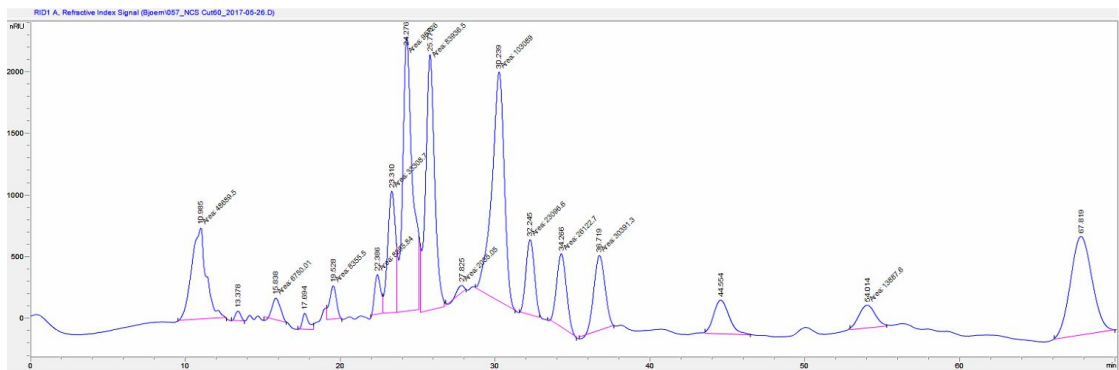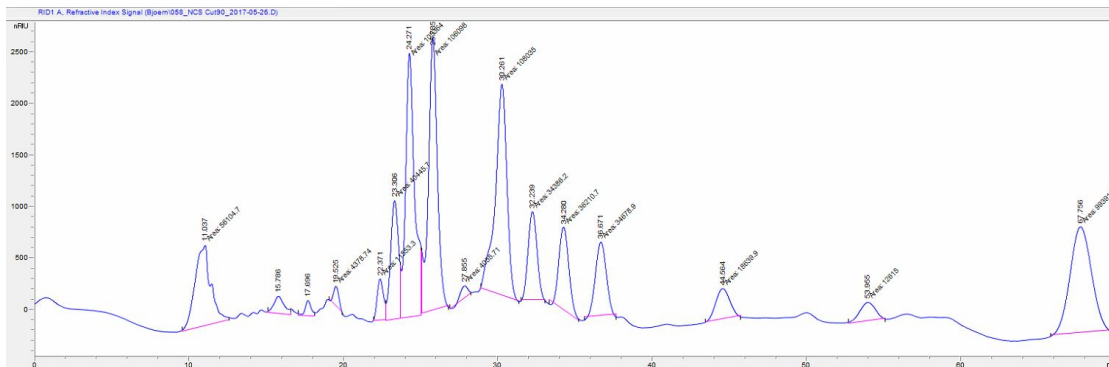**Figure D.32:** 0,99g Cellulose, 0,3g MgO-Cu/CNT, Sampling after 60min
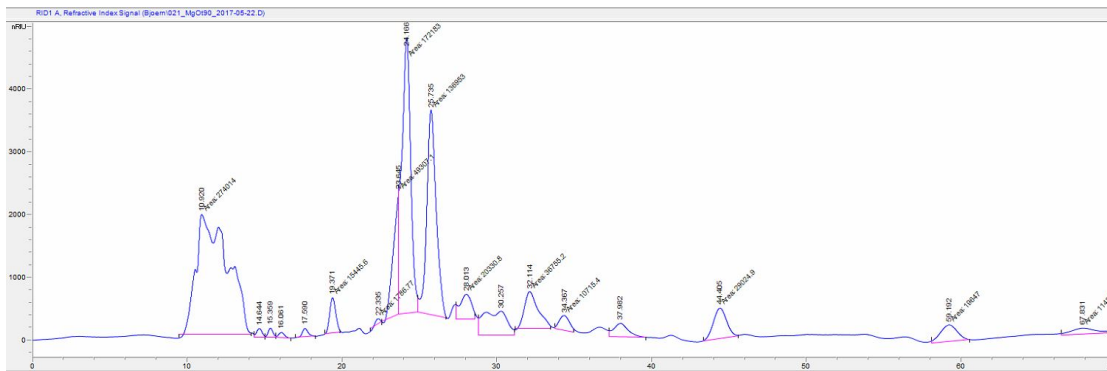
Figure D.33: 0,99g Cellulose, 0,3g MgO-Cu/CNT, Sampling after 90min
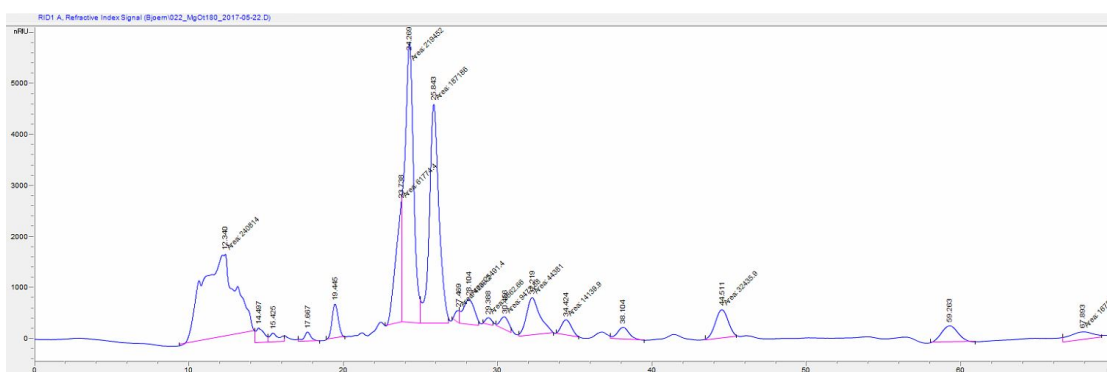
Figure D.34: 0,99g Cellulose, 0,3g MgO-Cu/CNT, Sampling after 0min

95

Figure D.35: 0,99g Cellulose, 0,3g MgO-Cu/CNT + 0,1g Ru/CNT, Sampling after 0min

Figure D.36: 0,99g Cellulose, 0,3g MgO-Cu/CNT + 0,1g Ru/CNT, Sampling after 15min

Figure D.37: 0,99g Cellulose, 0,3g MgO-Cu/CNT + 0,1g Ru/CNT, Sampling after 30min
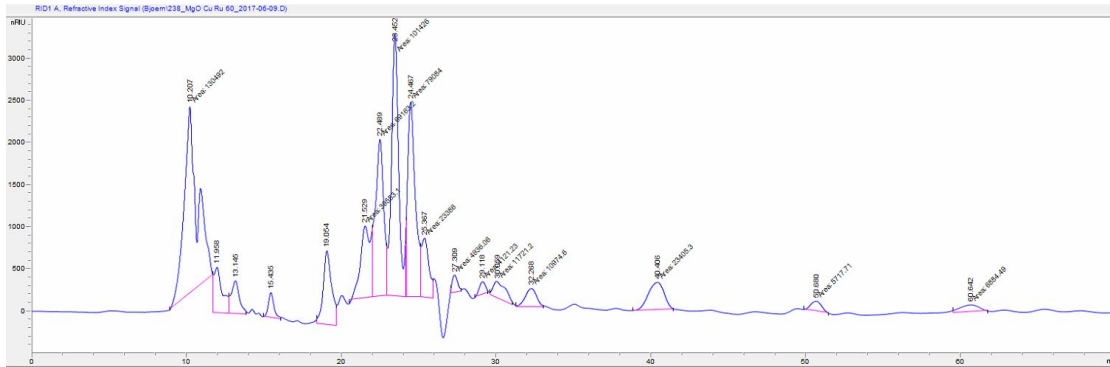
Figure D.38: 0,99g Cellulose, 0,3g MgO-Cu/CNT + 0,1g Ru/CNT, Sampling after 60min
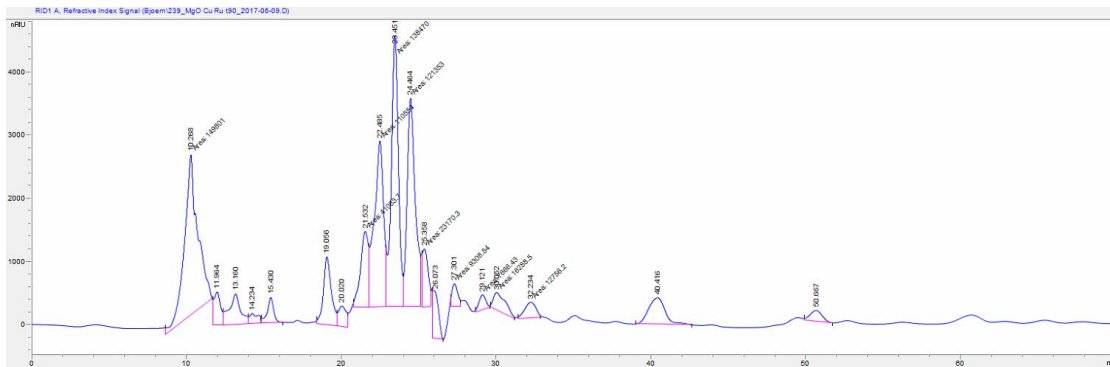
Figure D.39: 0,99g Cellulose, 0,3g MgO-Cu/CNT + 0,1g Ru/CNT, Sampling after 90min
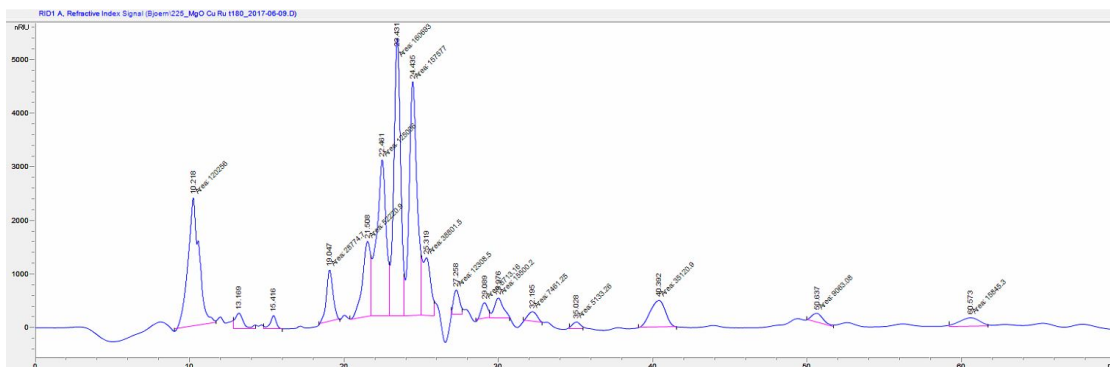
Figure D.40: 0,99g Cellulose, 0,3g MgO-Cu/CNT + 0,1g Ru/CNT, Sampling after 180min

Figure D.41: 0,99g Cellulose, 0,3g Cu/NCS, Sampling after 15min

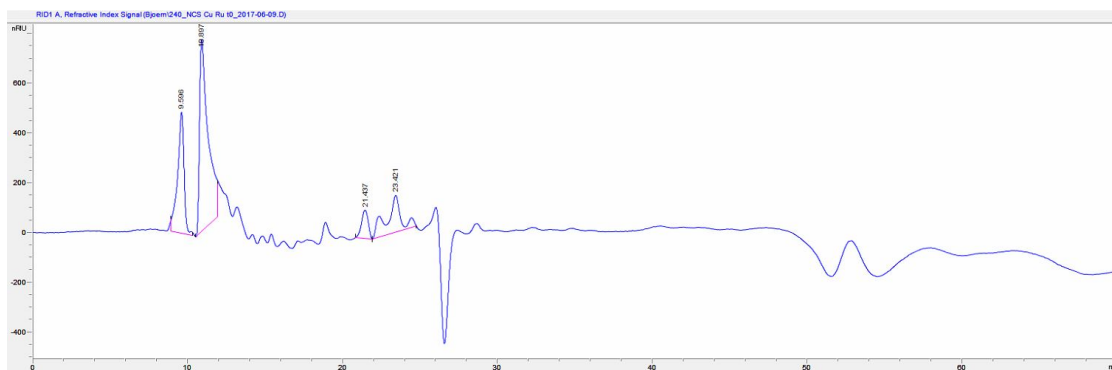**Figure D.42:** 0,99g Cellulose, 0,3g Cu/NCS, Sampling after 30min

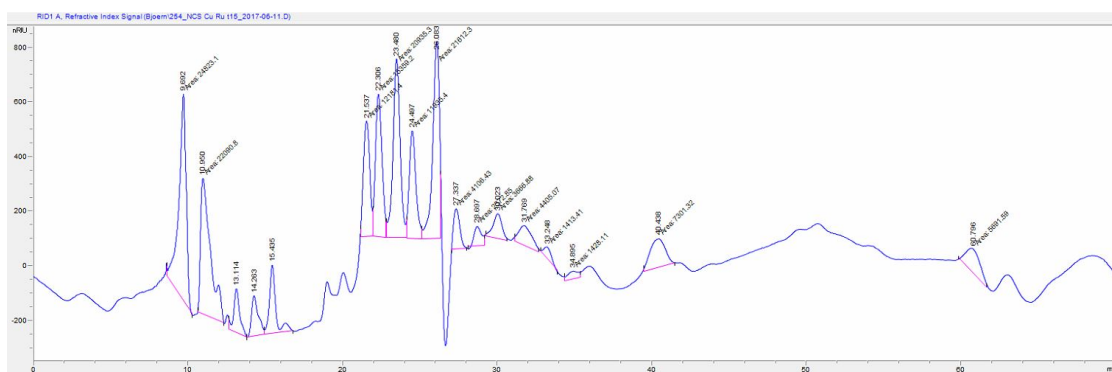**Figure D.43:** 0,99g Cellulose, 0,3g Cu/NCS, Sampling after 60min

Figure D.44: 0,99g Cellulose, 0,3g Cu/NCS, Sampling after 90min

Figure D.45: 0,99g Cellulose, 0,3g Cu/NCS, Sampling after 180min

99

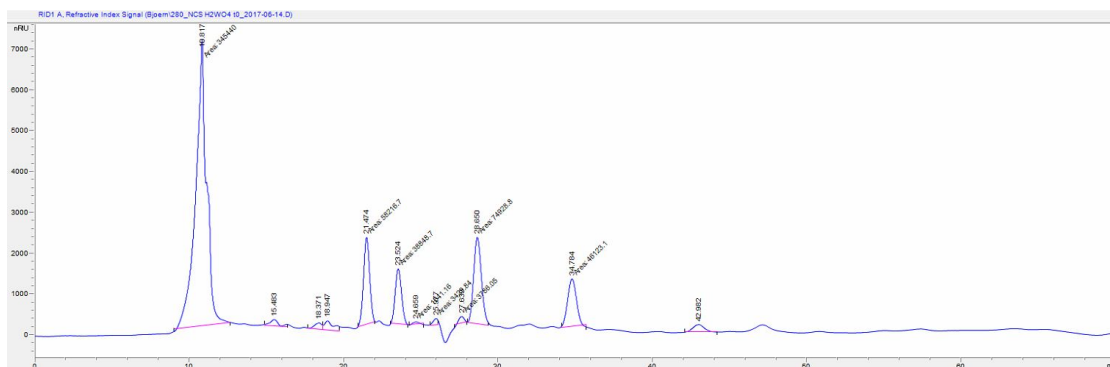**Figure D.46:** 0,99g Cellulose, 0,3g Cu/NCS, 0,1g Ru/CNT, Sampling after 0min

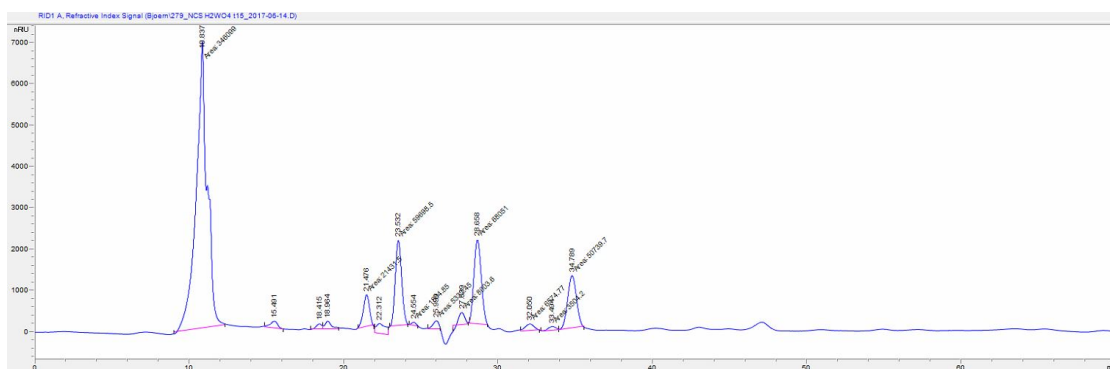**Figure D.47:** 0,99g Cellulose, 0,3g Cu/NCS, 0,1g Ru/CNT, Sampling after 15min

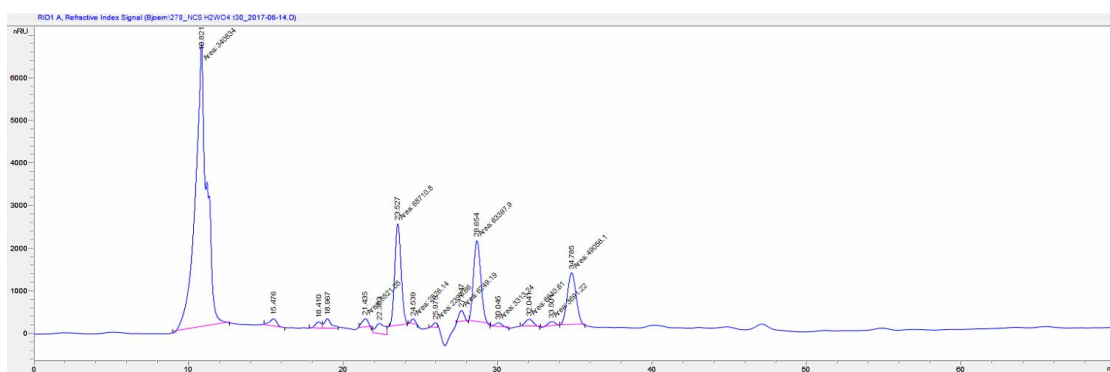**Figure D.48:** 0,99g Cellulose, 0,3g Cu/NCS, 0,1g Ru/CNT, Sampling after 30min
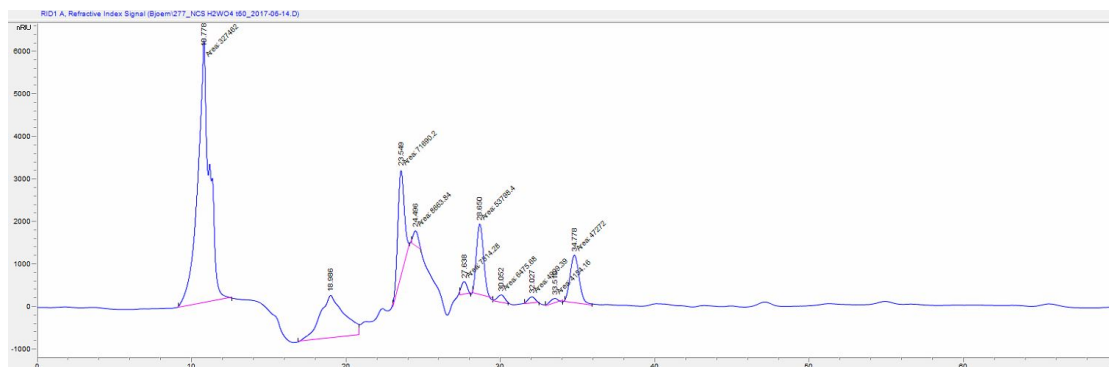
Figure D.49: 0,99g Cellulose, 0,3g Cu/NCS, 0,1g Ru/CNT, Sampling after 60min

Figure D.50: 0,99g Cellulose, 0,3g Cu/NCS, 0,1g Ru/CNT, Sampling after 90min

Figure D.51: 0,99g Cellulose, 0,3g Cu/NCS, 0,1g Ru/CNT, Sampling after 180min

101

Figure D.52: 0,99g Cellulose, 0,3g Cu/NCS, 0,1g H_2WO_4, Sampling after 0min

Figure D.53: 0,99g Cellulose, 0,3g Cu/NCS, 0,1g H_2WO_4, Sampling after 15min

Figure D.54: 0,99g Cellulose, 0,3g Cu/NCS, 0,1g H_2WO_4, Sampling after 30min

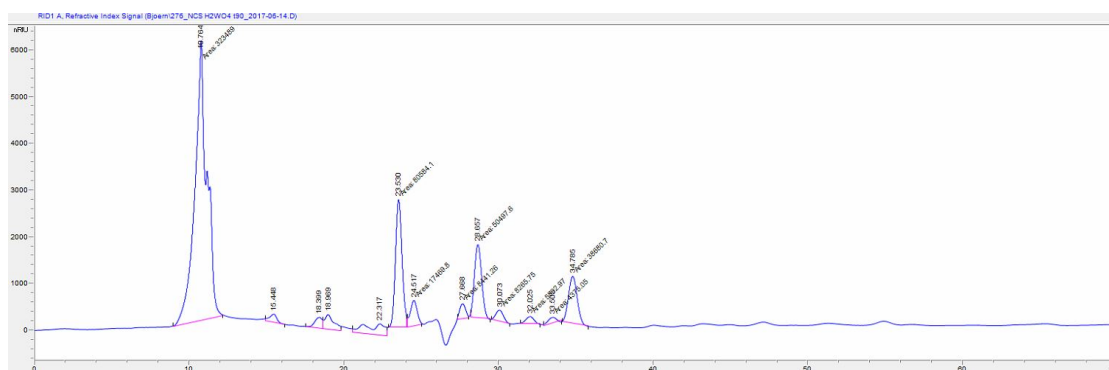**Figure D.55:** 0,99g Cellulose, 0,3g Cu/NCS, 0,1g H_2WO_4, Sampling after 60min

Figure D.56: 0,99g Cellulose, 0,3g Cu/NCS, 0,1g H_2WO_4, Sampling after 90min
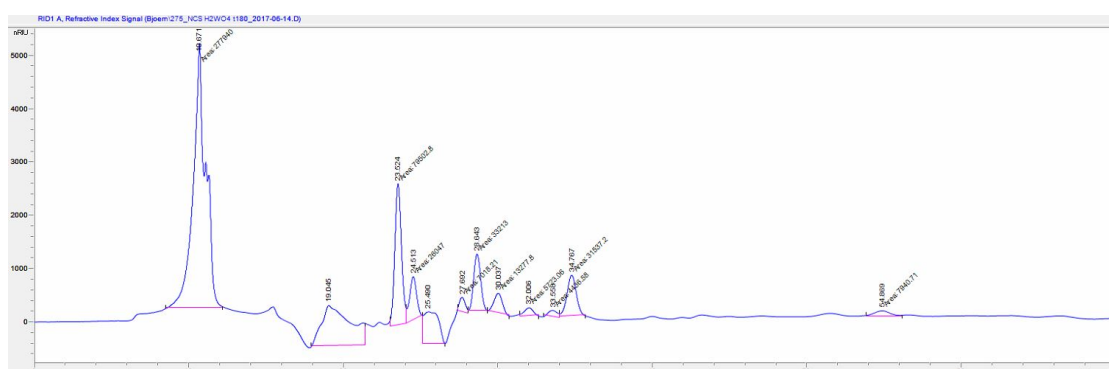

Figure D.57: 0,99g Cellulose, 0,3g Cu/NCS, 0,1g H_2WO_4, Sampling after 180min